UCLA
UCLA Electronic Theses and Dissertations

Title
Streamlined Development of Fully Human Antibody Fragments for ImmunoPET Imaging Using Phage Display Technology

Permalink
https://escholarship.org/uc/item/7db8c0n6

Author
Li, Keyu

Publication Date
2014

Peer reviewed|Thesis/dissertation

eScholarship.org Powered by the California Digital Library
University of California

UNIVERSITY OF CALIFORNIA

Los Angeles

Streamlined Development of Fully Human Antibody Fragments for ImmunoPET Imaging Using Phage Display Technology

A dissertation submitted in partial satisfaction of

the requirements for the degree

Doctor of Philosophy in Molecular and Medical Pharmacology

by

Keyu Li

2014

© Copyright by

Keyu Li

2014

ABSTRACT OF THE DISSERTATION

Streamlined Development of

Fully Human Antibody Fragments for ImmunoPET Imaging

Using Phage Display Technology

by

Keyu Li

Doctor of Philosophy in Molecular and Medical Pharmacology

University of California, Los Angeles, 2014

Professor Anna M. Wu, Chair

Exploiting antibodies' highly specific binding affinities to various biomarkers, immuno-positron emission tomography (immunoPET) provides a non-invasive way to obtain whole body information on *in vivo* molecular events that may be crucial for diagnosis and prognosis, which is increasingly important for diagnostics and prognostics. Small, fully human or humanized antibody fragments are preferred for immunoPET imaging probe development due to their favorable pharmacokinetic properties and low risk of immunogenicity. Phage display technology provides a convenient approach to rapidly generate fully human antibody candidates, showing the potential to accelerate and streamline the development process of antibody fragment based immunoPET

imaging probes, which is strongly needed as increasing numbers of targeted therapies are being developed every year. Chapter 2 and Chapter 3 describe the use of a traditional fully human scFv phage display library for developing anti-MET antibody fragments for both immunoPET imaging and potential therapeutic application. Multiple fully human anti-MET scFv clones were isolated and reformatted. Three cys-diabody clones showed high affinities (0.7 to 5.1 nM) and inhibitory effect on MET over-expressing cells. The H2 cys-diabody and minibody were able to distinguish a MET over-expressing gefitinib resistant tumor from the parental tumor at as early as 4 hours post injection, indicating the potential of same day imaging for patient stratification. To further exploit the benefit of the phage display technology and streamline the antibody fragment devlopment, as described in Chapter 4 and Chapter 5, two fully human scFv phage display libraries with customized linkers and restriction sites were constructed to simplify the antibody fragment reformatting process. The libraries were used for selections against several different targets and successfully generated multiple positive clones. ScFvs from these libraries were rapidly reformatted into diabodies using the restriction sites in the customized linkers. Size exclusion chromatography analysis of these antibody fragments proved the shortened linkers can successfully induce dimerization for the majority of the diabody clones. Together, the studies presented in this dissertation highlight a successful example of the use of phage display technology for developing fully human antibody fragments for immunoPET imaging and how phage display libraries can be improved to further streamline this process.

The dissertation of Keyu Li is approved.

Heather Christofk

Michael van Dam

Sherie L. Morrison

Anna M. Wu, Committee Chair

University of California, Los Angeles

2014

Dedicated to
my loving wife,
Lu,
for your support during the writing

and your trust over these years.

Table of Contents

Chapter 1: Introduction 1

1.1 Antibody and antibody imaging 3

1.1.1 Antibody 3

1.1.2 ImmunoPET 9

1.1.3 ImmunoPET using antibody fragments 14

1.2 Phage display 17

1.3 MET and cancer 20

1.4 Biblography 25

Chapter 2: Anti-MET antibody selection and *in vitro* characterization 35

2.1 Introduction 35

2.2 Materials and Methods 36

2.2.1 Cell lines 36

2.2.2 Phage library selection 37

2.2.3 Phage ELISA 38

2.2.4 Flow cytometry 39

2.2.5 Expression and purification of cys-diabody, minibody and scFv 39

2.2.6 Affinity determination by flow cytometry 42

2.2.7 ELISA to test cross reactivity 42

2.2.8 *In vitro* MTS assay 43

2.2.9 Signaling analysis using Western blot 43

2.3 Results 44

2.3.1 Anti-MET phage selection and screening 44

2.3.2 *In vitro* characterization of cys-diabodies 49

2.3.3 Cell growth inhibition assays 51

2.3.4 Downstream signaling analysis using Western blot 53

2.4 Discussion 55
2.5 Bibliography 59

Chapter 3: Anti-MET antibody fragments for immunoPET imaging 61
3.1 Introduction 61
3.2 Materials and methods 63
3.2.1 Cell lines and tumor models 63
3.2.2 Radiolabeling of cys-diabodies and minibodies 63
3.2.3 Binding and internalization assay of H2 cys-diabody 65
3.2.4 Small animal PET imaging and *ex vivo* biodistribution studies 65
3.3 Results 66
3.3.1 ^{89}Zr labeling of H2 cys-diabody and minibody 66
3.3.2 Internalization and uptake of ^{89}Zr labeled H2 cys-diabody 69
3.3.3 *In vivo* PET imaging using ^{89}Zr-DFO-mal-H2 cys-diabody 70
3.3.4 *In vivo* PET imaging using ^{89}Zr-DFO-SCN-H2 minibody 73
3.4 Discussion 75
3.5 Bibliography 78

Chapter 4: Construction of novel human scFv phage display libraries 79
4.1 Introduction 79
4.2 Materials and methods 82
4.2.1 Incorporating the new linkers into pHEN1 vector 82
4.2.2 Construction of the V_H and V_L libraries containing the new linkers 86
4.2.3 Construction of the scFv libraries containing the new linkers 88
4.2.4 Phage production from the new libraries 89
4.3 Results 93
4.3.1 Construction of the V_H and V_L libraries 93
4.3.2 Construction of the 17aa-SSA-scFv library and the 18aa-SX-scFv library 94
4.3.3 Phage production from the new libraries 96

4.4 Discussion 96
4.5 Bibliography 100

Chapter 5: Reformatting and analysis of antibody fragments from the new libraries 103
5.1 Introduction 103
5.2 Materials and methods 104
5.2.1 Phage library selection and phage ELISA 104
5.2.2 ScFv subcloning and reformatting 106
5.2.3 Expression and purification of scFvs and diabodies 106
5.2.4 Affinity determination by ELISA 107
5.2.5 Size exclusion chromatography 108
5.3 Results 108
5.3.1 Phage selections 108
5.3.2 Phage ELISA 110
5.3.3 *In vitro* characterization of anti-Ncad 17aa-SSA-scFvs 114
5.3.4 Linker length dependent dimerizations 116
5.4 Discussion 118
5.5 Bibliography 124

Chapter 6: Summary and future directions 125
6.1 Summary 125
6.2 Future Directions 129
6.3 Bibliography 131

Table of Figures

Chapter 1: Introduction

Figure 1.1: IgG structure and function. 5
Figure 1.2: Percentage of four types of mAbs in clinical development. 8
Figure 1.3: Principles of PET. 11
Figure 1.4: Antibody fragments with different serum half-lives. 16
Figure 1.5: Diabody and cys-diabody. 16
Figure 1.6: Principles of phage display library selections. 18
Figure 1.7: Streamlined development of immunoPET probes using a phage library. 20
Figure 1.8: The multidomain structure of MET and HGF. 22

Chapter 2: Anti-MET antibody selection and in vitro characterization

Figure 2.1: Distribution of duplicates among top 64 clones. 46
Figure 2.2: Anti-MET phage flow cytometry results. 48
Figure 2.3: SDS-PAGE of Anti-MET C2, H2 and H5 cys-diabodies. 49
Figure 2.4: Affinity determination of anti-MET cys-diabodies by flow cytometry. 50
Figure 2.5: Cross reactivity analysis of anti-MET cys-diabodies. 50
Figure 2.6: *In vitro* MTS assays to evaluate the off target toxicity of the cys-diabodies. 51
Figure 2.7: Anti-MET cys-diabodies inhibit growth of MET dependent cells. 52
Figure 2.8: Effects of anti-MET H2 Ab fragments on the growth of Hcc827-GR6. 53
Figure 2.9: Comparing the effects of H2 cysDb and scFv on downstream signaling. 54
Figure 2.10: Comparing the effects of H2 Ab fragments on downstream signaling. 55

Chapter 3: Anti-MET antibody fragments for immunoPET imaging

Figure 3.1: Site-specific conjugation of the H2 cys-diabody. 67
Figure 3.2: Random conjugation of the H2 minibody. 68
Figure 3.3: Internalization and uptake of radiolabeled H2 cys-diabody. 70
Figure 3.4: ImmunoPET using radiolabeled H2 cys-diabody. 72
Figure 3.5: ImmunoPET imaging using radiolabeled H2 minibody. 74

Chapter 4: Construction of novel human scFv phage display libraries

Figure 4.1: Reformatting selected scFvs from common phage libraries. 80

Figure 4.2: pHEN1 phagemid vector and different linkers. 83

Figure 4.3: Schematic outline of the library construction. 85

Chapter 5: Reformatting and analysis of antibody fragments from the new libraries

Figure 5.1: Counter selection to avoid unwanted phage clones. 105

Figure 5.2: *In vitro* characterization of anti-Ncad 17aa-SSA scFvs. 115

Figure 5.3: SEC analysis of anti-Ncad 17aa-linker scFvs and 7aa-linker diabodies. 117

Figure 5.4: SEC analysis of 18aa-linker scFvs and 5aa-linker diabodies. 117

Acknowledgments

First I want to thank my mentor, Dr. Anna Wu, for her enormous support and insightful suggestions over these years. She has always been encouraging and inspiring and has helped me to overcome numerous difficulties and challenges. I learned so much from her scientific experiences, her diligence and her enthusiastic attitude. With her help, I can finally make this dissertation possible and become a real scientist. I also want to thank my committee – Dr. Heather Christofk, Dr. Michael van Dam and Dr. Sherie Morrison – for all the feedbacks and suggestions on my research and on my dissertation.

I thank all the members of the Wu lab for the help and advice over the years, and also for making the lab such a fun place to work. I want to thank Eric Lepin for leading me through my rotation days at Wu lab. I thank Richard Tavaré and Kirstin Zettlitz for teaching me the techniques for radiolabeling, imaging and biodistribution studies. I thank Scott Knowles for his help on the imaging software and the mathematical models. I thank our lab manager, Felix Salazar, for always providing me supplies and teaching me all the tricks and secrets about everything in the lab, from the printer to the ÄKTA. I thank Shannon Sirk, Katelyn McCabe, Tove Olafsen, Vania Kenanova and all other past and present lab members for their support and help.

I also want to thank all of my collaborators, for working with me and providing me knowledge and techniques to make the projects becoming possible. A special thanks to Dr. Yu Zhou for

her help with the library construction, for being so patient in replying all my rookie questions.

I want to thank Waldemar Ladno, Darin Williams, John David and David Stout at the Crump Institute for their help with the PET/CT scans and the tail vein injections. I would like to thank Jeffery Calimlim and Ingrid Schmid at the Janis V. Giorgi Cytometry Core Facility for the help on flow cytometry experiments. I would also like to thank Sarah Starrett and Erika Corrin, who are the best administrators I have ever met.

In the end, I would like to thank all my friends and my family, for their support and the joy they have brought me these years. Especially, I want to thank my wife, Lu, for being supportive and patient, for encouraging me and helping me through difficult days. Thank you for your love and trust, and always being such a perfect wife. Thank you for making this dissertation possible.

Vita

2004-2006	Tsinghua Comprehensive Scholarship
2007	Undergraduate researcher,
	Dr. Guoqiang Chen's lab at Tsinghua University
	Microbiology and molecular biology
2007-2008	Undergraduate researcher,
	Dr. Ding Xue's lab at Tsinghua University
	Genetics in C. elegans
2008	Bachelor of Science, Biological Science and Biotechnology
	Tsinghua University
2008	Outstanding Graduate of Tsinghua University
2012	Student Travel Award
	UCLA, Department of Molecular and Medical Pharmacology

Patent Applications:

Keyu Li, Anna Wu. Fully human antibodies and fragments recognizing human c-MET. Patent application filed. Application number: PCT/US13/72668.

Keyu Li, Anna Wu. Fully Human Antibody Against EpCAM. Provisional patent filed. UCLA case number 2012-878.

Manuscripts:

Keyu Li, Richard Tavaré, Kirstin Zettlitz, Shannon Mumenthaler, Parag Mallick, Yu Zhou, James Marks, Anna Wu. Anti-MET immunoPET for non-small cell lung cancer using novel fully human antibody fragments. Manuscript submitted to Molecular Cancer Therapeutics.

Keyu Li, Yu Zhou, James Marks, Luke Lee, Parag Mallick, Robert Reiter, Anna Wu. Fully human scFv phage display libraries for rapid antibody fragments reformatting. Manuscript in preparation.

Presentations:

Keyu Li, Richard Tavaré, Kirstin Zettlitz, Scott Knowles, Matthew Rochefort, Felix Salazar, Anna Wu. Novel fully human anti-MET cys-diabodies show great potential for therapeutics and *in vivo* PET imaging for non-small cell lung cancer. Oral presentation at the World Molecular Imaging Congress, 2013.

Keyu Li, Richard Tavaré, Kirstin Zettlitz, Scott Knowles, Matthew Rochefort, Felix Salazar, Anna Wu. Novel fully human anti-MET antibody fragments for *in vivo* PET imaging and therapy of non-small cell lung cancer. Poster presentation at IBC's 24th Annual International Conference of Antibody Engineering, 2013.

Keyu Li, Richard Tavaré, Felix Salazar, Scott Knowles, Kirstin Zettlitz, Richard Gaster,, Lingyun Xu, Shan Wang, Anna Wu. Novel human antibody fragments against EpCAM and c-MET show great potential for therapeutic and diagnostic applications in targeted therapy of lung cancer. Poster presentation at IBC's 23rd Annual International Conference of Antibody Engineering, 2012.

Chapter 1: Introduction

In vitro diagnostic tests, such as immunohistochemistry and ELISA, rely on limited biopsy samples to evaluate the molecular status of a patient's disease. Small biopsy samples may provide misleading information if the target tissue is heterogeneous in nature. In the case of metastatic cancers, different metastatic lesions may have gone through different evolutionary history and have completely different characteristics. Limited biopsies cannot provide the overall information of these different lesions. Like the traditional immunohistochemistry, Immuno-positron emission tomography (immunoPET) also exploits antibodies' highly specific binding affinities to evaluate the expression levels of various biomarkers. However, instead of relying on limited biopsy samples, it provides a non-invasive way to obtain whole body information on *in vivo* molecular events that may be crucial for diagnosis and prognosis.

Like other *in vivo* clinical applications, humanized, or fully human antibodies are favored because of the relatively lower risk of immunogenicity. Meanwhile, instead of the intact antibodies commonly used in therapeutic applications, smaller antibody fragments are preferred for rapid, high contrast immunoPET because of their pharmacokinetic properties. Traditionally, in order to obtain humanized antibody fragments for imaging,

laborious and time consuming process of immunization, humanization, affinity maturation and antibody reformatting are required. As increasing numbers of targeted therapies are being developed every year, there is a strong need of numerous immunoPET probes to help analyze *in vivo* molecular characteristics. Therefore, it becomes extremely important for the field to accelerate the development process of imaging probes.

Fully human scFv (single-chain variable fragment) phage display libraries have been used for rapid generation of fully human antibody clones for years. Using such technology can bypass the need for immunization and humanization and greatly help accelerate the imaging probe development for clinical use. Chapter 2 and Chapter 3 describe the use of a traditional fully human scFv phage display library for developing anti-MET antibody fragments for immunoPET imaging. To further streamline phage display technology for developing engineered antibody fragments, Chapter 4 and Chapter 5 describe the construction of fully human scFv phage display libraries with customized linkers and restriction sites to simplify the antibody fragment reformatting process. Together, the present work highlights a successful example of the use of phage display technology for developing fully human antibody fragments for immunoPET imaging, and improvements to the technology to meet the needs of immunoPET and other applications where a variety of antibody fragments are desired. Prior to presenting the results, background information regarding antibody imaging, phage display technology and MET protein is provided.

1.1 Antibody and antibody imaging

1.1.1 Antibody

Antibodies, also called immunoglobulins, are natural proteins produced by animals that play an essential role in the immune system by recognizing and neutralizing foreign molecules called antigens. In mouse and human, antibodies come in five different classes called IgA, IgD, IgE, IgM and IgG, where “Ig” stands for immunoglobulin, each having different structures and biological activities. IgG is the most common class in the serum and is crucial for fighting invading pathogens (1). It is also the format used by almost all approved therapeutic intact antibodies (2, 3). IgG antibodies are 150 kDa, Y-shaped molecules composed of two identical heavy chains and two identical light chains, which are held together by both inter chain disulfide bonds and also non-covalent interactions. The light chain has one variable domain (V_L) and one constant domain (C_L), while the heavy chain has one variable domain (V_H)and three constant domains (C_H1, C_H2 and C_H3). Each of the two arms of the Y-shaped molecules consists of the whole light chain and the first two domains of the heavy chain (V_H and C_H1). It is named fragment antigen-binding (Fab) because of the antigen binding site located at the tip of the arm, which is determined primarily by the six complementarity determining regions (CDRs; H1, H2, H3 on V_H domain; L1, L2, L3 on V_L domain). The stem of the Y-shaped molecule is called fragment crystallizable region (Fc region). The antibody depends on the binding of the Fc region to various Fc receptors and complement proteins to initiate its

effector functions such as antibody-dependent cell-mediated cytotoxicity (ADCC) and complement-dependent cytotoxicity (CDC).The Fc region also contains the binding site for the neonatal Fc receptor (FcRn) that is responsible for the salvage of IgG antibodies which contributes to the exceptional long serum half-life (about 7 to 21 days) (4). Figure 1.1 depicts the structure and function of different subunits of a IgG molecule (5). Note that the Fc region contains glycosylation sites that are crucial for antibody effector functions. Successful expression of full length IgG proteins can only be done in mammalian cells, because bacterial expression systems lack such glycosylation capability.

The applications of antibodies in either scientific research or clinical use rely on their two major properties: antigen binding and effector functions. Antibodies are probably the most variable and reliable affinity reagents. Their unmatched high affinity and specificity have enabled their broad applications in scientific research and *in vitro* diagnosis to identify and quantify various biomarkers and other antigens. For *in vivo* therapeutics, their binding capabilities can be exploited to block the biological activities of target proteins by direct competition with their natural binding partners or by indirect inhibition through binding-induced conformational change. The effector functions of the Fc region can be employed to mount immune responses to pathogens or tumor cells. A functional Fc domain in a therapeutic antibody or antibody fragment also promises a long serum half-life that is useful for extending the dosing interval and can potentially reduce the cost of treatment. The distinct functions of different subunits of the antibody ensure the

possibility and necessity of antibody engineering to create optimized antibody fragments for different applications.

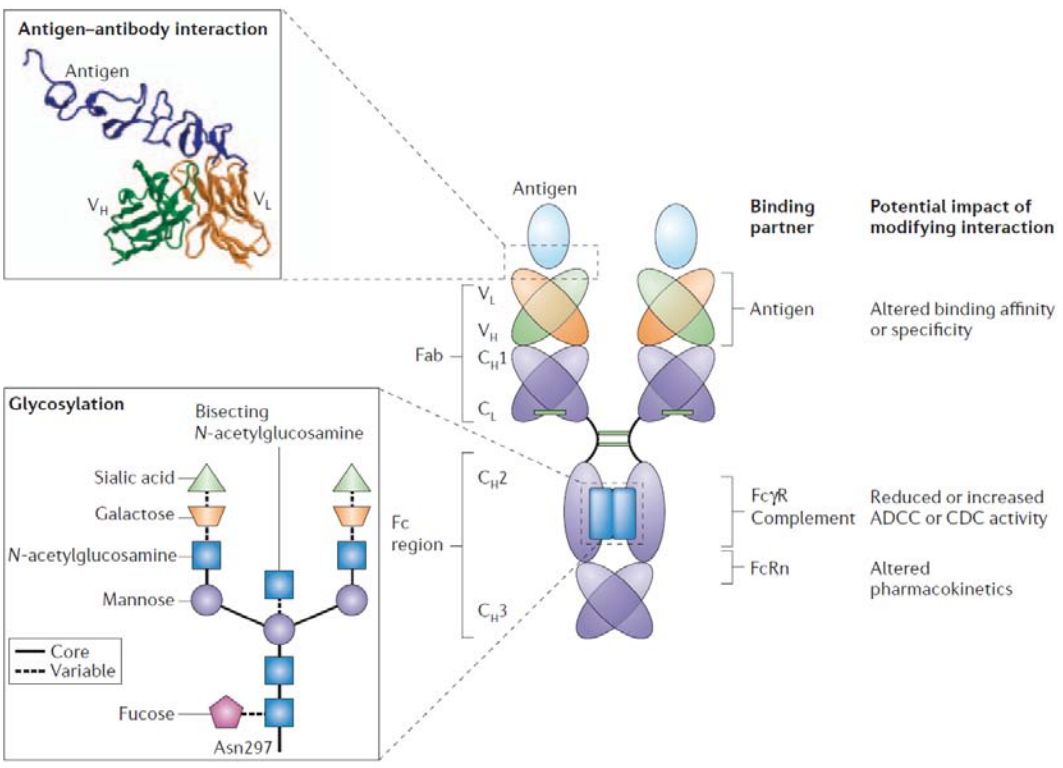

Figure 1.1: IgG structure and function.

IgG molecules are composed of two heavy chains and two light chains, which are linked by disulphide bonds (green bars). The light chain has one variable domain (V_L) and one constant domain (C_L), while the heavy chain has one variable domain (V_H) and three constant domains (C_H1, C_H2, C_H3). The antigens are recognized by the variable domains in which the complementarity-determining regions (CDRs) determine the binding specificity and affinity. The effector functions (ADCC and CDC) are dependent on the constant domains in the Fc region that interact with various Fcγ receptors (FcγR) and complement proteins. The proper glycosylation in this region is required for such interaction. Fc region also binds to the neonatal Fc receptor (FcRn), contributing to the long serum half-life of human IgG. Adapted from Carter, 2006. Reference (5).

While the half-life extending effect of the Fc domain is desirable for most therapeutic applications, the effector functions need to be avoided in some cases. One solution is to introduce mutations into the Fc region to abolish the effector functions while keeping the extended half-life, with the examples such as the anti-CD3 teplizumab and otelixizumab(6-9). Alternatively, an Fc-less fragment such as the Fab can be employed for these applications. In the case of Cimzia (certolizumab pegol), the Fab protein is also chemically conjugated to polyethylene glycol (PEGylated) to increase the serum half-life (6, 10). However, in the case of *in vivo* imaging, the long half-lives of the intact IgG proteins become less desirable because rapid and high contrast imaging requires fast blood clearance of the imaging tracer (11-14). Therefore, antibody fragments with shorter serum half-lives are very attractive for such applications (15-20).

Besides tweaking the functional subunits of the antibodies according to specific needs, another important aspect of antibody engineering is to reduce the immunogenicity. The first generation of therapeutic murine monoclonal antibodies (mAbs) came into clinical study during early 1980s, soon after the murine hybridoma technology was invented by Kohler and Milstein in 1975 (21). However, the intrinsic immunogenicity of murine antibodies can induce the production of human anti-mouse antibodies (HAMA) in patients, resulting in rapid clearance of the murine antibodies from the human body, and increasing the risk of allergic reactions (2, 22-26).Therefore, people started to reduce the immunogenicity by replacing parts of the mouse protein with human sequences. Morrison

et al. invented the chimeric mAbs in 1984, where murine constant domains were replaced by the human counter parts. Such change can reduce HAMA response for some antibodies and improve their efficacy, leading to several approved therapeutic chimeric mAbs such asrituximab and infliximab (2). Taking one step further, in 1986, Jones *et al*. developed humanized mAbs by replacing most of the sequences with the human version except for the CDRs (27). Approved humanized mAbs include daclizumab, trastuzumab, bevacizumab, etc (2). Another way to address the immunogenicity problem, naturally, is to use the antibodies of human origin, the so-called fully human antibodies. Early attempts focused on human hybridoma technology (28, 29), but the ethical restrictions on immunizing human subjects for antibody generation and the immune tolerance for human antigens surely limited its wider applications. More practical methods came later, when people cloned human antibody genes into other organisms to create phage display technology (30) and transgenic mice with human immunoglobulin genes (31, 32). The inherent low immunogenicity and the elimination of the humanization process make these fully human antibodies a preferred solution for mAb development (Figure 1.2).

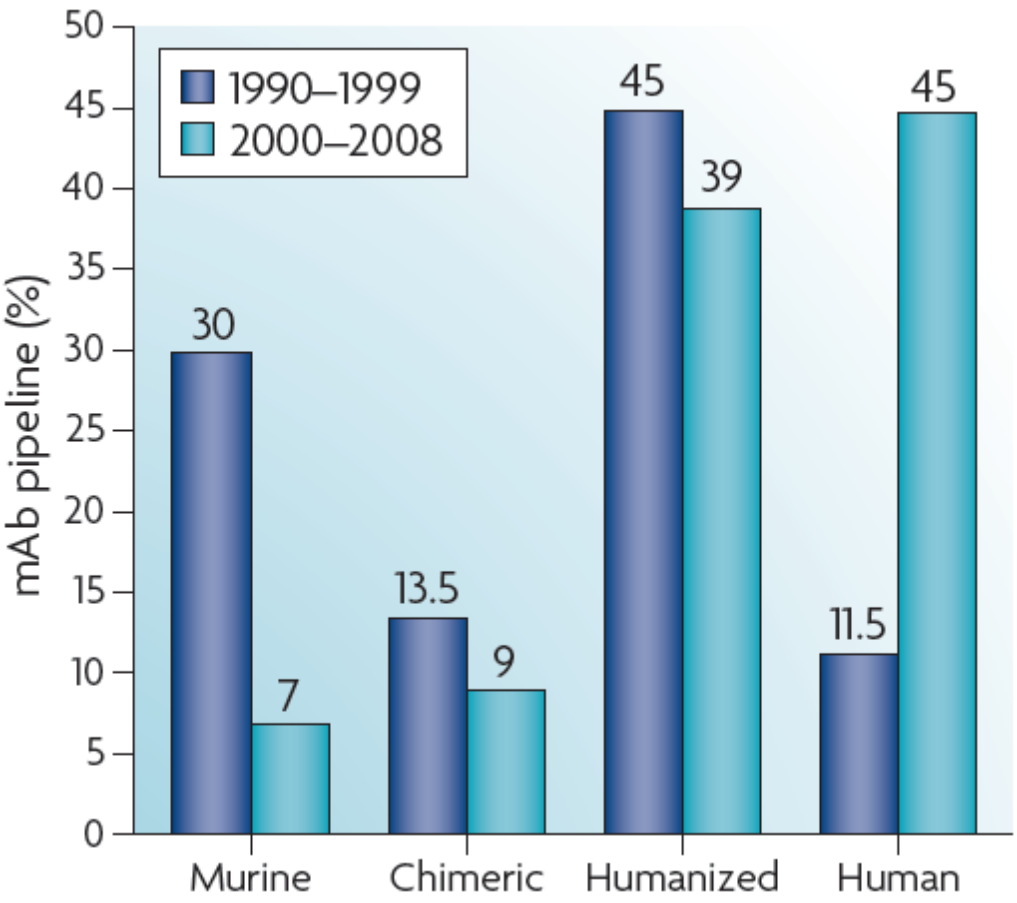

Figure 1.2: Percentage of four types of mAbs in clinical development.
Comparing the monoclonal antibodies that entered clinical study during 1990 – 1999 and 2000 – 2008, there is increasing interest in humanized and fully human antibodies. Adapted from Nelson *et al.*, 2010, reference (33).

Antibodies are also used to facilitate targeted delivery of other therapeutic agents in order to increase efficacy and reduce side effects (34-36). Common practices include the direct conjugation of the antibody or antibody fragment to chemotherapeutic drugs or cytotoxic radionuclides for chemoimmunotherapies or radioimmunotherapies. For example, approved for Hodgkin's lymphoma treatment, Brentuximab vedotin is composed of the CD30-specific chimeric mAb cAC10 and the cytotoxic agent, monomethyl auristatin E

(MMAE). It is rapidly internalized upon binding to CD30, and the subsequent proteolysis lead to the efficient release of MMAE, killing the target cell (37, 38). Zevalin (^{90}Y-labeled ibritumomab) and Bexxar (^{131}I-labeled tositumomab) are two examples of approved radioimmunotherapies for non-Hodgkin's lymphoma (35).Besides direct conjugation, antibodies can also be used to label nanoparticles loaded with drugs for targeted delivery. Such antibody-nanoparticle conjugates can potentially enable much higher drug to antibody ratios to maximize the drug concentration at the disease site. There are numerous active investigations using nanoparticles labeled with antibodies against various cell surface biomarkers, including Her2, EGFR, PSMA, etc (39).

All of these antibody-based, targeted therapies require a good understanding of the *in vivo* molecular status of the diseases, and this problem can be partly solved by one of the aforementioned antibody applications: antibody-based molecular imaging, such as immuno-positron emission tomography (immunoPET).

1.1.2 ImmunoPET

Traditional medical imaging has mostly been dominated by anatomy-based imaging such as computed tomography (CT) and magnetic resonance imaging (MRI). In order to conduct functional imaging to provide information on molecular targets and events, it is necessary to label biologically active molecules to generate detectable signals such as

near-infrared light or gamma-rays. In positron emission tomography (PET), the molecule of interest is labeled with a radionuclide that emits positrons. The emitted positron initially scatters in tissue until it collides with a nearby electron, leading to the annihilation that emits two 511 keV gamma-rays in opposite directions (~180°). The emitted photons are detected by a ring of scintillator crystals. The signals are then processed and reconstructed, resulting in a 3-D image showing the locations of all the annihilation events (Figure 1.3). PET is more sensitive than the earlier single-photon emission computed tomography (SPECT) by two to three orders of magnitude, and it also enables tracer quantitation at subnanomolar concentrations (40, 41). Combined with the anatomic information obtained from CT scans, PET can provide noninvasive and quantitative assessment of molecular status of numerous biological events in different organs and tissues.

The most widely used PET tracer today is the 2-[^{18}F] fluoro-2-deoxy-D-glucose (^{18}F-FDG). As a glucose analog, ^{18}F-FDG is transported into cells via the natural glucose transporters. Then ^{18}F-FDG is phosphorylated by hexokinase to form ^{18}F-FDG-6-phosphate; however it cannot serve as a substrate for subsequent glycolysis steps as can gluocose-6-phosphate, and is therefore retained in the cell in proportion to rate of glycolysis (42, 43). As a reflection of glucose metabolism, ^{18}F-FDG imaging is broadly used to monitor metabolic status of glucose-hungry organs such as brain and

heart, and it is also used to visualize tumors because of the increased glycolysis of tumors compared to normal tissue.

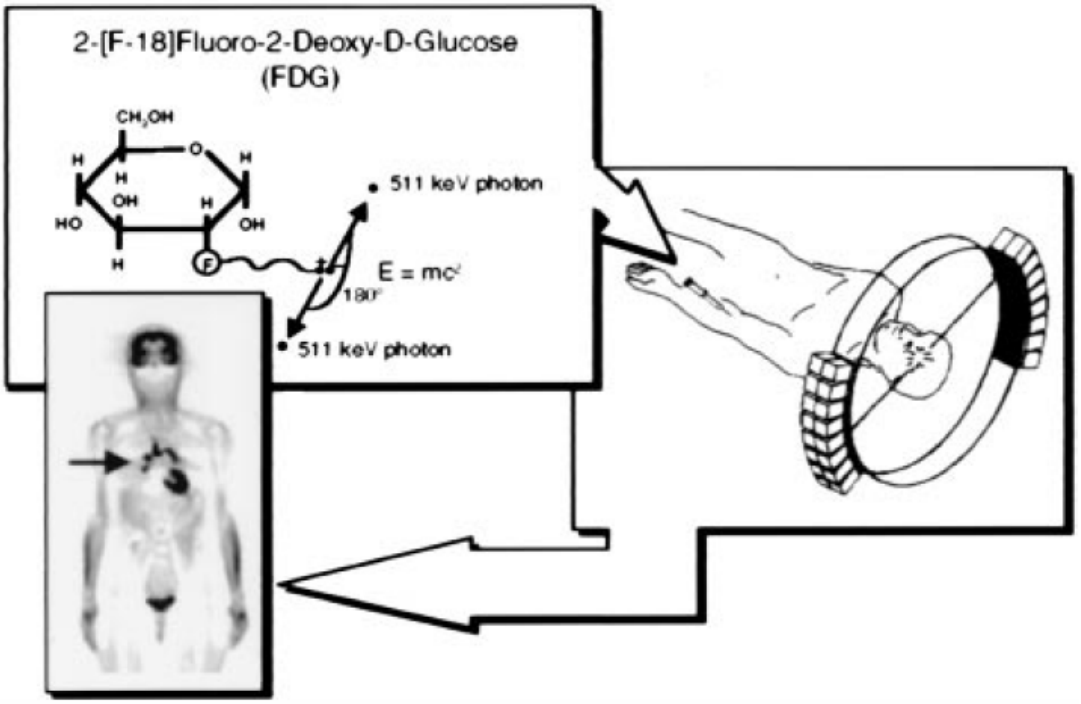

Figure 1.3: Principles of PET.
The molecule of interest labeled with a positron emitting radionuclide (18F-FDG is shown here as a example) is injected into a living subject. The positron emitted from the radionuclide (18F as shown here) travels a short distance before it collides and annihilates with a nearby electron. The annihilation results in two 511 keV photons (gamma-rays) traveling about 180°apart. The two photons are detected by the opposing detectors as a coincidence event, and the tomographic images are reconstructed according to the recorded signals. Adapted from Phelps, 2000, reference (44).

Researchers have developed many small molecule PET tracers that exploit different biological processes. For example, 3'-deoxy-3'-[^{18}F] fluorothymidine (^{18}F-FLT) is an analog of thymidine that can be used to examine thymidine transport and phosphorylation as a reflection of DNA synthesis(45). 1-(2-deoxy-2-[^{18}F] fluoro-arabinofuranosyl)-cytosine

(^{18}F-FAC) is a deoxycytidine analog that enables visualization of the salvage pathway for DNA synthesis that is extensively used in lymphoid organs, and can be used for imaging of immune activation (46). As there are more and more small molecule tracers being developed to help us understand intracellular activities, antibodies present themselves as very attractive PET tracers for molecular profiling of cell surface and extracellular biomarkers, leading to growing interest in the field of immuno-positron emission tomography (immunoPET).

Antibodies have been used for molecular profiling in *in vitro* diagnostic assays such as immunohistochemistry, immunofluorescence, flow cytometry, western blotting, and ELISAs for decades. Based on similar principles, they can also be used in PET scans to investigate *in vivo* molecular status. There are numerous important *in vivo* biomarkers that are accessible to radiolabeled antibody tracers, such as the classical tumor biomarkers such as carcinoembryonic antigen (CEA) (47), cell surface signaling receptors like human epidermal growth factor receptor 2 (HER2) (48) and hepatocyte growth factor receptor (HGFR, also known as MET) (14), cell- and tissue-specific markers such as CD8 (20), CD20 (49) and PSCA (prostate stem-cell antigen) (19). Quantitative evaluation of the *in vivo* expression level of these important markers can provide valuable information to help direct disease diagnosis and prognosis (40).

Compared to small molecule tracers, intact antibodies have longer biological half-lives, so their labeling require using radionuclides with similarly long half-lives, such as iodine-124 (^{124}I, $t_{1/2}$= 100.2 h), zirconium-89 (^{89}Zr, $t_{1/2}$= 78.4 h), copper-64 (^{64}Cu, $t_{1/2}$= 12.7 h) and yttrium-86 (^{86}Y, $t_{1/2}$= 14.7 h)(40). Another consideration regarding radiolabeling of antibodies is the choice between residualizing and non-residualizing radiolabeling. Non-residualizing labeling like direct iodination is excellent for producing high contrast, low background images for non-internalizing biomarkers, because all the non-bound tracers are eventually catabolized and secreted out of the body(40, 50). However, if the iodinated antibody tracer is rapidly internalized upon binding to the cell surface antigen, the intracellular catabolism and dehalogenation will result in the clearance of radioiodine, causing a loss of signal. In these cases, residualizing radiometal labeling (^{89}Zr, ^{64}Cu, etc) will be more suitable, because the internalized radioactive metabolites are trapped intracellularly, leading to accumulated signal over time. However, it will also increase the signals in the organs where the antibody tracers are metabolized (e.g. liver and kidney), because the radioactive metabolites are trapped there too (19, 40).

There are several successful examples of immunoPET in patients using radiolabeled intact antibodies. The ^{89}Zr-N-succinyldesferrioxamine (N-SucDf) –labeled chimeric antiCD44v6 U36 antibody was able to detect all primary tumors and detect metastatic lymph node levels with 72% sensitivity and 98% specificity in a study in 20 patients with squamous cell carcinoma of the head and neck (11, 40). ^{89}Zr-N-SucDf-labeled

trastuzumab also successfully detected most of the lesions in 14 patients with HER2-positive breast cancer (12, 40). ^{124}I-labeled anti-A33 antibody and ^{124}I-labeled anti-CA9 antibody also received promising results in colorectal cancer and clear cell carcinoma respectively (13, 40, 51-53). These successful studies definitely bring more optimism to the wider adoption of immunoPET in the future.

1.1.3 ImmunoPET using antibody fragments

Although antibodies have the unmatched flexibility and specificity in recognizing a broad spectrum of biomarkers, they also have a major drawback compared to the traditional small molecule PET tracers, namely, their long serum half-lives. While optimal images can be obtained within minutes or hours for most traditional small-molecule tracers, imaging using intact antibody tracers usually require several days of blood clearance before a PET scan can be acquired. This will lead to unnecessary radiation exposure to the patients and also increase the cost of care because of prolonged hospitalization. Preclinical studies have demonstrated that engineered antibody variants with shorter serum half-lives can enable immunoPET scans at earlier time points (15, 16, 40, 43, 54), which is desirable for clinical applications.

A single-chain variable fragment (scFv) is a small (25 -27 kDa) monovalent fragment consisting of the antibody V_H and V_L domains linked by a flexible linker. It has very rapid

blood clearance because of its small size and lack of interaction with the FcRn. Its reduced avidity limited its accumulation in the target tissue (40, 55), making it less attractive for general immunoPET applications. An scFv-Fc fragment (~110 kDa) is created when an scFv is fused to an Fc domain. The full Fc domain confers its interaction with the FcRn, leading to half-lives similar to intact antibodies. Furthermore, investigators have introduced mutations into the Fc region to tune its interaction with the FcRn, leading to scFv-Fc variants with shorter half-lives (56, 57). Deleting the C_H2 domain from the scFv-Fc fragment results in a smaller (~80 kDa) fragment called the minibody (scFv-C_H3). The interaction with the FcRn is abolished due to the deletion of C_H2 domain. This leads to terminal half-lives of 5 to 11 hours, which allows optimized immunoPET scans at 4-24 hours post injection (15, 19, 40). The smallest bivalent fragment, diabody (50-55 kDa), is created when the linker in a scFv is shortened (3 to 10 residues) to induce dimerization (58-61). The diabody fragment has a molecular weight below renal clearance threshold, so it is mainly cleared through kidneys, while larger fragments like minibodies are metabolized by liver. Diabodies also have very short half-lives of 3 to 7 hours, but the avidity effect causes higher uptake levels compared to scFvs (55), making them more favorable for rapid immunoPET imaging (15, 17, 48, 62). The structure and typical blood clearance curves of these popular antibody fragments are summarized in Figure 1.4 (40).

Although smaller antibody fragments have more favorable pharmacokinetic properties for immunoPET, they are more susceptible to losing immunoreactivity upon random labeling,

especially for diabodies. Therefore, C-terminal cysteines have been engineered into diabodies to create cys-diabodies for site-specific labeling using thiol-specific chemistry as shown in Figure 1.5 (18, 40, 63-65).

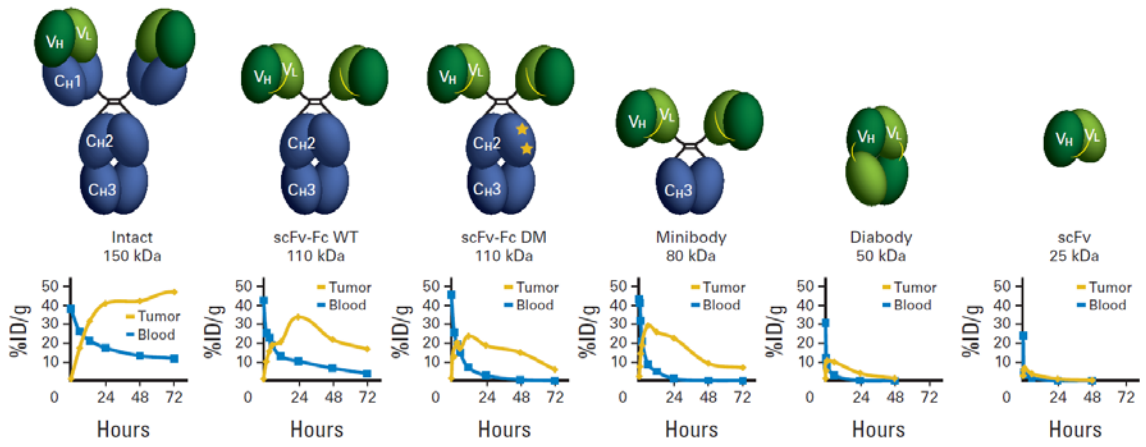

Figure 1.4: Antibody fragments with different serum half-lives.
The half-lives of antibody fragments can be modified by deleting domains or introduce mutations that change the interactions with the FcRn (scFv-Fc DM: scFv-Fc with H310A/H435Q double mutation). Different antibody fragments are optimized for imaging at different time points. Adapted from Knowles and Wu, 2012, reference (40).

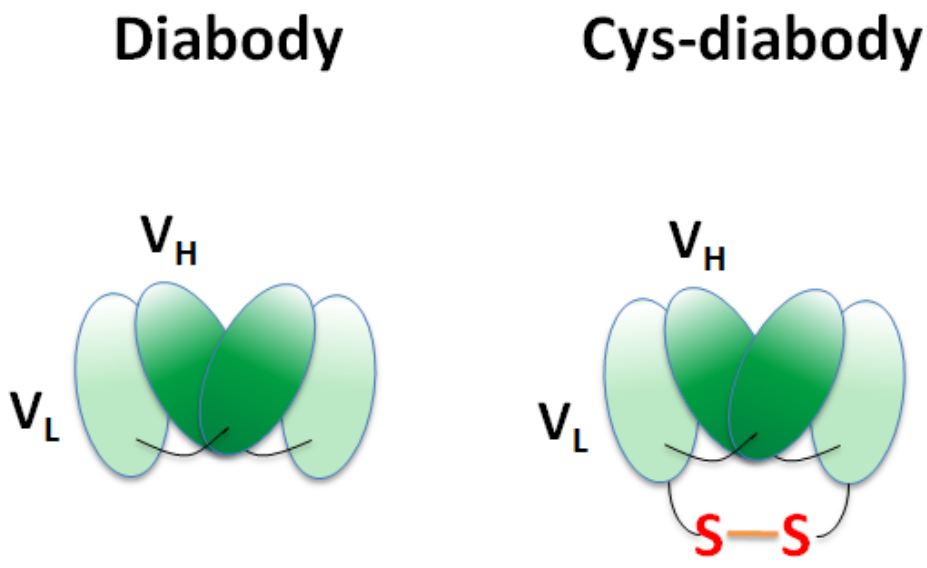

Figure 1.5: Diabody and cys-diabody.

The short half-lives of the antibody fragments also enable radiolabeling with short lived radionuclides such as ^{18}F. This will potentially further reduce the radiation exposure for patients in the clinic. The ^{18}F labeled diabodies have successfully produced high-contrast images in multiple murine xenograft models (62, 66, 67). However, considering the lower cost and easier handling, most preclinical immunoPET studies using antibody fragments still use radionuclides with longer half-lives (^{89}Zr, ^{124}I, etc) for routine labeling, but antibody probes can potentially benefit from the ^{18}F labeling at later stages of tracer development.

1.2 Phage display

Phage display is a technology that enables *in vitro* selection of proteins or polypeptides by fusing foreign gene sequences to the gene encoding bacteriophage coat proteins. Invented in 1980s, phage display technology demonstrated a new way for generating peptide affinity reagents *in vitro* by mimicking the selection strategies of the immune system (68-70). Soon after the invention of this technology, people found that some small antibody fragments like single chain variable fragment (scFv) and fragment antigen-binding (Fab) can also be properly displayed and selected (30, 71-74), leading to a revolutionary new route for antibody discovery and development. By cloning human antibody genes into the phage genome (75), it also enables the artificial selection of fully human antibodies that are greatly favored in clinical applications because of their

relatively lower risk of immunogenicity. Today, phage display technology has already become one of the major sources of fully human therapeutic antibodies and has led to therapeutics including Humira (adalimumab) and Benlysta (belimumab) (76). The principle of phage display library selections is illustrated in Figure 1.6.

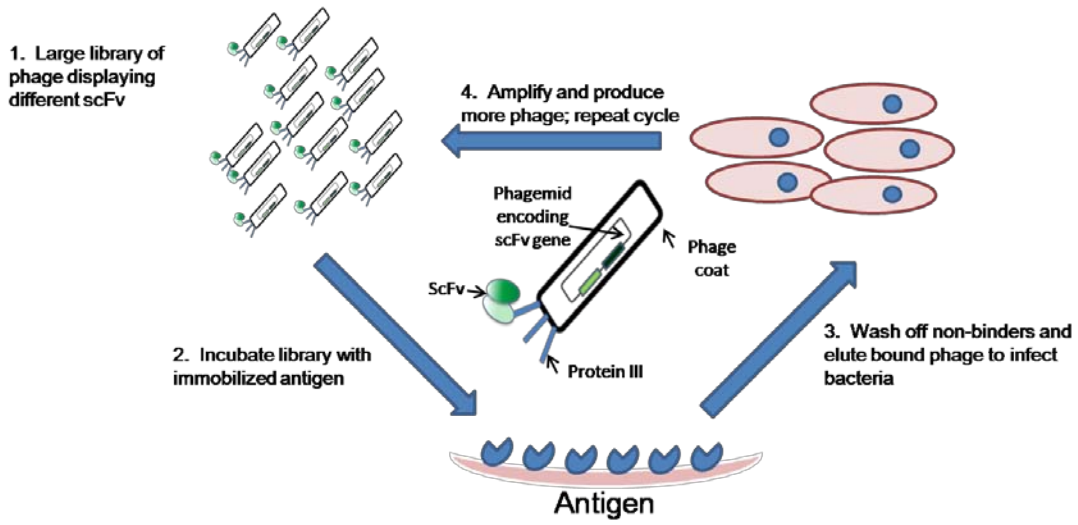

Figure 1.6: Principles of phage display library selections.

A small antibody fragment such as scFv is fused to the N-terminus of protein III of the M13 phage, and encoded in the phagemid. A large library of phage displaying numerous different scFvs is applied to the immobilized antigen. After washing off non-binders, the bound phage is eluted and used to infect bacteria and produce more phage for the next round of selection. Repeating the cycle for 3-4 times, and the binders will be enriched.

Besides intact full length antibodies, antibody fragments such as diabodies, minibodies and scFv-Fcs are also experiencing increasing interest for various *in vitro* and *in vivo* applications. While the small monovalent scFv and Fab are the preferred formats for phage display libraries (77, 78), researchers need to routinely reformat the selected scFv

and Fab into the aforementioned fragments or intact antibodies. Using the incorporated restriction sites in most phage display libraries, it is relatively easy to reformat a Fab into an intact antibody or reformat a scFv into a minibody or scFv-Fc by subcloning. However, reformatting a selected scFv into a diabody requires a reduction in the length of the polypeptide linker, which is usually done by the laborious and time consuming overlapping PCR (79). Being the smallest bivalent fragments, diabodies are easy to be produced in bacteria while still enjoy the benefit of bivalent avidity. Their small size and unique pharmacokinetic properties also make them attractive for nanoparticle labeling (80) and *in vivo* imaging (18, 62, 64, 79, 81). Therefore, a novel phage display library with specially designed restriction sites in the linker region that can be used for rapid and convenient linker shortening would greatly accelerate the development process of diabody fragments for various applications.

The other major means for generation of fully human antibody is through immunization of transgenic mice carrying human immunoglobulin genes (31, 32), this approach has also produced numerous therapeutic mAbs for clinical applications (33). However, compared to phage display technology, it is still less efficient and convenient for rapid generation of candidate antibody clones for large numbers of antigens (76). Furthermore, with carefully design of linkers and restriction sites, the antibody clones selected from a phage display library are more engineering-friendly, and can be easily reformatted to different antibody fragments (Figure 1.7 shows the streamlined development process of fully human

antibody fragments for immunoPET imaging using phage display technology). For this reason, phage display technology is a better choice for laboratories focusing on studies using fully human antibody fragments.

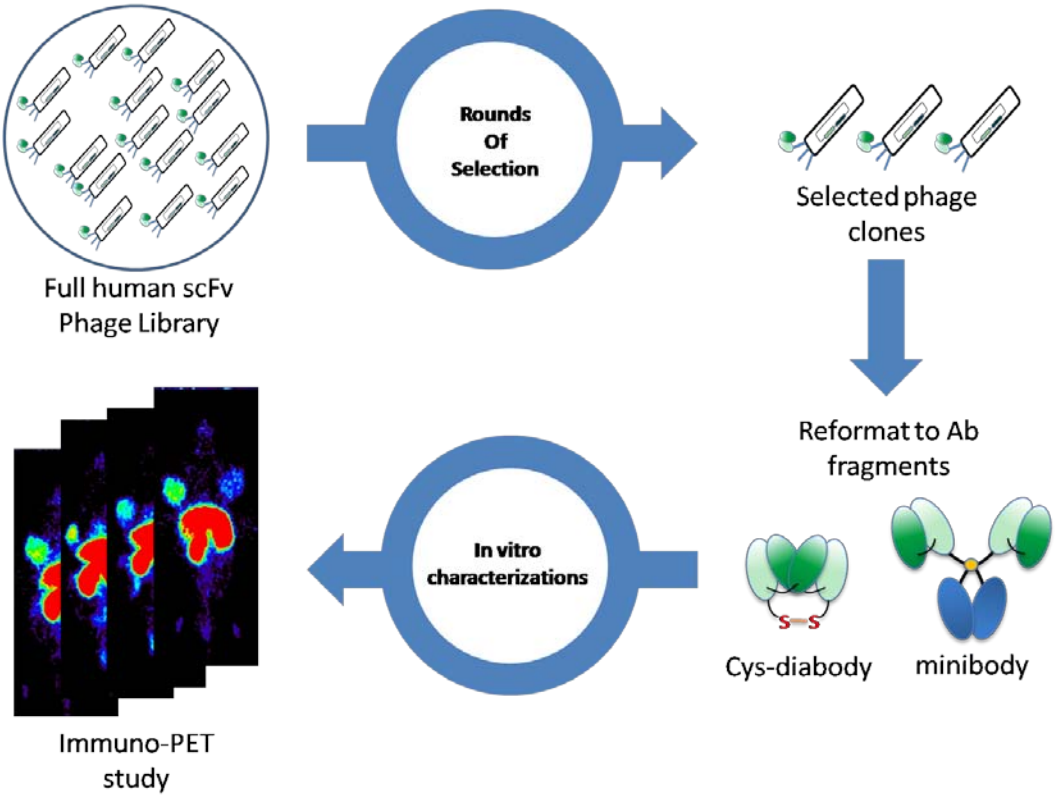

Figure 1.7: Streamlined development of immunoPET probes using a phage library.

1.3 MET and cancer

The MET oncogene was discovered in the mid-1980s, encoding a receptor tyrosine kinase with no known ligand at the time (82, 83). In 1991, the hepatocyte growth factor

(HGF, also known as scatter factor, SF) was found to be the ligand of MET receptor (84). The MET protein is composed of a short N-terminal α-chain and a long β-chain that are produced by proteolysis of a 1390-aa single-chain precursor (85). The mature protein has a N-terminal SEMA domain, a cysteine-rich domain, four immunoglobulin domains, transmembrane and juxtamembrane regions, and a kinase domain (86). The ligand, HGF consists of an N-terminal domain, four kringle domains, and a serine proteinase homology (SPH) domain. There are crystal structures available for several fragments and complexes, including the MET ectodomain binding to SPH domain or InlB (internalin B, a bacterial protein that is responsible for MET mediated bacterial internalization) (86-93).The structure of the MET and HGF proteins are depicted in Figure 1.8 (86). The binding of HGF induces the MET dimerization, causing the phosphorylation (Y1230, Y1234 and Y1235) and activation of the kinase domain, which in turn leads to the autophosphorylation of Y1349 and Y1356 in the C-terminal sequence, recruiting adaptor proteins including GAB1, Grb2, Src, etc. The subsequent downstream signaling is mainly mediated by the MAPK/Erk, Akt, Rap1 and Rac1-Cdc42 pathways, modulating cell survival, cell migration and cell adhesion (86). HGF-MET signaling is known to play crucial roles for embryonic survival, myogenic precursor cell migragion and liver growth during development (86, 94-97). It is also important for liver regeneration after partial hepatectomy (98-100) and wound repair in the skin, kidney, lung, skeletal muscle and heart in the adults (86, 101-104).

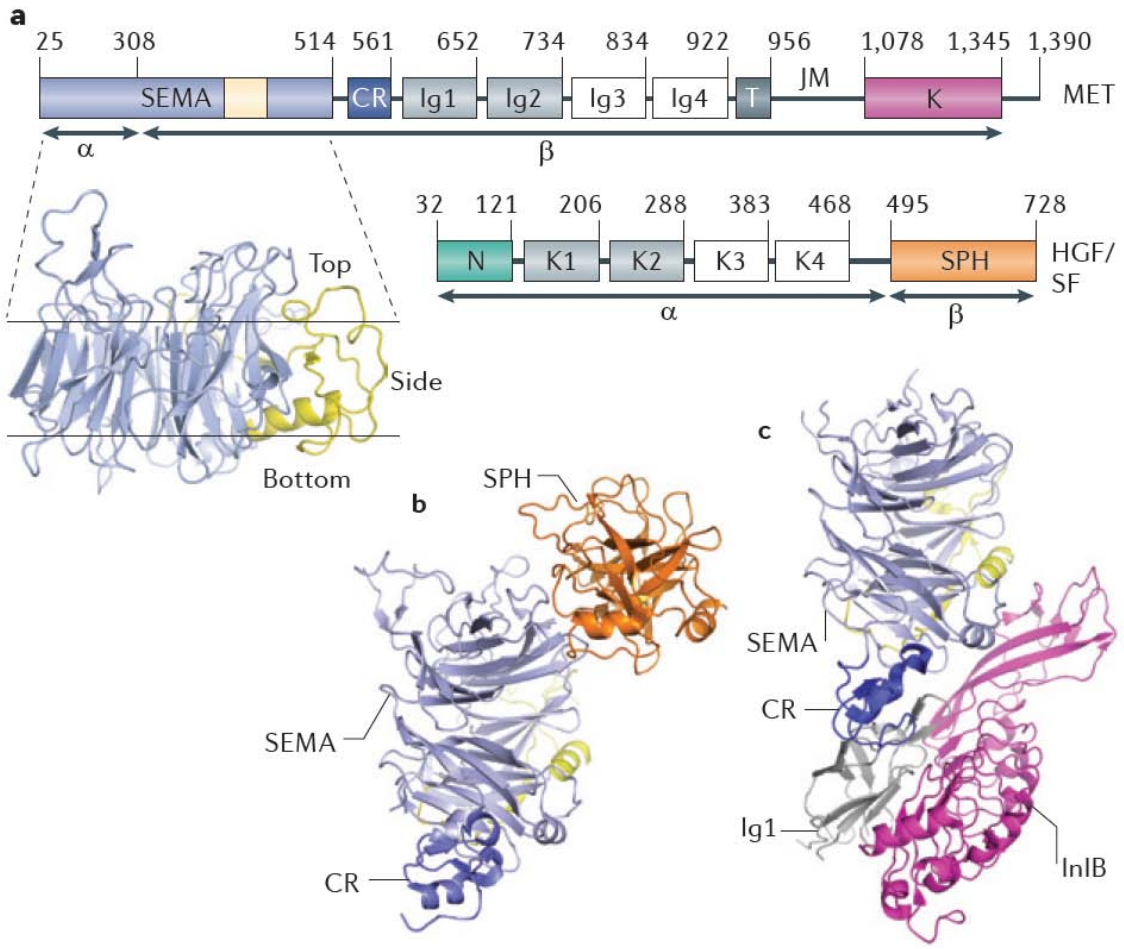

Figure 1.8: The multidomain structure of MET and HGF.

a. The MET protein is composed of an N-terminal SEMA domain, a cysteine-rich (CR) domain, a stalk structure formed with four immunoglobulin domains (Ig1-4), the transmembrane (T) and juxtamembrane (JM) sequences, the kinase(K) domain and the C-terminal sequence that involved in downstream signaling. HGF/SF is composed of the N-terminal (N) domain, four kringle domain (K1-4), and the serine proteinase homology (SPH) domain. **b.** The crystal structure showing SPH domain binding to the α-chain of MET. **c.** The crystal structure showing Internalin B binding to the Ig1 domain of MET. Adapted from Gherardi *et al.*, 2012, reference (86).

Because of its involvement in cell survival and motility (105), MET signaling is also a very important topic in cancer biology. Germline mutations in MET have been found in the patients with hereditary papillary renal carcinomas (106), strongly indicating a causal relationship between MET mutation and human cancer. Changes in HGF-MET signaling

have been found in numerous cancers summarized in the “HGF/SF-MET and cancer” online table (http://www.vai.org/Met/Index.aspx) (105). The role of HGF-MET signaling in metastasis has been demonstrated in murine models (86, 107-111). In the head and neck squamous-cell carcinoma patients, cancer cells expressing mutated MET are selected for as the lymphatic chain invading tumors, which suggests the relationship between MET signaling and cancer invasive growth (105, 112). MET amplification has also been found to be an important mechanism for acquired resistance to anti-EGFR therapies in non-small cell lung cancer through activation of ERBB3 (113, 114).

Because of the important roles of HGF-MET signaling in various cancers, many inhibitors targeting this pathway are currently being developed for clinical applications, including both small-molecule inhibitors and monoclonal antibodies (86). A humanized one-armed anti-MET antibody, onartuzumab (MetMAb), has been evaluated in clinical trials for advanced non-small cell lung cancer in combination with erlotinib. While patients with MET positive tumor benefited from such combination treatment, the MET negative patients actually had worse overall survival when treated with onartuzumab plus erlotinib, compared to with erlotinib plus placebo (115). Such results emphasize the importance of molecular profiling for this kind of targeted therapies.By providing *in vivo*, whole body information regarding the MET expression levels in both primary and metastatic tumors, immunoPET has the potential to greatly help patient stratification and improve the efficacy of MET targeted therapies.

Previously, anti-MET immunoPET imaging has been successfully demonstrated in preclinical mouse models using the intact monoclonal mouse antibody DN-30 or the humanized one-armed antibody onartuzumab (14, 116). However, these antibodies with full Fc domains require relatively long imaging delays (3 days to 1 week) to clear from the circulation in order to produce high contrast images. By using a fully human scFv phage display library, one can rapidly develop novel immunoPET probes using high-affinity, low-immunogenicity fully human antibody fragments with shorter serum half lives, such as diabodies and minibodies. Using these antibody fragment based probes, immunoPET can be performed at earlier time points with similar or even higher contrast, which is highly desired for clinical imaging applications (16, 34, 40, 43).

1.4 Biblography

1. Woof JM, Burton DR. Human antibody-Fc receptor interactions illuminated by crystal structures. Nature reviews Immunology. 2004;4:89-99.

2. Reichert JM, Rosensweig CJ, Faden LB, Dewitz MC. Monoclonal antibody successes in the clinic. Nature biotechnology. 2005;23:1073-8.

3. Sliwkowski MX, Mellman I. Antibody therapeutics in cancer. Science. 2013;341:1192-8.

4. Shakib F, Stanworth DR. Human IgG subclasses in health and disease. (A review). Part I. La Ricerca in clinica e in laboratorio. 1980;10:463-79.

5. Carter PJ. Potent antibody therapeutics by design. Nature reviews Immunology. 2006;6:343-57.

6. Chan AC, Carter PJ. Therapeutic antibodies for autoimmunity and inflammation. Nature reviews Immunology. 2010;10:301-16.

7. Alegre ML, Peterson LJ, Xu D, Sattar HA, Jeyarajah DR, Kowalkowski K, et al. A non-activating "humanized" anti-CD3 monoclonal antibody retains immunosuppressive properties *in vivo*. Transplantation. 1994;57:1537-43.

8. Woodle ES, Xu D, Zivin RA, Auger J, Charette J, O'Laughlin R, et al. Phase I trial of a humanized, Fc receptor nonbinding OKT3 antibody, huOKT3gamma1(Ala-Ala) in the treatment of acute renal allograft rejection. Transplantation. 1999;68:608-16.

9. Bolt S, Routledge E, Lloyd I, Chatenoud L, Pope H, Gorman SD, et al. The generation of a humanized, non-mitogenic CD3 monoclonal antibody which retains *in vitro* immunosuppressive properties. European journal of immunology. 1993;23:403-11.

10. Choy EH, Hazleman B, Smith M, Moss K, Lisi L, Scott DG, et al. Efficacy of a novel PEGylated humanized anti-TNF fragment (CDP870) in patients with rheumatoid arthritis: a phase II double-blinded, randomized, dose-escalating trial. Rheumatology (Oxford). 2002;41:1133-7.

11. Borjesson PK, Jauw YW, Boellaard R, de Bree R, Comans EF, Roos JC, et al. Performance of immuno-positron emission tomography with zirconium-89-labeled chimeric monoclonal antibody U36 in the detection of lymph node metastases in head and neck cancer patients. Clin Cancer Res. 2006;12:2133-40.

12. Dijkers EC, Oude Munnink TH, Kosterink JG, Brouwers AH, Jager PL, de Jong JR, et al. Biodistribution of 89Zr-trastuzumab and PET imaging of HER2-positive lesions in patients with metastatic breast cancer. Clinical pharmacology and therapeutics. 2010;87:586-92.

13. Carrasquillo JA, Pandit-Taskar N, O'Donoghue JA, Humm JL, Zanzonico P, Smith-Jones PM, et al. (124)I-huA33 antibody PET of colorectal cancer. Journal of nuclear medicine : official publication, Society of Nuclear Medicine. 2011;52:1173-80.

14. Perk LR, Stigter-van Walsum M, Visser GW, Kloet RW, Vosjan MJ, Leemans CR, et al. Quantitative PET imaging of Met-expressing human cancer xenografts with 89Zr-labelled monoclonal antibody DN30. Eur J Nucl Med Mol Imaging. 2008;35:1857-67.

15. Sundaresan G, Yazaki PJ, Shively JE, Finn RD, Larson SM, Raubitschek AA, et al. 124I-labeled engineered anti-CEA minibodies and diabodies allow high-contrast, antigen-specific small-animal PET imaging of xenografts in athymic mice. Journal of nuclear medicine : official publication, Society of Nuclear Medicine. 2003;44:1962-9.

16. Wu AM. Antibodies and antimatter: the resurgence of immuno-PET. Journal of nuclear medicine : official publication, Society of Nuclear Medicine. 2009;50:2-5.

17. Girgis MD, Kenanova V, Olafsen T, McCabe KE, Wu AM, Tomlinson JS. Anti-CA19-9 diabody as a PET imaging probe for pancreas cancer. The Journal of surgical research. 2011;170:169-78.

18. McCabe KE, Liu B, Marks JD, Tomlinson JS, Wu H, Wu AM. An engineered cysteine-modified diabody for imaging activated leukocyte cell adhesion molecule (ALCAM)-positive tumors. Molecular imaging and biology : MIB : the official publication of the Academy of Molecular Imaging. 2012;14:336-47.

19. Knowles SM, Zettlitz KA, Tavare R, Rochefort MM, Salazar FB, Stout DB, et al. Quantitative ImmunoPET of Prostate Cancer Xenografts with 89Zr- and 124I-Labeled Anti-PSCA A11 Minibody. Journal of nuclear medicine : official publication, Society of Nuclear Medicine. 2014.

20. Tavare R, McCracken MN, Zettlitz KA, Knowles SM, Salazar FB, Olafsen T, et al. Engineered antibody fragments for immuno-PET imaging of endogenous CD8+ T cells *in vivo*. Proc Natl Acad Sci U S A. 2014;111:1108-13.

21. Kohler G, Milstein C. Continuous cultures of fused cells secreting antibody of predefined specificity. Nature. 1975;256:495-7.

22. Lonberg N. Human antibodies from transgenic animals. Nature biotechnology. 2005;23:1117-25.

23. A randomized clinical trial of OKT3 monoclonal antibody for acute rejection of cadaveric renal transplants. Ortho Multicenter Transplant Study Group. The New England journal of medicine. 1985;313:337-42.

24. Kuus-Reichel K, Grauer LS, Karavodin LM, Knott C, Krusemeier M, Kay NE. Will immunogenicity limit the use, efficacy, and future development of therapeutic monoclonal antibodies? Clinical and diagnostic laboratory immunology. 1994;1:365-72.

25. Baert F, Noman M, Vermeire S, Van Assche G, G DH, Carbonez A, et al. Influence of immunogenicity on the long-term efficacy of infliximab in Crohn's disease. The New England journal of medicine. 2003;348:601-8.

26. Pendley C, Schantz A, Wagner C. Immunogenicity of therapeutic monoclonal antibodies. Current opinion in molecular therapeutics. 2003;5:172-9.

27. Jones PT, Dear PH, Foote J, Neuberger MS, Winter G. Replacing the complementarity-determining regions in a human antibody with those from a mouse. Nature. 1986;321:522-5.

28. Cole SP, Campling BG, Atlaw T, Kozbor D, Roder JC. Human monoclonal antibodies. Molecular and cellular biochemistry. 1984;62:109-20.

29. Carson DA, Freimark BD. Human lymphocyte hybridomas and monoclonal antibodies. Advances in immunology. 1986;38:275-311.

30. McCafferty J, Griffiths AD, Winter G, Chiswell DJ. Phage antibodies: filamentous phage displaying antibody variable domains. Nature. 1990;348:552-4.

31. Green LL, Hardy MC, Maynard-Currie CE, Tsuda H, Louie DM, Mendez MJ, et al. Antigen-specific human monoclonal antibodies from mice engineered with human Ig heavy and light chain YACs. Nature genetics. 1994;7:13-21.

32. Lonberg N, Taylor LD, Harding FA, Trounstine M, Higgins KM, Schramm SR, et al. Antigen-specific human antibodies from mice comprising four distinct genetic modifications. Nature. 1994;368:856-9.

33. Nelson AL, Dhimolea E, Reichert JM. Development trends for human monoclonal antibody therapeutics. Nature reviews Drug discovery. 2010;9:767-74.

34. Wu AM, Senter PD. Arming antibodies: prospects and challenges for immunoconjugates. Nature biotechnology. 2005;23:1137-46.

35. Steiner M, Neri D. Antibody-radionuclide conjugates for cancer therapy: historical considerations and new trends. Clinical cancer research : an official journal of the American Association for Cancer Research. 2011;17:6406-16.

36. Sievers EL, Senter PD. Antibody-drug conjugates in cancer therapy. Annual review of medicine. 2013;64:15-29.

37. Francisco JA, Cerveny CG, Meyer DL, Mixan BJ, Klussman K, Chace DF, et al. cAC10-vcMMAE, an anti-CD30-monomethyl auristatin E conjugate with potent and selective antitumor activity. Blood. 2003;102:1458-65.

38. Katz J, Janik JE, Younes A. Brentuximab Vedotin (SGN-35). Clinical cancer research : an official journal

of the American Association for Cancer Research. 2011;17:6428-36.

39. Fay F, Scott CJ. Antibody-targeted nanoparticles for cancer therapy. Immunotherapy. 2011;3:381-94.

40. Knowles SM, Wu AM. Advances in immuno-positron emission tomography: antibodies for molecular imaging in oncology. Journal of clinical oncology : official journal of the American Society of Clinical Oncology. 2012;30:3884-92.

41. Rahmim A, Zaidi H. PET versus SPECT: strengths, limitations and challenges. Nuclear medicine communications. 2008;29:193-207.

42. Phelps ME. Positron emission tomography provides molecular imaging of biological processes. Proceedings of the National Academy of Sciences of the United States of America. 2000;97:9226-33.

43. Gambhir SS. Molecular imaging of cancer with positron emission tomography. Nature reviews Cancer. 2002;2:683-93.

44. Phelps ME. PET: the merging of biology and imaging into molecular imaging. Journal of nuclear medicine : official publication, Society of Nuclear Medicine. 2000;41:661-81.

45. Shields AF, Grierson JR, Dohmen BM, Machulla HJ, Stayanoff JC, Lawhorn-Crews JM, et al. Imaging proliferation *in vivo* with [F-18]FLT and positron emission tomography. Nature medicine. 1998;4:1334-6.

46. Radu CG, Shu CJ, Nair-Gill E, Shelly SM, Barrio JR, Satyamurthy N, et al. Molecular imaging of lymphoid organs and immune activation by positron emission tomography with a new [18F]-labeled 2'-deoxycytidine analog. Nature medicine. 2008;14:783-8.

47. Hong H, Sun J, Cai W. Radionuclide-Based Cancer Imaging Targeting the Carcinoembryonic Antigen. Biomarker insights. 2008;3:435-51.

48. Robinson MK, Doss M, Shaller C, Narayanan D, Marks JD, Adler LP, et al. Quantitative immuno-positron emission tomography imaging of HER2-positive tumor xenografts with an iodine-124 labeled anti-HER2 diabody. Cancer Res. 2005;65:1471-8.

49. Olafsen T, Betting D, Kenanova VE, Salazar FB, Clarke P, Said J, et al. Recombinant anti-CD20 antibody fragments for small-animal PET imaging of B-cell lymphomas. Journal of nuclear medicine : official publication, Society of Nuclear Medicine. 2009;50:1500-8.

50. Nayak TK, Brechbiel MW. Radioimmunoimaging with longer-lived positron-emitting radionuclides: potentials and challenges. Bioconjugate chemistry. 2009;20:825-41.

51. O'Donoghue JA, Smith-Jones PM, Humm JL, Ruan S, Pryma DA, Jungbluth AA, et al. 124I-huA33 antibody uptake is driven by A33 antigen concentration in tissues from colorectal cancer patients imaged by immuno-PET. Journal of nuclear medicine : official publication, Society of Nuclear Medicine.

2011;52:1878-85.

52. Divgi CR, Pandit-Taskar N, Jungbluth AA, Reuter VE, Gonen M, Ruan S, et al. Preoperative characterisation of clear-cell renal carcinoma using iodine-124-labelled antibody chimeric G250 (124I-cG250) and PET in patients with renal masses: a phase I trial. The lancet oncology. 2007;8:304-10.

53. Pryma DA, O'Donoghue JA, Humm JL, Jungbluth AA, Old LJ, Larson SM, et al. Correlation of *in vivo* and *in vitro* measures of carbonic anhydrase IX antigen expression in renal masses using antibody 124I-cG250. Journal of nuclear medicine : official publication, Society of Nuclear Medicine. 2011;52:535-40.

54. Wu AM, Yazaki PJ, Tsai S, Nguyen K, Anderson AL, McCarthy DW, et al. High-resolution microPET imaging of carcinoembryonic antigen-positive xenografts by using a copper-64-labeled engineered antibody fragment. Proc Natl Acad Sci U S A. 2000;97:8495-500.

55. Adams GP, Tai MS, McCartney JE, Marks JD, Stafford WF, 3rd, Houston LL, et al. Avidity-mediated enhancement of *in vivo* tumor targeting by single-chain Fv dimers. Clin Cancer Res. 2006;12:1599-605.

56. Kenanova V, Olafsen T, Crow DM, Sundaresan G, Subbarayan M, Carter NH, et al. Tailoring the pharmacokinetics and positron emission tomography imaging properties of anti-carcinoembryonic antigen single-chain Fv-Fc antibody fragments. Cancer research. 2005;65:622-31.

57. Olafsen T, Kenanova VE, Wu AM. Tunable pharmacokinetics: modifying the *in vivo* half-life of antibodies by directed mutagenesis of the Fc fragment. Nature protocols. 2006;1:2048-60.

58. Hudson PJ, Kortt AA. High avidity scFv multimers; diabodies and triabodies. Journal of immunological methods. 1999;231:177-89.

59. Holliger P, Prospero T, Winter G. "Diabodies": small bivalent and bispecific antibody fragments. Proceedings of the National Academy of Sciences of the United States of America. 1993;90:6444-8.

60. Kortt AA, Lah M, Oddie GW, Gruen CL, Burns JE, Pearce LA, et al. Single-chain Fv fragments of anti-neuraminidase antibody NC10 containing five- and ten-residue linkers form dimers and with zero-residue linker a trimer. Protein engineering. 1997;10:423-33.

61. Atwell JL, Breheney KA, Lawrence LJ, McCoy AJ, Kortt AA, Hudson PJ. scFv multimers of the anti-neuraminidase antibody NC10: length of the linker between VH and VL domains dictates precisely the transition between diabodies and triabodies. Protein engineering. 1999;12:597-604.

62. Olafsen T, Sirk SJ, Olma S, Shen CK, Wu AM. ImmunoPET using engineered antibody fragments: fluorine-18 labeled diabodies for same-day imaging. Tumour biology : the journal of the International Society for Oncodevelopmental Biology and Medicine. 2012;33:669-77.

63. Li L, Olafsen T, Anderson AL, Wu A, Raubitschek AA, Shively JE. Reduction of kidney uptake in

radiometal labeled peptide linkers conjugated to recombinant antibody fragments. Site-specific conjugation of DOTA-peptides to a Cys-diabody. Bioconjugate chemistry. 2002;13:985-95.

64. Girgis MD, Federman N, Rochefort MM, McCabe KE, Wu AM, Nagy JO, et al. An engineered anti-CA19-9 cys-diabody for positron emission tomography imaging of pancreatic cancer and targeting of polymerized liposomal nanoparticles. The Journal of surgical research. 2013;185:45-55.

65. Olafsen T, Cheung CW, Yazaki PJ, Li L, Sundaresan G, Gambhir SS, et al. Covalent disulfide-linked anti-CEA diabody allows site-specific conjugation and radiolabeling for tumor targeting applications. Protein engineering, design & selection : PEDS. 2004;17:21-7.

66. Cai W, Olafsen T, Zhang X, Cao Q, Gambhir SS, Williams LE, et al. PET imaging of colorectal cancer in xenograft-bearing mice by use of an 18F-labeled T84.66 anti-carcinoembryonic antigen diabody. Journal of nuclear medicine : official publication, Society of Nuclear Medicine. 2007;48:304-10.

67. Liu K, Lepin EJ, Wang MW, Guo F, Lin WY, Chen YC, et al. Microfluidic-based 18F-labeling of biomolecules for immuno-positron emission tomography. Molecular imaging. 2011;10:168-76, 1-7.

68. Cwirla SE, Peters EA, Barrett RW, Dower WJ. Peptides on phage: a vast library of peptides for identifying ligands. Proceedings of the National Academy of Sciences of the United States of America. 1990;87:6378-82.

69. Parmley SF, Smith GP. Antibody-selectable filamentous fd phage vectors: affinity purification of target genes. Gene. 1988;73:305-18.

70. Smith GP. Filamentous fusion phage: novel expression vectors that display cloned antigens on the virion surface. Science. 1985;228:1315-7.

71. Hoogenboom HR, Griffiths AD, Johnson KS, Chiswell DJ, Hudson P, Winter G. Multi-subunit proteins on the surface of filamentous phage: methodologies for displaying antibody (Fab) heavy and light chains. Nucleic acids research. 1991;19:4133-7.

72. Barbas CF, 3rd, Kang AS, Lerner RA, Benkovic SJ. Assembly of combinatorial antibody libraries on phage surfaces: the gene III site. Proceedings of the National Academy of Sciences of the United States of America. 1991;88:7978-82.

73. Garrard LJ, Yang M, O'Connell MP, Kelley RF, Henner DJ. Fab assembly and enrichment in a monovalent phage display system. Biotechnology (N Y). 1991;9:1373-7.

74. Breitling F, Dubel S, Seehaus T, Klewinghaus I, Little M. A surface expression vector for antibody screening. Gene. 1991;104:147-53.

75. Marks JD, Hoogenboom HR, Bonnert TP, McCafferty J, Griffiths AD, Winter G. By-passing immunization. Human antibodies from V-gene libraries displayed on phage. Journal of molecular biology.

1991;222:581-97.

76. Schirrmann T, Meyer T, Schutte M, Frenzel A, Hust M. Phage display for the generation of antibodies for proteome research, diagnostics and therapy. Molecules. 2011;16:412-26.

77. de Haard HJ, van Neer N, Reurs A, Hufton SE, Roovers RC, Henderikx P, et al. A large non-immunized human Fab fragment phage library that permits rapid isolation and kinetic analysis of high affinity antibodies. The Journal of biological chemistry. 1999;274:18218-30.

78. Sheets MD, Amersdorfer P, Finnern R, Sargent P, Lindquist E, Schier R, et al. Efficient construction of a large nonimmune phage antibody library: the production of high-affinity human single-chain antibodies to protein antigens. Proceedings of the National Academy of Sciences of the United States of America. 1998;95:6157-62.

79. Shimazaki K, Lepin EJ, Wei B, Nagy AK, Coulam CP, Mareninov S, et al. Diabodies targeting epithelial membrane protein 2 reduce tumorigenicity of human endometrial cancer cell lines. Clin Cancer Res. 2008;14:7367-77.

80. Barat B, Sirk SJ, McCabe KE, Li J, Lepin EJ, Remenyi R, et al. Cys-diabody quantum dot conjugates (immunoQdots) for cancer marker detection. Bioconjugate chemistry. 2009;20:1474-81.

81. Sirk SJ, Olafsen T, Barat B, Bauer KB, Wu AM. Site-specific, thiol-mediated conjugation of fluorescent probes to cysteine-modified diabodies targeting CD20 or HER2. Bioconjugate chemistry. 2008;19:2527-34.

82. Cooper CS, Park M, Blair DG, Tainsky MA, Huebner K, Croce CM, et al. Molecular cloning of a new transforming gene from a chemically transformed human cell line. Nature. 1984;311:29-33.

83. Park M, Dean M, Cooper CS, Schmidt M, O'Brien SJ, Blair DG, et al. Mechanism of met oncogene activation. Cell. 1986;45:895-904.

84. Bottaro DP, Rubin JS, Faletto DL, Chan AM, Kmiecik TE, Vande Woude GF, et al. Identification of the hepatocyte growth factor receptor as the c-met proto-oncogene product. Science. 1991;251:802-4.

85. Komada M, Hatsuzawa K, Shibamoto S, Ito F, Nakayama K, Kitamura N. Proteolytic processing of the hepatocyte growth factor/scatter factor receptor by furin. FEBS letters. 1993;328:25-9.

86. Gherardi E, Birchmeier W, Birchmeier C, Vande Woude G. Targeting MET in cancer: rationale and progress. Nature reviews Cancer. 2012;12:89-103.

87. Chirgadze DY, Hepple JP, Zhou H, Byrd RA, Blundell TL, Gherardi E. Crystal structure of the NK1 fragment of HGF/SF suggests a novel mode for growth factor dimerization and receptor binding. Nature structural biology. 1999;6:72-9.

88. Ultsch M, Lokker NA, Godowski PJ, de Vos AM. Crystal structure of the NK1 fragment of human

hepatocyte growth factor at 2.0 A resolution. Structure. 1998;6:1383-93.

89. Tolbert WD, Daugherty-Holtrop J, Gherardi E, Vande Woude G, Xu HE. Structural basis for agonism and antagonism of hepatocyte growth factor. Proc Natl Acad Sci U S A. 2010;107:13264-9.

90. Stamos J, Lazarus RA, Yao X, Kirchhofer D, Wiesmann C. Crystal structure of the HGF beta-chain in complex with the Sema domain of the Met receptor. The EMBO journal. 2004;23:2325-35.

91. Niemann HH, Jager V, Butler PJ, van den Heuvel J, Schmidt S, Ferraris D, et al. Structure of the human receptor tyrosine kinase met in complex with the Listeria invasion protein InlB. Cell. 2007;130:235-46.

92. Schiering N, Knapp S, Marconi M, Flocco MM, Cui J, Perego R, et al. Crystal structure of the tyrosine kinase domain of the hepatocyte growth factor receptor c-Met and its complex with the microbial alkaloid K-252a. Proc Natl Acad Sci U S A. 2003;100:12654-9.

93. Gherardi E, Sandin S, Petoukhov MV, Finch J, Youles ME, Ofverstedt LG, et al. Structural basis of hepatocyte growth factor/scatter factor and MET signalling. Proc Natl Acad Sci U S A. 2006;103:4046-51.

94. Birchmeier C, Birchmeier W, Gherardi E, Vande Woude GF. Met, metastasis, motility and more. Nature reviews Molecular cell biology. 2003;4:915-25.

95. Schmidt C, Bladt F, Goedecke S, Brinkmann V, Zschiesche W, Sharpe M, et al. Scatter factor/hepatocyte growth factor is essential for liver development. Nature. 1995;373:699-702.

96. Uehara Y, Minowa O, Mori C, Shiota K, Kuno J, Noda T, et al. Placental defect and embryonic lethality in mice lacking hepatocyte growth factor/scatter factor. Nature. 1995;373:702-5.

97. Bladt F, Riethmacher D, Isenmann S, Aguzzi A, Birchmeier C. Essential role for the c-met receptor in the migration of myogenic precursor cells into the limb bud. Nature. 1995;376:768-71.

98. Michalopoulos GK, DeFrances MC. Liver regeneration. Science. 1997;276:60-6.

99. Borowiak M, Garratt AN, Wustefeld T, Strehle M, Trautwein C, Birchmeier C. Met provides essential signals for liver regeneration. Proc Natl Acad Sci U S A. 2004;101:10608-13.

100. Huh CG, Factor VM, Sanchez A, Uchida K, Conner EA, Thorgeirsson SS. Hepatocyte growth factor/c-met signaling pathway is required for efficient liver regeneration and repair. Proc Natl Acad Sci U S A. 2004;101:4477-82.

101. Huelsken J, Vogel R, Erdmann B, Cotsarelis G, Birchmeier W. beta-Catenin controls hair follicle morphogenesis and stem cell differentiation in the skin. Cell. 2001;105:533-45.

102. Snippert HJ, Haegebarth A, Kasper M, Jaks V, van Es JH, Barker N, et al. Lgr6 marks stem cells in the hair follicle that generate all cell lineages of the skin. Science. 2010;327:1385-9.

103. Chmielowiec J, Borowiak M, Morkel M, Stradal T, Munz B, Werner S, et al. c-Met is essential for wound healing in the skin. The Journal of cell biology. 2007;177:151-62.

104. Nakamura T, Mizuno S, Matsumoto K, Sawa Y, Matsuda H. Myocardial protection from ischemia/reperfusion injury by endogenous and exogenous HGF. J Clin Invest. 2000;106:1511-9.

105. Boccaccio C, Comoglio PM. Invasive growth: a MET-driven genetic programme for cancer and stem cells. Nature reviews Cancer. 2006;6:637-45.

106. Schmidt L, Duh FM, Chen F, Kishida T, Glenn G, Choyke P, et al. Germline and somatic mutations in the tyrosine kinase domain of the MET proto-oncogene in papillary renal carcinomas. Nature genetics. 1997;16:68-73.

107. Rong S, Segal S, Anver M, Resau JH, Vande Woude GF. Invasiveness and metastasis of NIH 3T3 cells induced by Met-hepatocyte growth factor/scatter factor autocrine stimulation. Proc Natl Acad Sci U S A. 1994;91:4731-5.

108. Meiners S, Brinkmann V, Naundorf H, Birchmeier W. Role of morphogenetic factors in metastasis of mammary carcinoma cells. Oncogene. 1998;16:9-20.

109. Gallego MI, Bierie B, Hennighausen L. Targeted expression of HGF/SF in mouse mammary epithelium leads to metastatic adenosquamous carcinomas through the activation of multiple signal transduction pathways. Oncogene. 2003;22:8498-508.

110. Jeffers M, Fiscella M, Webb CP, Anver M, Koochekpour S, Vande Woude GF. The mutationally activated Met receptor mediates motility and metastasis. Proc Natl Acad Sci U S A. 1998;95:14417-22.

111. Moshitch-Moshkovitz S, Tsarfaty G, Kaufman DW, Stein GY, Shichrur K, Solomon E, et al. *In vivo* direct molecular imaging of early tumorigenesis and malignant progression induced by transgenic expression of GFP-Met. Neoplasia. 2006;8:353-63.

112. Di Renzo MF, Olivero M, Martone T, Maffe A, Maggiora P, Stefani AD, et al. Somatic mutations of the MET oncogene are selected during metastatic spread of human HNSC carcinomas. Oncogene. 2000;19:1547-55.

113. Engelman JA, Zejnullahu K, Mitsudomi T, Song Y, Hyland C, Park JO, et al. MET amplification leads to gefitinib resistance in lung cancer by activating ERBB3 signaling. Science. 2007;316:1039-43.

114. Zucali PA, Ruiz MG, Giovannetti E, Destro A, Varella-Garcia M, Floor K, et al. Role of cMET expression in non-small-cell lung cancer patients treated with EGFR tyrosine kinase inhibitors. Annals of oncology : official journal of the European Society for Medical Oncology / ESMO. 2008;19:1605-12.

115. Surati M, Patel P, Peterson A, Salgia R. Role of MetMAb (OA-5D5) in c-MET active lung malignancies. Expert opinion on biological therapy. 2011;11:1655-62.

116. Jagoda EM, Lang L, Bhadrasetty V, Histed S, Williams M, Kramer-Marek G, et al. Immuno-PET of the hepatocyte growth factor receptor Met using the 1-armed antibody onartuzumab. Journal of nuclear medicine : official publication, Society of Nuclear Medicine. 2012;53:1592-600.

Chapter 2: Anti-MET antibody selection and *in vitro* characterization

2.1 Introduction

MET, the receptor of the hepatocyte growth factor (HGF), plays important roles in embryonic development, wound repair and tumorigenesis. Because of its importance in various cancers, more and more MET inhibitors are being developed for clinical applications (1).In non-small cell lung cancer, MET amplification has been found to be an important mechanism for acquired resistance to anti-EGFR therapies (gefitinib, erlotinib, etc), and the recent MET-targeted clinical trial using onartuzumab (MetMab) in combination with erlotinib got strikingly different responses from MET positive and MET negative tumors (2). This further emphasizes the importance of molecular profiling for MET targeted therapies, showing a strong need for diagnostic tools for *in vivo* MET expression level evaluation.

Antibody fragment based immuno-positron emission tomography (immunoPET) has the potential to rapidly quantify *in vivo* MET expression levels for drug response evaluation and patient stratification. Phage display technology provides a robust approach to rapidly generate fully human antibody fragments. There are already successful examples of using phage library derived antibody fragments for

immunoPET imaging (3-5). To generate novel fully human anti-MET antibody fragments, we performed the selection using a large naïve human scFv phage display library constructed by Sheets *et al.* (6). This library contains 6.7 x 10^9 members, and it has previously yielded high affinity scFv clones against various targets with dissociation constants as low as 0.2 nM (6-8). Three rounds of panning were performed on immobilized recombinant human MET protein, and 93 random phage clones were tested for binding by phage ELISA. Positive clones were sequenced, and binding to native cell surface antigen was confirmed by phage flow cytometry. Considering the benefit of site-specific labeling and the relatively easy expression in bacteria, phage clones were first reformatted into cys-diabodies for *in vitro* characterization. The cys-diabodies were also used to treat different cell lines with or without gefitinib and erlotinib, in order to evaluate their biological activities. Initial downstream signaling analysis was performed by western blot. The minibody and scFv-Fc version of one of the clones (H2) were also produced and analyzed.

2.2 Materials and Methods

2.2.1 Cell lines

Hcc827 parental cells and the gefitinib resistant Hcc827-GR6 cells were obtained from Jeffrey A. Engelman's laboratory (Massachusetts General Hospital) (9). Hcc827-/+ cells (provided by Drs. Shannon Mumenthaler and Parag Mallick, USC and Stanford) were derived from Hcc827 cells by 15 days of treatment with 50 ng/mL HGF

and 1 μM erlotinib (LC Laboratories)(replenished every 3 days). H1975 and H1650 cells were obtained from ATCC (American Type Culture Collection). All these cell lines were maintained with RPMI 1640 media (Cellgro) supplemented with 10% FBS (fetal bovine serum, Gemini), 1mM sodium pyruvate (Cellgro) and 1% penicillin-streptomycin (Gibco). The Hcc827-GR6 media was also supplemented with 100nM gefitinib (Santa Cruz biotechnology), and Hcc827-/+ cells were maintained with 1 μM erlotinib. All cell cultures and incubation were performed at 37°C with 5% CO_2 unless otherwise stated.

2.2.2 Phage library selection

A naïve human scFv phage display library from James D. Marks' laboratory (UCSF) (6) was used to perform three rounds of selection against recombinant human MET protein using previously published methods(10). Briefly, for the first round, 100μg of recombinant MET protein (R&D Systems, 358-MT/CF) in 2 mL PBS was used to coat an immunotube (Nunc) overnight at 4°C. After washing with PBS and blocking with 2% milk-PBS (non fat dry milk, Bio-rad, #170-6404), the immunotube was washed with PBS 3 times and then incubated with 10^{12}~10^{13} phage in 2mL 1% milk-PBS for 2 hours at room temperature. After washing with PBS twice, the bound phage were eluted with 1mL of 100mM triethylamine for 8 minutes and neutralized with 0.5mL of 1M Tris-HCl (pH = 7.5). Half of the eluted phage were used to infect 10mL exponentially growing *E. coli* TG1, and then plated on 2YT plates with 100μg/mL

ampicillin and 2% glucose. Colonies were scraped from the plates after overnight culture, and then used to produce phage for the next round of selection. Reduced amounts of MET protein from another supplier (Sino Biological Inc., 10692-H08H) and multiple washes using 0.05% PBS-Tween and PBS were used for the following 2 rounds to increase the stringency of selection.

2.2.3 Phage ELISA

Antibody-displaying phage were expressed from 93 clones from the 3rd round of selection as previously described(10). 50μL of supernatant of the overnight culture was used for the ELISA (helper phage that displays no scFv was used for negative controls). 0.5μg of human MET protein in 0.1 mL PBS was used to coat each well. Blocking, washing and phage incubations were conducted as previously described (10). 100μL of 1:2000 diluted HRP conjugated anti-M13 antibody (GE Healthcare, Cat#: 27-9421-01) was added to each well and incubated for 1 hour. After washing with PBS-Tween and PBS 3 times, the plate was incubated with 100μL per well of 0.1mg/mL ABTS substrate solution (Sigma, A9941, dissolved in 0.05M phosphate-citrate buffer, pH = 5.0; 1/1000 of 50% $H_2O_2$was added before use) at room temperature for 10 to 30 minutes before reading A_{405}. The 64 clones with the highest positive signals were subjected to DNA sequencing.

2.2.4 Flow cytometry

For the standard anti-MET flow cytometry, murine anti-human MET antibody (Cell Signaling Technology, #5631) was used for primary incubation and FITC or PE conjugated goat anti-mouse IgG (Jackson ImmunoResearch) was used for secondary incubation. To determine the copy number of MET protein per cell, quantitative flow was performed using QIFIKIT (Dako, K0078) according to the recommended protocol.

For phage flow cytometry, 30X concentrated phage were incubated with cells in flow buffer (PBS / 1% FBS / 2 mM EDTA) with 4% milk on ice for 1 hour. After washing 3 times with flow buffer, FITC conjugated anti-M13 antibody (Santa Cruz Biotech, sc-53005 FITC) was added to detect the phage.

2.2.5 Expression and purification of cys-diabody, minibody and scFv

The scFv clones with 15-residue linkers (GGGGSGGGGSGGGGS) from the phage library were converted into cys-diabodies by shortening the linker to 6-residue (GGGGGS) via overlap extension PCR. The PCR product was then cloned into a modified pSYN1 vector, pSYN1-cys, using the NcoI and NotI restriction sites. The original pSYN1 vector (11, 12) has built-in Myc tag and 6-his tag at the downstream of the NotI site. A C-terminal cysteine was engineered into the vector via isothermal DNA assembly (13) to generate the pSYN1-cys vector for cys-diabody production. Therefore, after cloning into the pSYN1-cys vector, the diabody clones are fused to a

C-terminal sequence containing Myc tag, 6-his tag, and a cysteine residue (AAAEQKLISEEDLNGAAHHHHHHC, “AAA” is the NotI site). The constructs were then transformed into chemical competent TG1 bacteria (Zymo Research) for protein production. Briefly, the bacteria were inoculated into 2YT medium with 100 μg/mL ampicillin and 0.1% glucose, and then grown at 37 °C with shaking (300 rpm) until A_{600}=0.9. Then the protein expression was induced with 0.5mM IPTG (Isopropyl β-D-1-thiogalactopyranoside) at 20 °C with shaking (300 rpm). The next day, the bacteria cells were pelleted and the expressed cys-diabody was released from bacteria by sonication or BugBuster (Novagen) treatment. After centrifugation, the supernatant containing antibody fragments was filtered and loaded to the HisTrap HP column (GE Healthcare). The column was then washed with the washing buffer (30 mM imidazole, 500 mM NaCl, 50 mM sodium phosphate buffer, pH = 7.4), and the gradient elution was carried out to recover the bound antibody fragments. The fractions containing the antibody fragments were identified by SDS-PAGE and combined for dialysis to PBS. The protein samples were concentrated, filtered and then stored at 4 °C. H2 scFv with a 17-residue linker (GGSTGGGSGGGGSTGAP, refer to chapter 4 for the generation of this 17aa-SSA linker) was cloned into the original pSYN1 vector to fused to C-terminal Myc tag and 6-his tag, and the scFv protein was produced and purified using the similar method.

The H2 scFv (with the original 15-residue linker) was also converted into a minibody or a scFv-Fc by subcloning the scFv into pSecTag2 vectors (Life Technologies)

containing a human IgG1 C_H3 domain or a mouse IgG2a Fc domain (vectors modified and provided by Dr. Kirstin Anja Zettlitz). The minibody and scFv-Fc constructs were transfected into human 293F cells (Gibco) for antibody production. The transfected cells were maintained with DMEM media supplemented with 10% FBS, 1% non-essential amino acids (Cellgro) and selected with Zeocin (Life Technologies). The cells were then expanded into triple flasks (Corning). The medium was changed to serum free Opti-MEM (Life Technologies) after the cells reached confluency for protein production. The minibody and scFv-Fc proteins were purified from the supernatant by protein A affinity chromatography. Briefly, the concentrated supernatant was filtered and loaded to the protein A column. The column was washed with PBS. Gradient elution using 0.2M citric acid was carried out to recover the bound antibody fragments. Each 1 mL fraction was neutralized with 0.3 mL of 1M Tris (pH8.2). The fractions containing the antibody fragments were identified by SDS-PAGE and combined for dialysis to PBS. The protein samples were concentrated, filtered and then stored at 4 °C.

Protein concentrations were calculated according to the extinction coefficient and the absorbance at 280 nm (the extinction coefficient was calculated using online tools: http://web.expasy.org/protparam/).

2.2.6 Affinity determination by flow cytometry

Serial diluted cys-diabodies were incubated with 1 x 10^5 Hcc827-GR6 cells at 4°C for 2 hours, then cells were quickly washed with flow buffer and incubated on ice with excess mouse anti-MYC IgG for 20 minutes, and washed again before a final incubation on ice with excess PE-conjugated goat anti-mouse IgG. Mean fluorescence intensities (MFI) at different concentrations were calculated using FlowJo software, and the binding curves were analyzed using Graphpad Prism to calculate dissociation constants using the “one site-specific binding” model.

2.2.7 ELISA to test cross reactivity

1µg of purified anti-MET cys-diabodies in 100µL PBS were used to coat each well at 4°C overnight. Anti-EpCAM cys-diabody or 2% milk-PBS were used for negative controls. The overnight coated plate was then washed with PBS and blocked with 2% milk-PBS. The plate was then washed with PBS before adding 0.1µg human or mouse MET-hIgG Fc fusion protein (Sino Biological Inc.) in 100µL 2% milk-PBS to each well. After 1.5 hours of incubation at room temperature, the plate was washed with PBS-Tween and PBS. The captured human or mouse MET-hIgG Fc were detected with alkaline phosphatase conjugated goat anti-human IgG (Jackson ImmunoResearch). Each combination was done in triplicate.

2.2.8 *In vitro* MTS assay

Cell growth and inhibition were evaluated by MTS assay using the CellTiter96 AQueous Assay Kit from Promega (Cat#: G5421), according to the recommended protocol. 1 x 10^4 cells were seeded in each well of the 96-well plates and treated with different combination of antibodies and drugs for 3 days before the MTS assay. Each combination of cell line and drug and antibody treatment was evaluated in at least triplicate wells. The results were normalized to the cells treated with medium only.

2.2.9 Signaling analysis using Western blot

Hcc827 or Hcc827-GR6 cells were seeded in to 6-well plates (10^6 cells per well) and cultured overnight with serum free RPMI 1640 media (Cellgro) supplemented with 1mMsodium pyruvate (Cellgro) and 1% penicillin-streptomycin (Gibco). The next day, the medium was changed to fresh medium with serum (RPMI 1640 media / 10% FBS / 1mM sodium pyruvate / 1% penicillin-streptomycin) and the cells were treated with anti-MET antibody fragments or the MET inhibitor PHA665752 in combination with gefitinib for 6 hours. After incubation, the medium was discarded and cells were washed with PBS (2mL per well). 200 µL modified RIPA buffer (10 mM β-glycerophosphate / 1 mM EDTA / 1 mM Vanadate / 1 mM NaF / 1% NP-40 / 0.25% sodium deoxycolate / 150mM NaCl / 50 mM Tris-HCl, pH 7.4; 1/2 tablet of Roche Complete protease inhibitor was dissolved in 25 mL buffer) was added to each well, and the cells were incubated on ice for 15 min with occasional mixing. The cell debris

and the buffer were then collected into Eppendorf tubes and incubated on ice for another 10 min prior to micro-centrifugation (14,000g) at 4°C for 1 min. 20 µL of the supernatant (lysate) from each sample were used for polyacrylamide gel electrophoresis (PAGE) and then transferred to nitrocellulose membranes (0.2 µm pore size, Biorad) for western blot analysis.

Primary antibodies used for the western blot were anti-phospho-MET (Tyr1234/1235) (D26) rabbit mAb (Cell Signaling, #3077P), anti-phospho-p44/42 MAPK (Erk 1/2) (Thr202/Tyr204) (D13.14.4E) rabbit mAb (Cell Signaling, #4370), anti-phospho-Akt (Ser473) (D9E) rabbit mAb (Cell Signaling, #4060) and Mouse anti-human-β-actin mAb. The rabbit or mouse primary antibodies were detected with fluorescent labeled seconday antibodies (IRDye 680 Goat anti-Rabbit IgG, and IRDye 800 Goat anti-Mouse IgG from LI-COR) and scanned with the Odyssey infrared imaging system from LI-COR.

2.3 Results

2.3.1 Anti-MET phage selection and screening

Three rounds of selection were performed on immobilized recombinant MET protein; the details of each round are summarized in Table 2.1. MET-human IgG Fc fusion protein from R&D was used for the first round, and MET protein from Sino Biological was used for the second and third rounds. Only two PBS washes were performed in

round 1, in order to retain more of the positive clones, to allow amplification and enrichment in the subsequent rounds. As the washing stringencies were greatly increased in round 2 and round 3, the number of output phage and the output / input ratios both decreased compared to the first round.

Table 2.1: Results of phage library selection on human MET protein.

	Antigen and washes	Phage input	Phage output	Output / input ratio
Round 1	100 µg MET-Fc (R&D), 2 PBS washes	6.8×10^{12}	3.6×10^{8}	5.3×10^{-5}
Round 2	30 µg MET (Sino Bio), 30 min of PBS-Tween incubation + 4 PBS washes	2.0×10^{13}	7.0×10^{6}	3.5×10^{-7}
Round 3	20 µg MET (Sino Bio), 30 min of PBS-Tween incubation + 30 min of PBS incubation + 9 PBS washes	1.0×10^{14}	5.0×10^{6}	5.0×10^{-8}

Following the selections, 93 clones were randomly picked and their binding to MET protein was evaluated via phage ELISA. The absorbance signal is shown in Table 2.2, where the numbers are the A_{405} values for the corresponding wells on a 96-well plate; the wells are color coded according to the signal strength. Note that F12, G12 and H12 are negative controls using helper phage that displays no scFv.

The clones were ranked according to the ELISA signal and DNA sequencing results of the top 64 clones revealed 19 distinct functional sequences. The representative clones and the number of repeats are summarized in Figure 2.1. As shown here,

among the top 64 positive clones, 8 distinct sequences have two or more duplicated clones, and 11 sequences have only one copy each. This indicates the pool of anti-MET phage clones is still highly diversified after 3 rounds of selection.

Table 2.2: Phage ELISA results (A_{405}) of 93 random Anti-MET phage clones.

<>	1	2	3	4	5	6	7	8	9	10	11	12
A	0.1924	0.4359	0.0521	0.4477	0.1402	0.2917	0.2291	0.2798	0.1702	0.1793	0.2520	0.4693
B	0.0613	0.2803	0.0523	0.1366	0.1516	0.1707	0.0570	0.2321	0.0560	0.0544	0.1787	0.2576
C	0.3452	0.1784	0.0520	0.2599	0.0545	0.1563	0.1718	0.1641	0.1854	0.0593	0.1983	0.1947
D	0.0578	0.1781	0.1589	0.1906	0.1476	0.1640	0.1647	0.1622	0.1686	0.0521	0.1811	0.3060
E	0.0579	0.1382	0.1620	0.0582	0.1687	0.1871	0.1530	0.1635	0.1623	0.1620	0.2141	0.1768
F	0.3066	0.1898	0.1560	0.1623	0.0859	0.1744	0.1798	0.1641	0.1940	0.1692	0.1922	0.0587
G	0.1436	0.1426	0.1382	0.1472	0.2450	0.0613	0.0733	0.0680	0.1714	0.1899	0.1550	0.0535
H	0.1766	0.2393	0.2399	0.1941	0.2035	0.0578	0.0563	0.1260	0.2173	0.1841	0.2288	0.0545

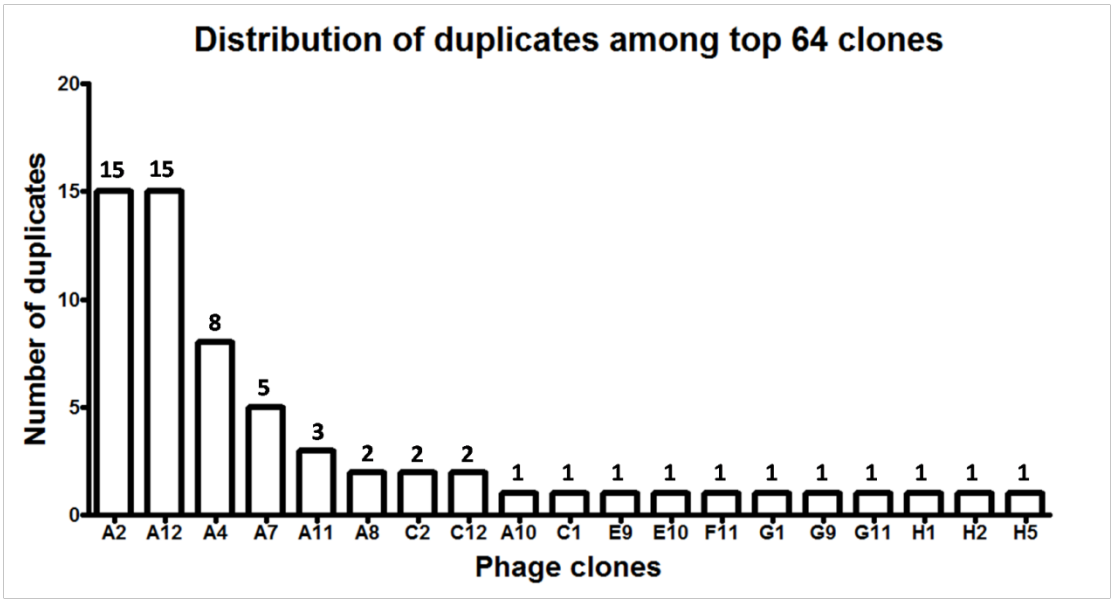

Figure 2.1: Distribution of duplicates among top 64 clones.
Following 3 rounds of anti-MET selection, clones were ranked based on binding to MET protein via phage ELISA. DNA sequencing results of the top 64 clones reveal 19 distinct functional sequences, 8 of which have two or more duplicates while 11 clones have only one copy each.

Determined by quantitative flow, Hcc827-GR6 cell line has 2.6 x 10^5 cell surface MET per cell while the parental Hcc827 cell line has 6.7 x 10^4 per cell. To further confirm binding to the native cell surface antigen, all 19 phage clones were incubated with MET positive Hcc827-GR6 cells and analyzed by flow cytometry in three separate experiments, as summarized in Figure 2.2. According to the binding profiles in flow analysis, nine of the clones (A2, A12, C1, C2, E9, F11, G1, H2 and H5) were chosen for subsequent studies.

These clones were reformatted into cys-diabodies by shortening the 15-residue linker to 6-residue linker and incorporation of C-terminal tags (see Materials and Methods). Three of the cys-diabody clones, C2, H2 and H5, were successfully expressed, purified (yields ranging from 1 – 3 mg/L) and characterized further. Other clones were dropped because of low expression levels and purities. As expected, C2, H2 and H5 cys-diabodies all migrated as covalent dimers under non-reducing conditions, but as monomers under reducing conditions (Figure 2.3).

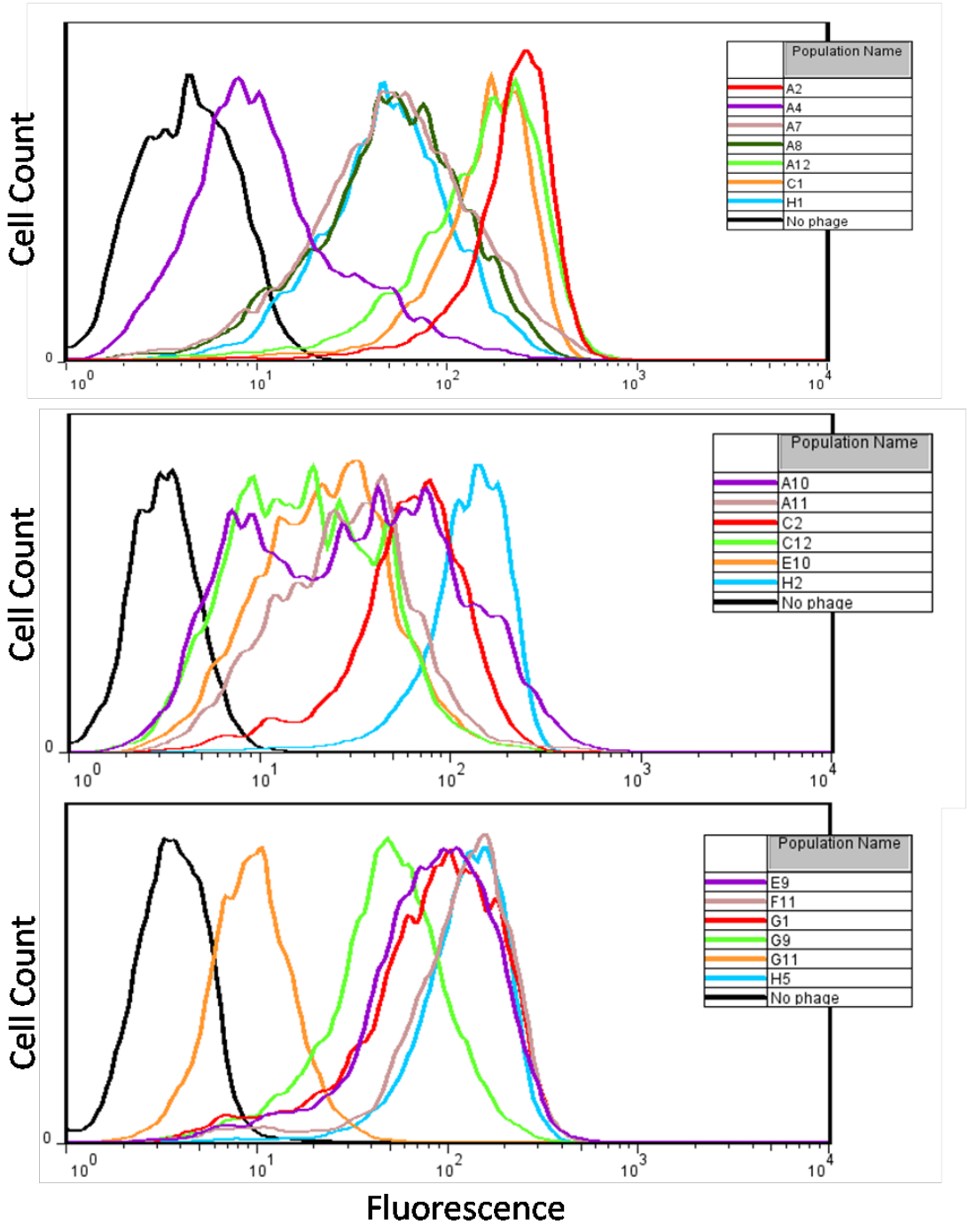

Figure 2.2: Anti-MET phage flow cytometry results.

19 distinct anti-MET phage clones were analyzed by phage flow cytometry using Hcc827-GR6 cells. According to the binding profiles in flow analysis, nine of the clones (A2, A12, C1, C2, E9, F11, G1, H2 and H5) were chosen for subsequent studies.

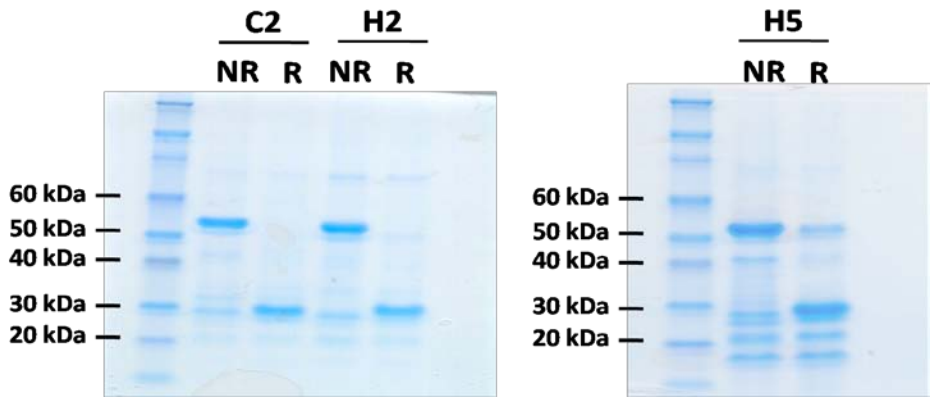

Figure 2.3: SDS-PAGE of Anti-MET C2, H2 and H5 cys-diabodies.
SDS-PAGE of purified Anti-MET C2, H2 and H5 under non-reducing (NR) and reducing conditions. The non-reduced cys-diabodies migrated as covalent dimers (approximately 55 kDa), and the reduced cys-diabodies migrated as monomers (approximately 27 kDa). 2 µg of C2 and H2 cys-diabodies were loaded to each lane, while 4 µg of H5 cys-diabody was to for each lane.

2.3.2 *In vitro* characterization of cys-diabodies

The purified C2, H2 and H5 cys-diabodies retained the ability to bind to MET positive cells. The affinities were estimated by flow cytometry. Binding curves on Hcc827-GR6 showed H2 cys-diabody has the highest binding affinity (K_D = 0.73 ± 0.10 nM), while the other two cys-diabodies also have low nanomolar affinities (C2 cys-diabody: K_D=2.4 ± 0.2 nM; H5 cys-diabody: K_D =5.1 ± 0.5 nM) as shown in Figure 2.4.

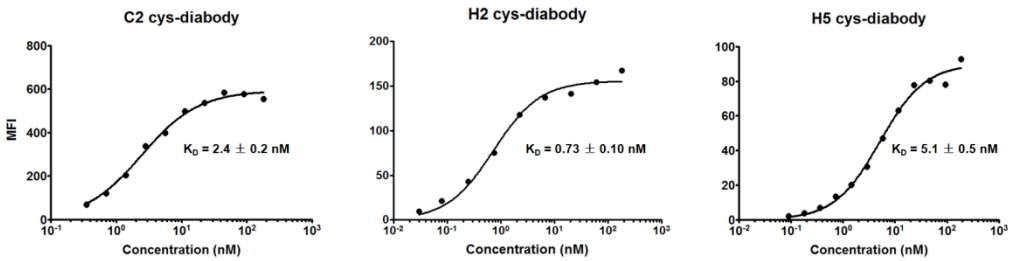

Figure 2.4: Affinity determination of anti-MET cys-diabodies by flow cytometry.
Purified anti-MET C2, H2 and H5 cys-diabodies were incubated with the MET positive Hcc827-GR6 cells to determine their affinities. The binding curves were analyzed using Graphpad Prism to calculate dissociation constants using the "one site-specific binding" model.

To determine their cross reactivities to mouse MET protein, the cys-diabodies were also tested for the ability to capture human and mouse MET protein by ELISA. The results showed that the H2 cys-diabody clearly bound to both human and mouse MET, while C2 and H5 have no significant cross reactivity to the mouse MET (Figure 2.5).

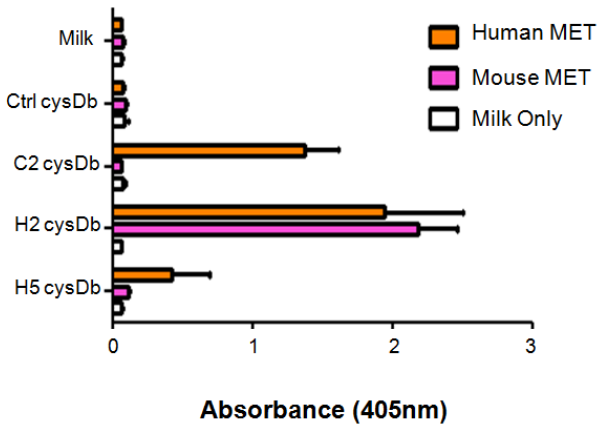

Figure 2.5: Cross reactivity analysis of anti-MET cys-diabodies.
Binding of C2, H2 and H5 cys-diabodies (cysDb) to immobilized human and mouse MET in ELISA. Only the H2 cys-diabody showed cross-reactivity, while C2 and H5 bind to human MET exclusively. Non-specific cysDb (ctrl cysDb) and secondary Ab only were included as controls.

2.3.3 Cell growth inhibition assays

The cys-diabodies were also tested for their effects on the growth of cell cultures *in vitro*. To assess off-target toxicity, first, the parental Hcc827 cells were treated with cys-diabodies alone for 3 days in culture medium. No significant effects were observed for all 3 cys-diabodies at up to 180 nM concentration (Figure 2.6A). Next, the cys-diabodies were used to treat two gefitinib resistant cell lines lacking MET amplification, H1650 and H1975, in combination with gefitinib. No significant inhibitory effects were observed on these two cell lines (Figure 2.6B).

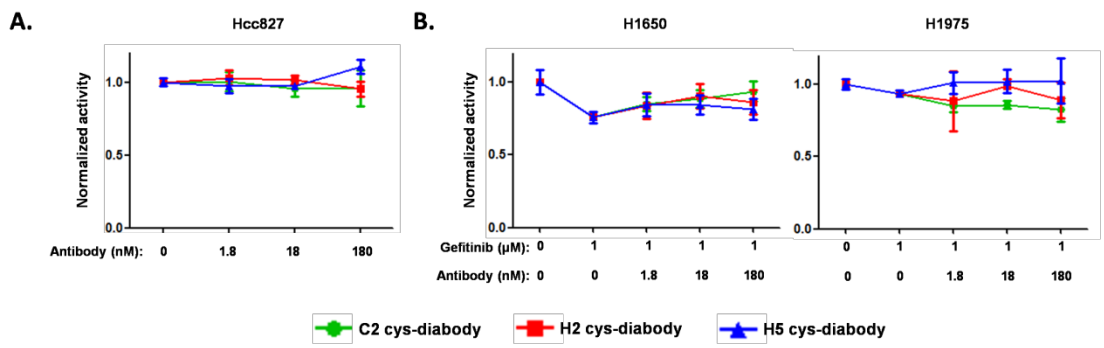

Figure 2.6: *In vitro* MTS assays to evaluate the off target toxicity of the cys-diabodies.
Different cell lines were treated with combinations of anti-MET antibody fragments (1.8 – 180 nM) and gefitinib (1 μM) for 3 days as indicated. Cell viability was assessed by MTS assay and normalized to untreated cells. **A.** Hcc827 parental cell line treated with cys-diabodies. **B.** Two gefitinib-resistant cell lines without MET amplification (H1650 and H1975) treated with the cys-diabodies in combination with gefitinib.

The anti-MET inhibitory effects were tested by applying these cys-diabodies to two cell lines with amplified MET signaling, Hcc827-GR6 and Hcc827-/+. The Hcc827-GR6 cell line was generated through prolonged selection from the parental Hcc827 treated with gefitinib (9). The Hcc827-/+ cells were obtained by short-term treatment of Hcc827 with HGF and erlotinib (see Materials and Methods). The cells

were treated with different concentrations of cys-diabodies in combination with either gefitinib (Figure 2.7A) or erlotinib (Figure 2.7B) for 3 days before MTS assays. The results are similar regardless of which anti-EGFR drug was used, both showing H2 has the strongest inhibitory effect at lowest concentration, while C2 has little or no inhibitory effect.

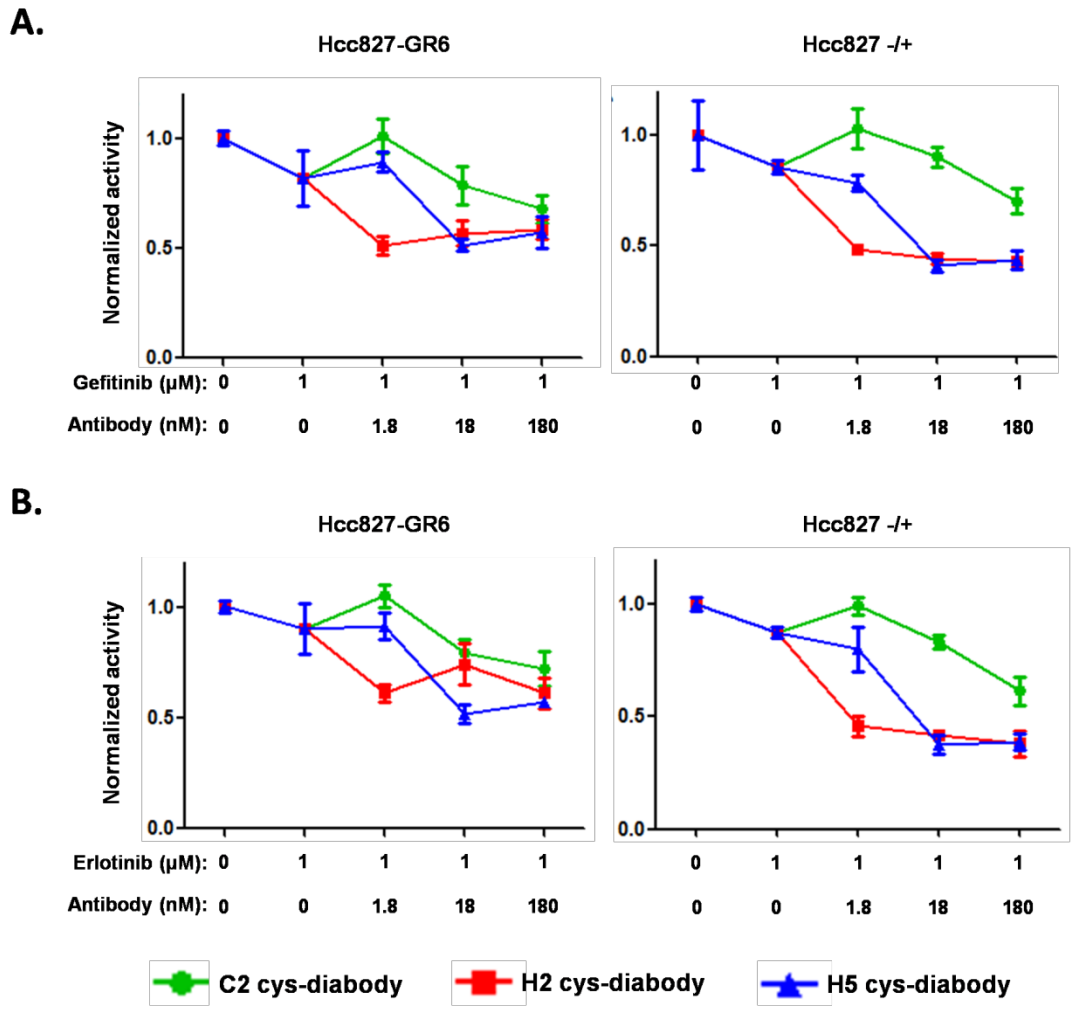

Figure 2.7: Anti-MET cys-diabodies inhibit growth of MET dependent cells.

Two cell lines with amplified MET signal, Hcc827-GR6 and Hcc827-/+ cells, were treated with combinations of anti-MET antibody fragments (1.8 – 180 nM) and **A.**gefitinib (1 μM) or **B.**erlotinib (1 μM) for 3 days as indicated. Cell viability was assessed by MTS assay and normalized to untreated cells.H2 showed the strongest inhibitory effect at lowest concentration.

Because of the high affinity and inhibitory effect of H2 cys-diabody, we further reformatted H2 into scFv, minibody (with human IgG1 C_H3 domain) and scFv-Fc (with mouse IgG2a Fc domain). Their inhibitory effects on Hcc827-GR6 were tested in two separate experiments, with one comparing scFv, minibody and cys-diabody, the other comparing scFv-Fc, minibody and cys-diabody. Interestingly, cys-diabody and minibody both show similar inhibitory effects while scFv and scFv-Fc both failed to inhibit the cell growth (Figure 2.8).

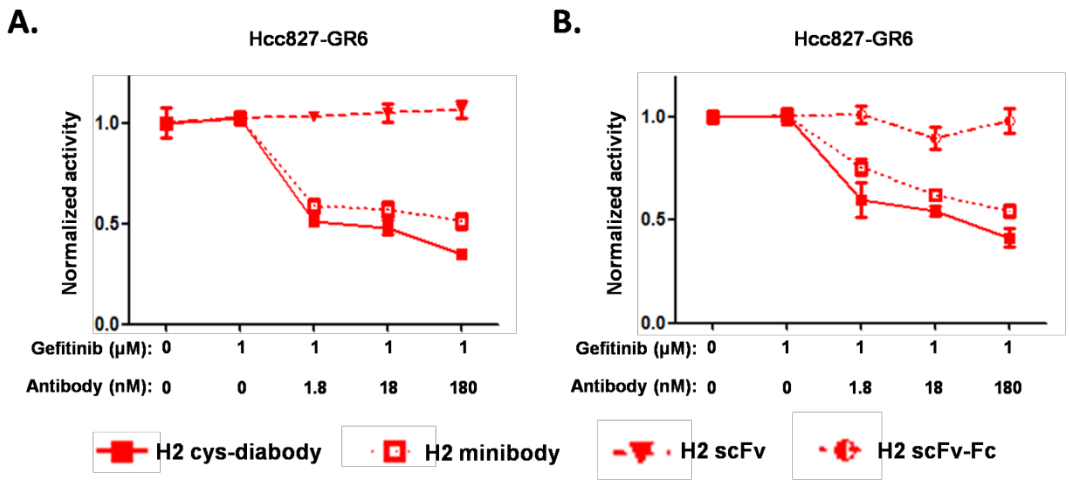

Figure 2.8: Effects of anti-MET H2 Ab fragments on the growth of Hcc827-GR6.
Hcc827-GR6 wastreated with combinations of anti-MET antibody fragments (1.8 – 180 nM) and gefitinib (1 μM) for 3 days as indicated. Cell viability was assessed by MTS assay and normalized to untreated cells.**A.** One experiment compared scFv, minibody and cys-diabody.**B.**Another experiment compared scFv-Fc, minibody and cys-diabody. The cys-diabody and minibody showed similar inhibitory effects.

2.3.4 Downstream signaling analysis using Western blot

Given the fact that H2 cys-diabody can inhibit the growth of MET dependent cell lines, we evaluated the changes in downstream signaling in Hcc827-GR6 and Hcc827upon

treatment of H2 antibody fragments. First the effects of cys-diabody (cysDb) and scFv were compared, in order to determine whether bivalent binding is essential for any change in downstream signaling. In the Hcc827-GR6 cells, the small molecule MET inhibitor PHA665752 can abolish the phospho-MET signal and most of the downstream phospho-Akt (p-Akt) and phospho-Erk (p-Erk) signal. The H2 cys-diabody had no significant effect on the MET phosphorylation, but it reduced the downstream p-Akt and p-Erk signaling. In contrast, H2 scFv had no effect. These results suggest the bivalent binding is required for down regulating p-Akt and p-Erk signaling (Figure 2.9A). However, the Hcc827 parental cells are dependent on EGFR signaling, and the treatment of H2 antibody fragments had no effect at all in the absence of gefitinib, but the H2 cysDb can partially rescue the p-Akt and p-Erk signaling in the presence of gefitinib (Figure 2.9B).

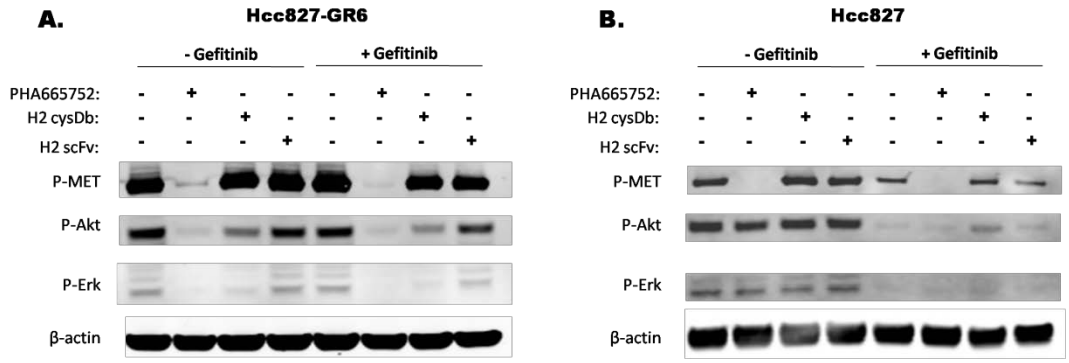

Figure 2.9: Comparing the effects of H2 cysDb and scFv on downstream signaling.
Hcc827-GR6 or Hcc827 cells were treated with different combinations of drugs and H2 antibody fragments before lysed for western blot analysis. H2 cysDb can reduce the p-Akt and p-Erk signaling in the Hcc827-GR6 cells, but it also partially rescue the p-Akt and p-Erk signaling in the Hcc827 cells in the presence of gefitinib. (Gefitinib: 1 μM; PHA665752: 1 μM; H2 cysDb: 10 μg/mL; H2 scFv: 40 μg/mL.)

After we observed the surprisingly different effects of H2 minibody and scFv-Fc on the growth of Hcc827-GR6, all four H2 Ab fragments were tested by western blot analysis.

In Hcc827-GR6 cells, only cysDb and minibody can down regulate the downstream p-Akt and p-Erk signaling, consistent with the observation that only these two fragments can inhibit the growth of Hcc827-GR6 cells (Figure 2.10A). In the Hcc827 cells, none of the four fragments has any effect in the absence of gefitinib. However, all the bivalent fragments (cysDb, minibody, and scFv-Fc) can rescue the p-Akt and p-Erk signaling in the presence of gefitinib (Figure 2.10B).

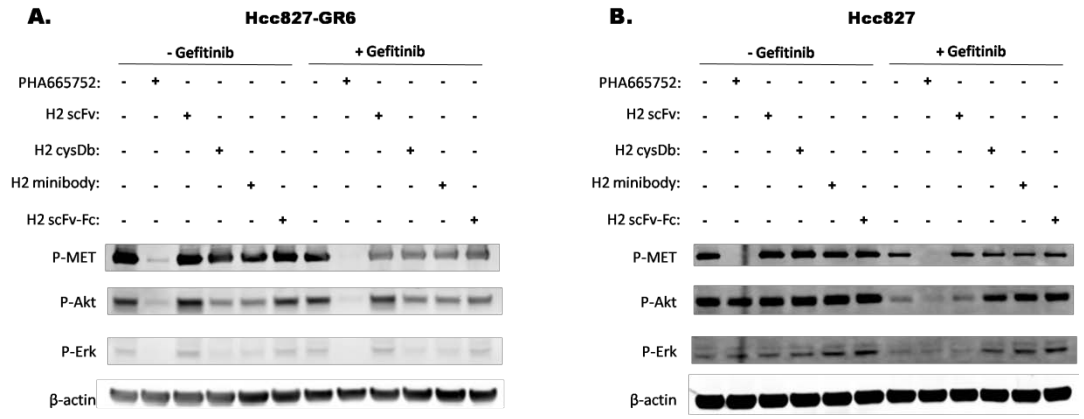

Figure 2.10: Comparing the effects of H2 Ab fragments on downstream signaling.
Hcc827-GR6 or Hcc827 cells were treated with different combinations of drugs and H2 antibody fragments before lysed for western blot analysis. H2 cysDb and minibody can reduce the p-Akt and p-Erk signaling in the Hcc827-GR6 cells. All bivalent fragments can partially rescue the p-Akt and p-Erk signaling in the Hcc827 cells in the presence of gefitinib. (Gefitinib: 1 μM; PHA665752: 1 μM; H2 scFv: 40 μg/mL; H2 cysDb: 10 μg/mL; H2 minibody: 20 μg/mL; H2 scFv-Fc: 20 μg/mL.)

2.4 Discussion

Since its invention in 1980s, phage display technology has been a proven success for rapid generation of affinity reagents (peptides, antibody fragments, and alternative scaffolds) against essentially any targets. With FDA approved Humira (adalimumab) and Benlysta (belimumab), and dozens more in clinical trials (14), phage display

technology has also become one of the major sources of fully human monoclonal antibodies for therapeutic applications. Since the fully human antibody gene sequences are already in hand following phage display selection, reformatting the scFv into diabodies or minibodies is very fast and simple. This approach has been employed to generate several previous antibody fragment imaging probes from phage libraries (3-5). As immunoPET is playing an increasingly important role in diagnosis, and in the development and implementation of targeted therapies (15, 16), phage display can be an effective path for the rapid generation of antibody fragment-based imaging probes. Instead of the months required to generate and screen conventional hybridomas, isolate the antibody genes, humanize, and conduct affinity maturation, by using phage display technology, fully human antibodies can be identified and reformatted in just a few weeks.

Here we sequenced 64 positive phage clones and found 19 distinct antibody sequences, 11 of which occurred only once, indicating significant diversity of the MET binding phage in the library. Among the solitary isolates, the H2 scFv showed excellent affinity, and reformatted versions were employed as immunoPET agents, producing high contrast images of MET-positive tumor xenografts. It is likely that there are additional good candidates in the phage pool remaining after the third round of selection. During the phage selection process, high affinity candidates are not always the most enriched ones. Individual antibody sequences can vary in the ability to be expressed, or may encode proteins that are toxic or inhibit robust growth of the host

bacterium. Rare clones may express antibodies that perform better *in vivo* due to unique pharmacokinetic properties and stability. With the advent of deep sequencing, low-cost gene synthesis, and high throughput screening methods, there is the potential to discover and reformat many more antibody sequences in parallel for characterization in order to obtain the best possible targeting agents from the library.

While the intent was to isolate antibody fragments for *in vivo* PET imaging, it was also important to avoid antibodies that may stimulate MET signaling. H2 and H5 cys-diabodies inhibited cell proliferation of two MET-activated cell lines (Hcc827-GR6 and Hcc827-/+), but showed no effects on two other gefitinib-resistant cell lines lacking MET amplification (H1650 and H1975), indicating the inhibitory effects were MET specific. Focusing on the H2 clone alone, the cys-diabody, minibody, scFv and scFv-Fc formats were further compared in both the cell growth assay and the western blot analysis of downstream signaling. Interestingly, while the bivalentH2 cys-diabody and minibody showed similar inhibitory effects on Hcc827-GR6 cells, both the monovalent scFv and the bivalent scFv-Fc failed to inhibit the growth and the downstream signaling of the MET over-expressing Hcc827-GR6 cells. The failure of the H2 scFv to inhibit cell growth and signaling probably implies bivalent binding is required for the anti-MET inhibitory effect. Previously, many anti-MET antibodies that have been isolated exhibit a partial agonistic effect, limiting their potential utility as cancer therapeutics. Despite blocking HGF-induced activation, the bivalent engagement of anti-MET antibodies appeared to cause at least partial activation of

MET signaling. To address this problem, DN-30 and MetMAb (onartuzumab) were engineered into monovalent fragments, in order to exert their inhibitory effects without activating MET kinase (17-19). Engelman *et al.* showed that Hcc827-GR6 acquired gefitinib resistance by activating ERBB3 through MET over-expression (9). Given the requirement of bivalency, it is unlikely that H2 antibody fragments' inhibitory effects are due to competition with HGF or directly blocking of binding site for other cell surface receptors such as ERBB3. Furthermore, the western blot analysis revealed no change in MET phosphorylation. A possible mechanism is that the bivalent binding of H2 antibody fragments can lock MET into a conformation that prohibits downstream signaling. The lack of activity of the scFv-Fc format may be due to its size or unique orientation of the two arms, forbidding the specific engagement that is required for the inhibitory effect. Another very interesting and unexpected observation is that despite no significant change in MET phosphorylation, all the bivalent fragments can partially rescue p-Akt and p-Erk signaling suppressed by gefitinib in the Hcc827. The fact that H2 scFv-Fc can rescue the p-Akt and p-Erk signaling in Hcc827 cells but cannot affect signaling in Hcc827-GR6 cells is intriguing. It suggests that the H2 antibody fragments may exert their functions in the Hcc827 and Hcc827-GR6 cells through different mechanisms, one of which may have very specific requirements with regard to the size and conformation of the fragment that a scFv-Fc cannot fulfill. Investigation of the detailed mechanism is ongoing.

2.5 Bibliography

1. Gherardi E, Birchmeier W, Birchmeier C, Vande Woude G. Targeting MET in cancer: rationale and progress. Nature reviews Cancer. 2012;12:89-103.

2. Surati M, Patel P, Peterson A, Salgia R. Role of MetMAb (OA-5D5) in c-MET active lung malignancies. Expert opinion on biological therapy. 2011;11:1655-62.

3. Robinson MK, Doss M, Shaller C, Narayanan D, Marks JD, Adler LP, *et al.*. Quantitative immuno-positron emission tomography imaging of HER2-positive tumor xenografts with an iodine-124 labeled anti-HER2 diabody. Cancer Res. 2005;65:1471-8.

4. McCabe KE, Liu B, Marks JD, Tomlinson JS, Wu H, Wu AM. An engineered cysteine-modified diabody for imaging activated leukocyte cell adhesion molecule (ALCAM)-positive tumors. Molecular imaging and biology : MIB : the official publication of the Academy of Molecular Imaging. 2012;14:336-47.

5. Fu M, Brewer S, Olafsen T, Wu AM, Gordon LK, Said J, et al. Positron emission tomography imaging of endometrial cancer using engineered anti-EMP2 antibody fragments. Molecular imaging and biology : MIB : the official publication of the Academy of Molecular Imaging. 2013;15:68-78.

6. Sheets MD, Amersdorfer P, Finnern R, Sargent P, Lindquist E, Schier R, et al. Efficient construction of a large nonimmune phage antibody library: the production of high-affinity human single-chain antibodies to protein antigens. Proc Natl Acad Sci U S A. 1998;95:6157-62.

7. Poul MA, Becerril B, Nielsen UB, Morisson P, Marks JD. Selection of tumor-specific internalizing human antibodies from phage libraries. Journal of molecular biology. 2000;301:1149-61.

8. McCall AM, Amoroso AR, Sautes C, Marks JD, Weiner LM. Characterization of anti-mouse Fc gamma RII single-chain Fv fragments derived from human phage display libraries. Immunotechnology : an international journal of immunological engineering. 1998;4:71-87.

9. Engelman JA, Zejnullahu K, Mitsudomi T, Song Y, Hyland C, Park JO, et al. MET amplification leads to gefitinib resistance in lung cancer by activating ERBB3 signaling. Science. 2007;316:1039-43.

10. Marks JD, Bradbury A. Selection of Human Antibodies from Phage Display Libraries. In: Lo BKC, editor. Antibody engineering : methods and protocols. Totowa, N.J.: Humana Press; 2004. p. 161 p.

11. Schier R, Marks JD, Wolf EJ, Apell G, Wong C, McCartney JE, et al. *In vitro* and *in vivo* characterization of a human anti-c-erbB-2 single-chain Fv isolated from a filamentous phage antibody library. Immunotechnology : an international journal of immunological engineering. 1995;1:73-81.

12. Bai J, Sui J, Zhu RY, Tallarico AS, Gennari F, Zhang D, et al. Inhibition of Tat-mediated transactivation and HIV-1 replication by human anti-hCyclinT1 intrabodies. J Biol Chem. 2003;278:1433-42.

13. Gibson DG, Young L, Chuang RY, Venter JC, Hutchison CA, 3rd, Smith HO. Enzymatic assembly of DNA molecules up to several hundred kilobases. Nature methods. 2009;6:343-5.

14. Nelson AL, Dhimolea E, Reichert JM. Development trends for human monoclonal antibody therapeutics. Nature reviews Drug discovery. 2010;9:767-74.

15. McCabe KE, Wu AM. Positive progress in immunoPET--not just a coincidence. Cancer biotherapy & radiopharmaceuticals. 2010;25:253-61.

16. van Dongen GA, Vosjan MJ. Immuno-positron emission tomography: shedding light on clinical antibody therapy. Cancer biotherapy & radiopharmaceuticals. 2010;25:375-85.

17. Pacchiana G, Chiriaco C, Stella MC, Petronzelli F, De Santis R, Galluzzo M, et al. Monovalency unleashes the full therapeutic potential of the DN-30 anti-Met antibody. J Biol Chem. 2010;285:36149-57.

18. Martens T, Schmidt NO, Eckerich C, Fillbrandt R, Merchant M, Schwall R, et al. A novel one-armed anti-c-Met antibody inhibits glioblastoma growth *in vivo*. Clin Cancer Res. 2006;12:6144-52.

19. Merchant M, Ma X, Maun HR, Zheng Z, Peng J, Romero M, et al. Monovalent antibody design and mechanism of action of onartuzumab, a MET antagonist with anti-tumor activity as a therapeutic agent. Proc Natl Acad Sci U S A. 2013;110:E2987-96.

Chapter 3: Anti-MET antibody fragments for immunoPET imaging

3.1 Introduction

As demonstrated in chapter 2, multiple anti-MET scFv clones have been isolated from a large naïve fully human scFv phage display library (1). Three clones have been reformatted into bivalent cys-diabodies with affinities to cell surface MET protein ranging from 0.7 nM to 5.1 nM. The H2 clone had the highest affinity and the best anti-MET inhibitory effect. It also showed cross reactivity to the mouse MET protein, which will help to generate more realistic imaging results in the presence of endogenous MET antigen. Therefore, the H2 clone was chosen for further immunoPET imaging studies.

Previously, the intact monoclonal mouse antibody DN-30 and the humanized one-armed antibody onartuzumab have already been used for anti-MET immunoPET imaging studies in murine xenograft models(2, 3).MET amplification has also been found to be an important mechanism for acquired resistance against EGFR targeted therapies in non-small cell lung cancer by Engelman *et al.* (4).Recent clinical trials using onartuzumab in combination with erlotinib for non-small cell lung cancer revealed surprising adverse effects of these MET-targeting therapies on patients

without MET over-expression, and further demonstrated the necessity of accurate molecular profiling. ImmunoPET imaging using small antibody fragments such as diabodies and minibodies can produce high contrast images at earlier time points, making it easier to rapidly evaluate *in vivo* MET expression levels, and potentially improve MET-targeted therapies in non-small cell lung cancer and other malignancies.

In this study, anti-MET H2 cys-diabody and minibody were radiolabeled with ^{89}Zr for immunoPET imaging of MET-positive xenografts in SCID mice. The faster blood clearance of cys-diabodies enables rapid PET scans at earlier time points, but it also limits the exposure time of the target tumors to the imaging probe, leading to lower uptake levels in the tumors. Different imaging applications require different formats of antibody fragments to achieve optimized balance between fast blood clearance and enough tumor uptake. Three tumor xenograft models were used to study whether the ^{89}Zr labeled cys-diabody and minibody imaging probes can distinguish the differences between the gefitinib resistant Hcc827-GR6 tumors with high MET expression, the parental Hcc827 tumors with low MET expression, and the MET-negative C6 tumors.

3.2 Materials and methods

3.2.1 Cell lines and tumor models

Hcc827 parental cells and the gefitinib resistant Hcc827-GR6 cells were obtained from Jeffrey A. Engelman's laboratory (Massachusetts General Hospital) (4). Hcc827 parental cells were maintained with 1640 media (Cellgro) supplemented with 10% FBS (fetal bovine serum, Gemini), 1mM sodium pyruvate (Cellgro) and 1% penicillin-streptomycin (Gibco). The Hcc827-GR6 cells were maintained in the same media supplemented with 100 nM gefitinib (Santa Cruz biotechnology). The MET negative C6 rat glioma cells were maintained in Deficient DME High Glucose media (Irvine Scientific) supplemented with 10% FBS, 1% penicillin-streptomycin and 2 mM L-glutamine. All cells were cultured at 37°C with 5% CO_2. Female SCID mice (Jackson Laboratories) were injected subcutaneously into the left or right shoulders with cells (2–4 x 10^6) in growth media: 50% Matrigel (BD Biosciences). The tumors were allowed to develop for 2–4 weeks before imaging. All animal studies were carried out under a protocol approved by the Chancellor's Animal Research Committee of the University of California in Los Angeles.

3.2.2 Radiolabeling of cys-diabodies and minibodies

All antibody fragments were first dialyzed into metal-free PBS (0.5–2mg/mL) before conjugation. 200 to 500 µg of cys-diabody was reduced with 15–20 fold excess of tris(2-carboxyethyl)phosphine (TCEP) for approximately 2 hours at room temperature.

20-fold excess deferoxamine-maleimide (Macrocyclics) was then incubated with the cys-diabody for 3 to 4 hours at room temperature. The minibody was randomly conjugated with deferoxamine-p-SCN (Macrocyclics), using a modified method of Vosjan *et al.* (5). Briefly, the pH of the minibody was adjusted to 9 using Na_2CO_3 before being incubated with 4-fold molar excess of deferoxamine-p-SCN at 37°C for 1 hour. The conjugated cys-diabody and minibody were then purified using a PD-10 column (GE Health).

^{89}Zr oxalic acid solution (Washington University or 3D Imaging) was neutralized with Na_2CO_3 and HEPES buffer to pH = 7, reacted with the deferoxamine (DFO) conjugated protein (protein concentration: 1 mg/mL; use 100 to 300 MBq activity for 1 mg of protein) at room temperature for 1 hour, followed by PD-10 column purification. The labeling efficiency and radiochemical purity were determined by ITLC (instant thin-layer chromatography). To assess immunoreactivity, a small amount of radiolabeled antibody fragment (~20 ng) was incubated with excess antigen positive Hcc827-GR6or antigen negative C6 cells (~100 million cells in 0.3 mL PBS with 1% FBS) for 1 hour at room temperature, after which the cells were pelleted and washed with 1mL PBS twice. The radioactivity of the combined supernatant and cell pellet was measured by a Wizard 3' 1480 Automatic Gamma Counter (Perkin-Elmer, Covina, CA). The immunoreactivity is calculated by dividing the radioactivity in the cell pellet with the total radioactivity of supernatant and cell pellet.

3.2.3 Binding and internalization assay of H2 cys-diabody

MET positive Hcc827-GR6 cells were seeded into a 24-well plate and cultured until confluent. The media was removed and the cells were incubated with ice cold PBS / 1% FBS with excess ^{89}Zr labeled H2 cys-diabody for 1 hour to saturate cell surface MET. Following washing with ice cold PBS-1% FBS three times, the cells were incubated at 37°C in growth media with excess ^{89}Zr labeled cys-diabody. At each time point (0 h, 1 h, 2 h, 4 h, and 24 h), cells were washed with ice cold PBS and the membrane bound cys-diabody was stripped with two 3-min treatment of 1 mL cold stripping buffer (0.1 M glycine, 0.15 M NaCl, pH = 2.5). The 2 mL stripping buffer was combined and considered as the membrane bound fraction. The cells were then lysed with 1 mL lysis buffer (PBS / 10 mM Tris / 0.5% SDS, pH = 7.4) at room temperature for 3 min. Each well was washed one more time with 1 mL lysis buffer and the combined lysis buffer was considered as internalized fraction. The radioactivity of each fraction was measured by gamma counting. The assay was performed in triplicate for each time point.

3.2.4 Small animal PET imaging and *ex vivo* biodistribution studies

Tumor bearing mice (tumor weight: 58 to 467 mg) were injected via tail vein with approximately 13 to 25µg of ^{89}Zr labeled cys-diabody or minibody in PBS (specific activity: 0.08 - 0.2 MBq/µg). 10-minute microPET acquisitions were performed at 4 and 20 hours post injection for cys-diabody, and 24 and 44 hours post injection for

minibody, with an Inveon microPET Scanner (Siemens). The mice were anesthetized with 2% isoflurane during the scanning process. MicroPET images were reconstructed using a filtered back projection algorithm, and analyzed with AMIDE software (6). *Ex vivo* biodistribution studies were performed after the final imaging time point. Organs, tumors and blood were harvested and weighed, and the radioactivities were measured by gamma counting. The percent injected dose per gram of tissue (%ID/g) was calculated after decay correction to evaluate the uptake level in each organ. About half of the Hcc827-GR6 tumors were cystic, and the biodistribution of these tumors was calculated excluding the cystic fluid. The radioactivities of some kidney samples were too high to be accurately measured by gamma counting, so the uptake levels were estimated by image quantitation using a previously described method (7), and the cylinder factor used for the image quantitation was provided by Dr. Scott Knowles.

3.3 Results

3.3.1 ^{89}Zr labeling of H2 cys-diabody and minibody

The H2 cys-diabody was first treated with TCEP to reduce the C-terminal cysteines. Then the deferoxamine-maleimide was conjugated to the C-terminal cysteines. The H2 cys-diabody and DFO-mal-H2 cys-diabody were analyzed by Superdex 75 size exclusion chromatography (SEC) and compared with protein size markers (BSA, 66 kDa, eluted at 20.29 min; Carbonic Anhydrase, 29 kDa, eluted at 24.08 min;

Cytochrome C, 12.4 kDa, eluted at 27.25 min). Both proteins ran as dimers (~55 kDa) in SEC. This also proved the H2 diabody with the 6-residue linker (GGGGGS) formed non-covalent dimers without the C-terminal disulfide bond. The peak for the conjugated H2 cys-diabody ran slightly earlier than the un-conjugated cys-diabody (22.34 min vs. 23.11 min), probably due to a change in charge and conformation of the molecule due to the conjugation (Figure 3.1).

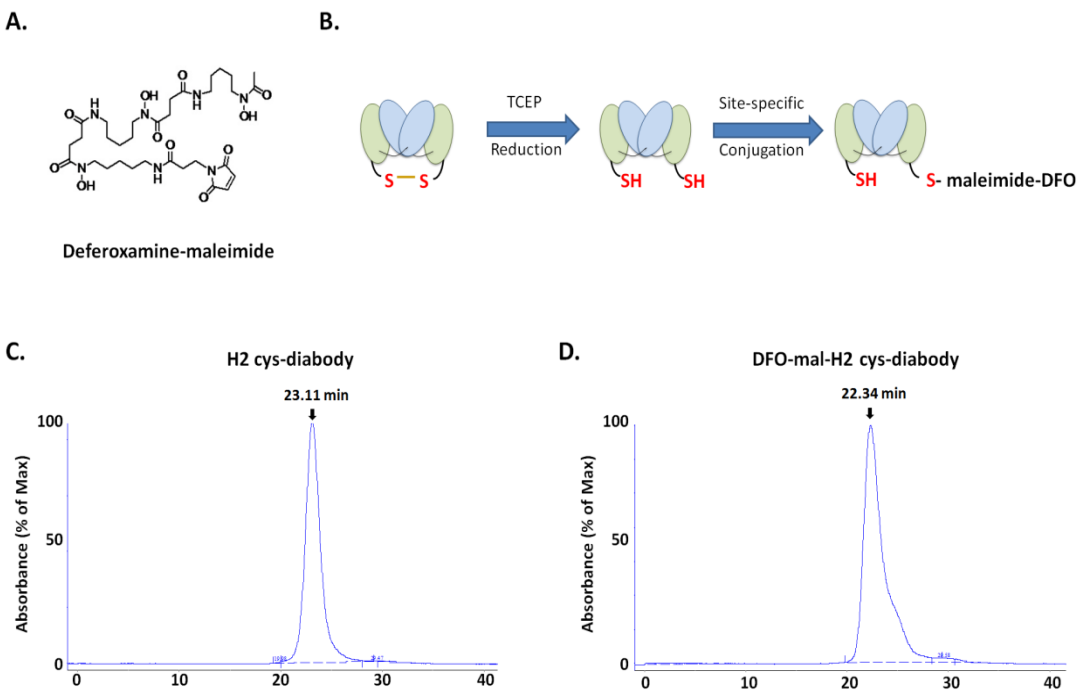

Figure 3.1: Site-specific conjugation of the H2 cys-diabody.
H2 cys-diabody was site-specifically conjugated with deferoxamine-maleimide. **A.** The structure of deferoxamine-maleimide (adopted from Macrocyclics' website). **B.** The C-terminal disulfide bond of the H2 cys-diabody was first reduced with TCEP, and then conjugated to DFO-maleimide. **C.** Superdex 75 size exclusion chromatography analysis of the purified H2 cys-diabody. The H2 cys-diabody ran as a single peak at 23.11 min. **D.** Superdex 75 size exclusion chromatography analysis of the site-specifically conjugated H2 cys-diabody (DFO-mal-H2 cys-diabody). The peak came at 22.34 min, slightly earlier than the un-conjugated protein.

The deferoxamine-p-SCN was randomly conjugated to primary amine groups (lysines and the N-terminal amines) on the H2 minibody. The majority of the un-conjugated minibody ran as dimers in the Superdex 200 SEC analysis at 30.64 min, but there was also a minor peak of the higher molecular-weight multimers at 28.17 min. However, after conjugation, most of the protein ran as dimers at 30.66 min (Figure 3.2).

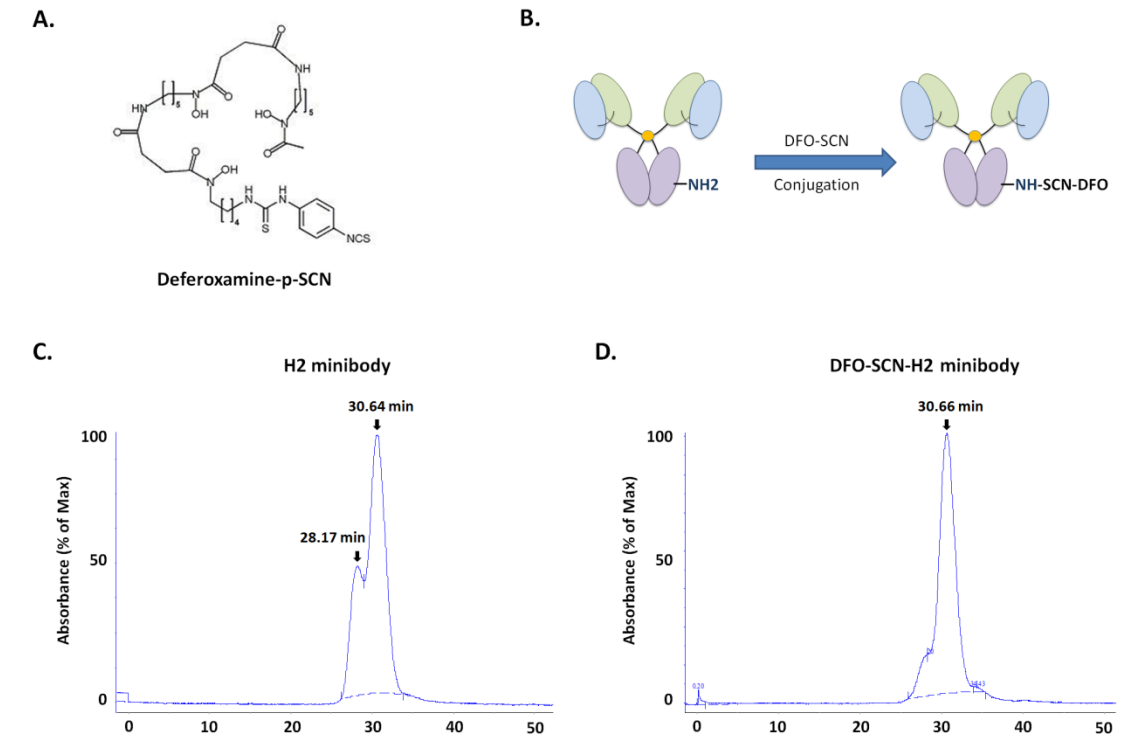

Figure 3.2: Random conjugation of the H2 minibody.

The H2 minibody was randomly conjugated with deferoxamine-p-SCN. A. The structure of deferoxamine-p-SCN (adopted from Macrocyclics' website). **B.** Random primary amine groups on the minibody were conjugated to DFO-SCN. **C.** Superdex 200 size exclusion chromatography analysis of the H2 minibody. The majority of the protein ran as dimers (~80 kDa) at 30.64 min. There was a minor peak of higher molecular-weight multimers at 28.17 min. **D.** Superdex 200 size exclusion chromatography analysis of the DFO-SCN conjugated H2 minibody (DFO-SCN-H2 minibody). The conjugated protein ran as dimers at 30.66 min.

The DFO conjugated H2 cys-diabody and minibody were then radiolabeled with ^{89}Zr for cell internalization assays and *in vivo* imaging studies. The labeling efficiencies

ranged from 27% to 88%, the immunoreactivities ranged from 65% to 78%, and the radiochemical purities were higher than 91%. Refer to Table 3.1 and Table 3.2 for detailed immunoreactivity (the MET negative C6 cells were used as negative controls for the immunoreactivity assays, and showed 5.5 ± 0.2% background activity) and radiochemical purity for each imaging experiment.

3.3.2 Internalization and uptake of ^{89}Zr labeled H2 cys-diabody

Following site-specific conjugation of H2 cys-diabody with maleimide-DFO and radiolabeling with ^{89}Zr, the labeling efficiency was 49%, the radiochemical purity was 95% after column purification, and the specific activity was 0.13 MBq/µg. When MET expressing Hcc827-GR6 cells were cultured with excess radiolabeled H2 cys-diabody (^{89}Zr-DFO-mal-H2 cys-diabody), the membrane bound radioactivity decreased in the first 6 hours while the internalized activity increased, giving a constant total cell radioactivity in the first few hours. The membrane radioactivity remained low and the internalized ^{89}Zr activity continued to accumulate over the 24 hour time course. Such results indicate rapid internalization of the radiolabeled H2 cys-diabody, making it necessary to use residualizing isotope to achieve better imaging results. The results of the internalization and uptake assay are summarized in Figure 3.3.

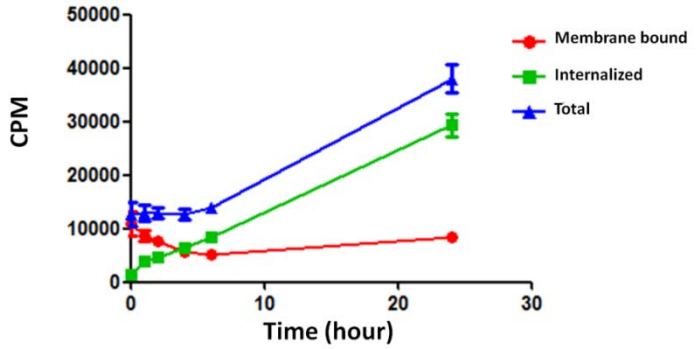

Time (hour)	Membrane bound activity (CPM)	Internalized activity (CPM)	Total activity (CPM)
0	$1.1 \pm 0.2 \times 10^4$	$1.41 \pm 0.02 \times 10^3$	$1.3 \pm 0.2 \times 10^4$
1	$8.6 \pm 1.1 \times 10^3$	$3.9 \pm 0.4 \times 10^3$	$1.3 \pm 0.2 \times 10^4$
2	$7.7 \pm 0.7 \times 10^3$	$4.7 \pm 0.3 \times 10^3$	$1.3 \pm 0.1 \times 10^4$
4	$5.7 \pm 0.6 \times 10^3$	$6.5 \pm 0.5 \times 10^3$	$1.3 \pm 0.1 \times 10^4$
6	$5.2 \pm 0.2 \times 10^3$	$8.4 \pm 0.1 \times 10^3$	$1.40 \pm 0.02 \times 10^4$
24	$8.3 \pm 0.5 \times 10^3$	$2.9 \pm 0.2 \times 10^4$	$3.8 \pm 0.3 \times 10^4$

Figure 3.3: Internalization and uptake of radiolabeled H2 cys-diabody.

3.3.3 *In vivo* PET imaging using ^{89}Zr-DFO-mal-H2 cys-diabody

^{89}Zr-DFO-mal-H2 cys-diabody was initially used for immunoPET studies in mice bearing MET positive tumors (Hcc827 or Hcc827-GR6) and MET negative C6 tumors. It showed specific uptake in antigen positive tumors (Hcc827, Hcc827-GR6) and high contrast images were obtained at as early as 4 hours post injection. As shown in Figure 3.4A and Figure 3.4B, tracer uptake in MET positive tumors was higher than the MET negative C6 tumors in the PET scans at both 4 hours and 20 hours post injection. The *ex vivo* biodistribution data confirmed these observations. In the Hcc827 vs. C6 group, the MET positive Hcc827 tumors had uptake levels of 1.1 ± 0.1 %ID/g while the negative C6 tumors showed uptake levels of 0.47 ± 0.02 %ID/g (positive tumor : negative tumor = 2.4 ± 0.2, p = 0.001; positive tumor : blood = 18 ± 2; positive tumor : muscle = 12±4). In the Hcc827-GR6 vs. C6 group, the Hcc827-GR6

tumors had higher uptake levels of 1.8 ± 0.2 %ID/g, and the negative C6 tumors had uptake levels of 0.65 ± 0.15 %ID/g (positive tumor : negative tumor = 2.9 ± 0.8, p = 0.003; positive tumor : blood = 23 ± 5; positive tumor : muscle = 13 ± 7). For better comparison of Hcc827-GR6 and Hcc827 tumors, the high-MET gefitinib resistant tumor and the low-MET parental tumor were imaged in the same mouse as shown in Figure 3.4C. The images show clear differences between high-MET Hcc827-GR6 tumor and the low-MET Hcc827 parental tumor, confirmed by the *ex vivo* biodistribution analysis. The high-MET Hcc827-GR6 tumors had uptake levels of 3.4 ± 0.3 %ID/g (Hcc827-GR6 tumor : Hcc827 tumor = 1.9 ± 0.1, p = 0.007; Hcc827-GR6 tumor : blood = 22 ± 2; Hcc827-GR6 tumor: muscle = 27 ± 14).

Table 3.1 summarizes the *ex vivo* biodistribution study of the H2 cys-diabody imaging. The kidney uptakes were not shown in the biodistribution results because the signals were too high to be accurately measured by the gamma counter. However, we estimated the uptake levels to be about 83 to 104 %ID/g (Hcc827 vs. C6 group: 85 ± 1 %ID/g; Hcc827-GR6 vs. C6 group: 99 ± 2 %ID/g; Hcc827-GR6 vs. Hcc827 group: 98 ± 9 %ID/g) by image quantitation using previously described method (7). The high kidney uptakes are due to the renal clearance of these low molecular weight cys-diabody proteins.

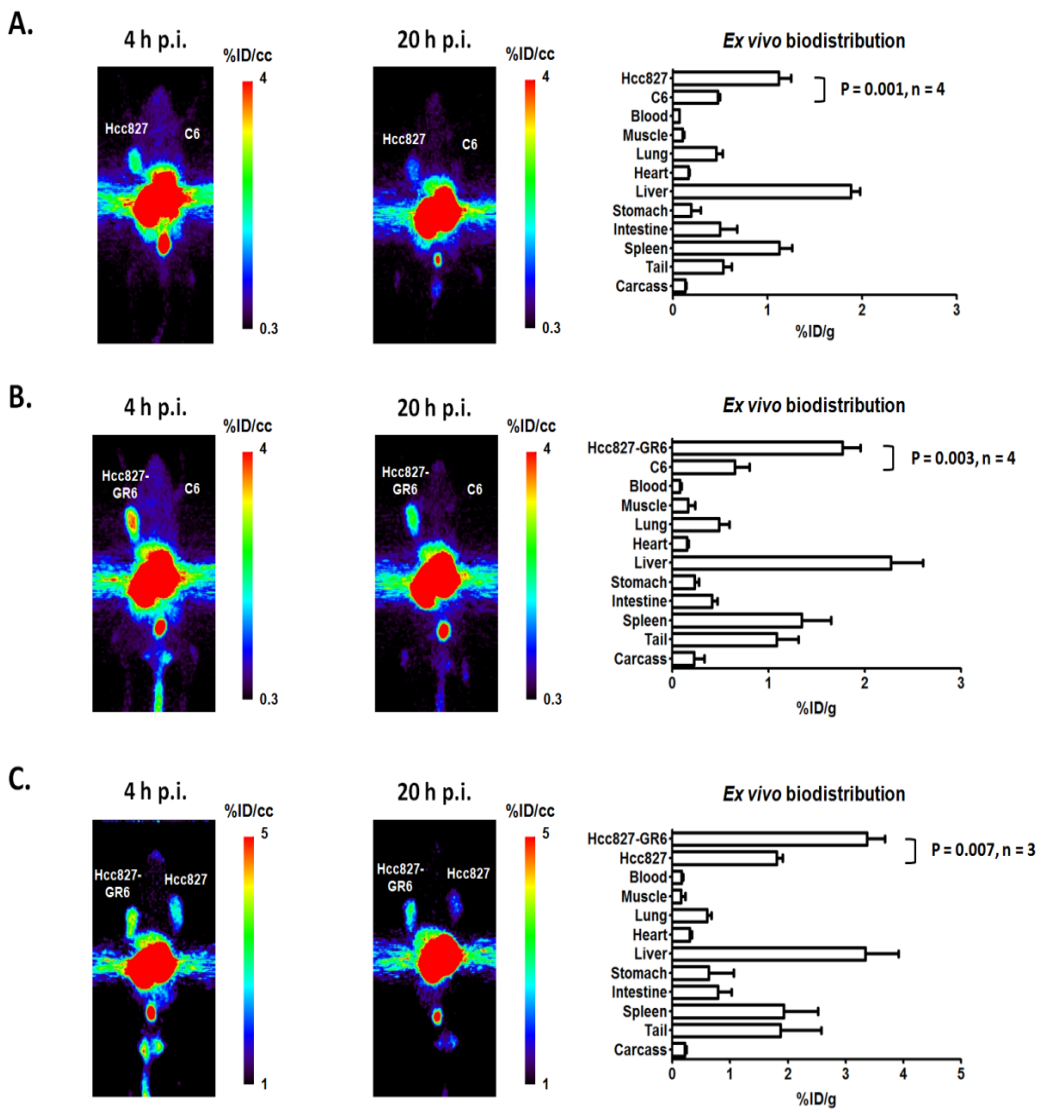

Figure 3.4: ImmunoPET using radiolabeled H2 cys-diabody.

H2 cys-diabody was site-specifically conjugated with DFO-maleimide, and then radiolabeled with ^{89}Zr for *in vivo* PET imaging.**A.** *In vivo* imaging of MET expressing Hcc827 tumor in a SCID mouse with Hcc827 tumor (212 mg) on left shoulder and C6 tumor (101 mg) on right shoulder. The ex vivo biodistribution analysis was performed at 20 hours post injection (n = 4). **B.** *In vivo* imaging of MET expressing Hcc827-GR6 tumor in a SCID mouse bearing Hcc827-GR6 tumor (262 mg) and C6 tumor (59 mg). The ex vivo biodistribution analysis was performed at 20 hours post injection (n = 4). **C.** *In vivo* imaging of MET expressing Hcc827-GR6 tumor (202 mg) and Hcc827 tumor (295 mg) in a SCID mouse. The ex vivo biodistribution analysis was performed at 20 hours post injection (n = 3).

Table 3.1: Ex vivo biodistribution of ^{89}Zr-DFO-mal-H2 cysDb at 20 hours post injection in female SCID mice bearing MET-positive (Hcc827, Hcc827-GR6) and MET-negative (C6) tumors.

	Hcc827 vs. C6 (n = 4)	**Hcc827-GR6 vs. C6 (n = 4)**	**Hcc827-GR6vs. Hcc827 (n = 3)**
Immuno-reactivity	67%	71%	78%
Radiochemical purity	99.7%	99.6%	99.6%
Injected dose (µg, MBq)	13 µg, 2.7 MBq	19 µg, 3.4 MBq	22 µg, 1.7 MBq
Tissue:	**%ID/g (mean ± SD)**		
Hcc827 tumor	1.1 ± 0.1	N.A.	1.8 ± 0.1
Hcc827-GR6 tumor	N.A.	1.8 ± 0.2	3.4 ± 0.3
C6 tumor	0.47 ± 0.02	0.65 ± 0.15	N.A.
Blood	0.064 ± 0.002	0.080 ± 0.012	0.16 ± 0.02
Muscle	0.10 ± 0.02	0.16 ± 0.07	0.15 ± 0.07
Lung	0.46 ± 0.07	0.48 ± 0.11	0.60 ± 0.07
Heart	0.16 ± 0.01	0.15 ± 0.02	0.29 ± 0.04
Liver	1.9 ± 0.1	2.3 ± 0.3	3.3 ± 0.6
Stomach	0.19 ± 0.11	0.23 ± 0.05	0.63 ± 0.43
Intestine	0.50 ± 0.18	0.41 ± 0.06	0.79 ± 0.23
Spleen	1.1 ± 0.1	1.3 ± 0.3	1.9 ± 0.6
Tail	0.53 ± 0.09	1.1 ± 0.2	1.9 ± 0.7
Carcass	0.13 ± 0.01	0.22 ± 0.11	0.21 ± 0.03
Ratios:	**Mean ± SD**		
High-MET tumor/Blood	18 ± 2	23 ± 5	22 ± 2
High-MET tumor/Muscle	12 ± 4	13 ± 7	27 ± 14
High-MET Tu/Low-MET Tu	2.4 ± 0.2	2.9 ± 0.8	1.9 ± 0.1

3.3.4 *In vivo* PET imaging using ^{89}Zr-DFO-SCN-H2 minibody

H2 minibody was also evaluated in immunoPET studies. For the minibody imaging, tumor bearing SCID mice were scanned at 24 hours and 44 hours post injection. Figure 3.5 shows clear differences in uptake levels between the high-MET Hcc827-GR6 tumor and the low-MET Hcc827 tumor, both at 24 hours and 44 hours post injection. Due to the longer serum persistence of the minibody, the *ex vivo* biodistribution analysis at 44 hours post injection revealed higher uptake levels of 8.6

± 0.5%ID/g in Hcc827-GR6 tumors, and the Hcc827 tumors also showed higher uptake level of 4.5 ± 0.4%ID/g. However, the image contrast was not improved due to higher background signal in the blood (Hcc827-GR6 Tumor: Blood = 4.2 ± 0.5). The detailed results of the *ex vivo* biodistribution study of the H2 minibody imaging are summarized in Table 3.2.

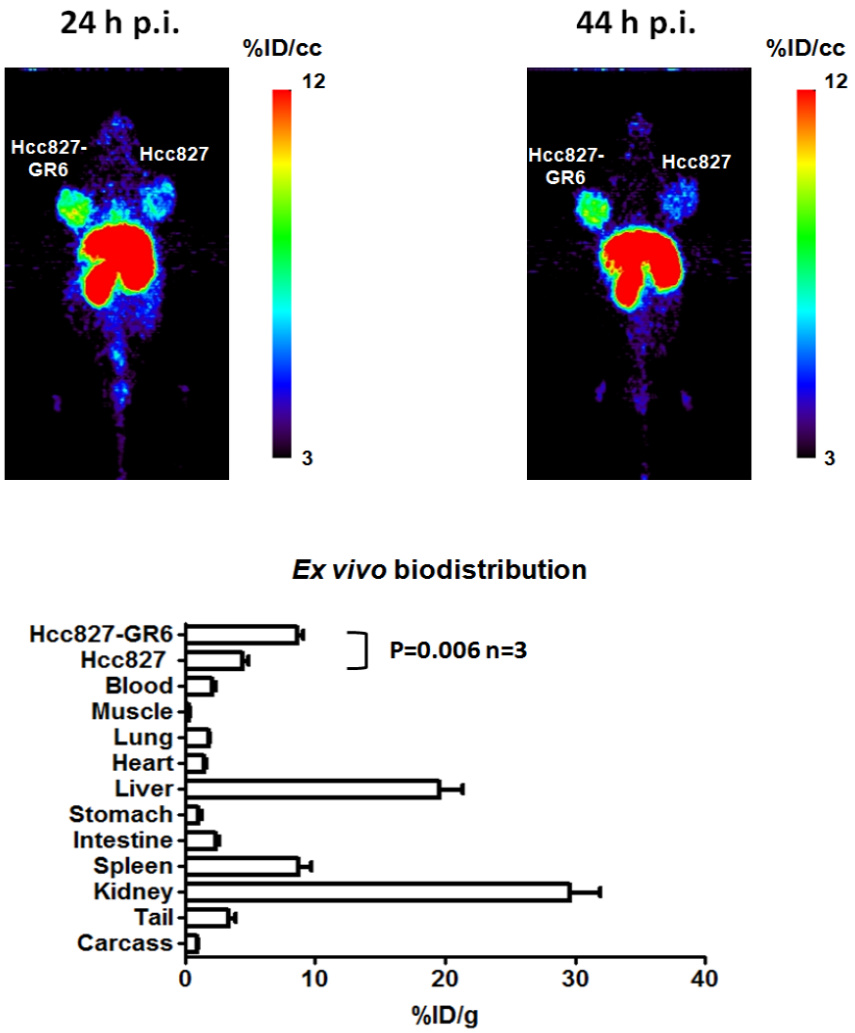

Figure 3.5: ImmunoPET imaging using radiolabeled H2 minibody.
H2 minibody was randomly conjugated with SCN-DFO, and then radio labeled with ^{89}Zr. Shown here are the imaging results of a SCID mouse with Hcc827-GR6 tumor (270mg) and Hcc827 parental tumor (306mg). The ex vivo biodistribution analysis were performed at 44 hours post injection (n = 3).

Table 3.2: Ex vivo biodistribution of ^{89}Zr-DFO-maleimide-H2 cysDb at 44 hours post injection in female SCID mice bearing Hcc827 and Hcc827-GR6 tumors.

	Hcc827-GR6 vs. Hcc827 (n=3)
Immuno-reactivity	65%
Radiochemical purity	91%
Injected dose (μg, MBq)	25 μg, 0.74 MBq
Tissue:	**%ID/g (mean ± SD)**
Hcc827 tumor	4.5 ± 0.4
Hcc827-GR6 tumor	8.6 ± 0.5
Blood	2.1 ± 0.3
Muscle	0.33 ± 0.3
Lung	1.8 ± 0.1
Heart	1.5 ± 0.2
Liver	20 ± 2
Stomach	1.0 ± 0.2
Intestine	2.4 ± 0.2
Spleen	8.7 ± 1.0
Kidney	30 ± 2
Tail	3.4 ± 0.5
Carcass	0.96 ± 0.07
Ratios:	**Mean ± SD**
Hcc827-GR6 Tu/Blood	4.2 ± 0.5
Hcc827-GR6 Tu/Muscle	26 ± 1
Hcc827-GR6 Tu/Hcc827 Tu	1.9 ± 0.2

3.4 Discussion

Demonstrated in this chapter is the successful application of ^{89}Zr labeled anti-MET H2 cys-diabody and minibody for immunoPET imaging in SCID mice carrying MET positive non-small cell lung cancer xenografts. The ^{89}Zr radiolabeled H2 cys-diabody and minibody were able to distinguish a MET over-expressing gefitinib resistant tumor from the parental tumor at as early as 4 hours post injection, indicating the potential of same day imaging for patient stratification.

The internalization and uptake assay using the ^{89}Zr labeled H2 cys-diabody showed the rapid internalization of the H2 antibody fragment upon binding to cell surface MET. Therefore, the residualizing radiolabeling approach using chelated ^{89}Zr was selected for the imaging studies, the same as two previous preclinical anti-MET immunoPET studies (2, 3). It is difficult to directly compare among these studies because of the differences in tumor models and mouse strains. However, it is known that radiolabeled diabodies usually have lower tumor uptake levels compared to larger fragments or intact antibodies, but high contrast images can be produced at earlier time points, due to the rapid blood clearance (8). With the high tumor-to-blood ratio (~20:1) at only 20 hours post injection, these results once more demonstrated the unique advantage of diabodies for rapid and high contrast immunoPET imaging.

In the current cys-diabody imaging studies, some variations were observed between experiments. For example, the cys-diabody imaging of mice bearing dual Hcc827-GR6 and Hcc827 tumors showed higher tumor uptake levels relative to the other experiments. This may reflect the effects of variations in radiolabeling, tail vein injection, or perhaps the ages of the mice and variations in physiology. Despite difference in absolute uptake levels, the tumor-to-blood ratios remain similar among the three groups, suggesting that the variations in uptake levels are likely caused by differences in availability of the radiotracer in the blood.

Compared to cys-diabodies, minibodies have longer serum persistence, allowing higher tracer uptake in the tumors. The imaging and biodistribution results indeed showed improved tumor uptake levels when using H2 minibody, but the tumor-to-blood contrast was less impressive (~4:1, at 44 hours post injection). Overall, cys-diabody is the preferred choice for rapid immunoPET applications. A further potential advantage of the H2 antibody fragments is their cross reactivity to mouse MET, allowing more representative imaging studies in the presence of endogenous MET expression in normal tissues of the mouse.

Phage display technology has been employed to generate several previous antibody fragment imaging probes in previous studies (9-11). Chapter 2 and chapter 3 demonstrate one more successful example of rapid development of fully human antibody fragment based immunoPET probes from a human scFv phage display library, proving the potential of this method. In the next two chapters, we will focus on how this valuable tool can be further optimized to rapidly generate various antibody fragments.

3.5 Bibliography

1. Sheets MD, Amersdorfer P, Finnern R, Sargent P, Lindquist E, Schier R, et al. Efficient construction of a large nonimmune phage antibody library: the production of high-affinity human single-chain antibodies to protein antigens. Proc Natl Acad Sci U S A. 1998;95:6157-62.

2. Perk LR, Stigter-van Walsum M, Visser GW, Kloet RW, Vosjan MJ, Leemans CR, et al. Quantitative PET imaging of Met-expressing human cancer xenografts with 89Zr-labelled monoclonal antibody DN30. Eur J Nucl Med Mol Imaging. 2008;35:1857-67.

3. Jagoda EM, Lang L, Bhadrasetty V, Histed S, Williams M, Kramer-Marek G, et al. Immuno-PET of the hepatocyte growth factor receptor Met using the 1-armed antibody onartuzumab. Journal of nuclear medicine : official publication, Society of Nuclear Medicine. 2012;53:1592-600.

4. Engelman JA, Zejnullahu K, Mitsudomi T, Song Y, Hyland C, Park JO, et al. MET amplification leads to gefitinib resistance in lung cancer by activating ERBB3 signaling. Science. 2007;316:1039-43.

5. Vosjan MJ, Perk LR, Visser GW, Budde M, Jurek P, Kiefer GE, et al. Conjugation and radiolabeling of monoclonal antibodies with zirconium-89 for PET imaging using the bifunctional chelate p-isothiocyanatobenzyl-desferrioxamine. Nature protocols. 2010;5:739-43.

6. Loening AM, Gambhir SS. AMIDE: a free software tool for multimodality medical image analysis. Molecular imaging. 2003;2:131-7.

7. Knowles SM, Zettlitz KA, Tavare R, Rochefort MM, Salazar FB, Stout DB, et al. Quantitative ImmunoPET of Prostate Cancer Xenografts with 89Zr- and 124I-Labeled Anti-PSCA A11 Minibody. Journal of nuclear medicine : official publication, Society of Nuclear Medicine. 2014.

8. Sundaresan G, Yazaki PJ, Shively JE, Finn RD, Larson SM, Raubitschek AA, et al. 124I-labeled engineered anti-CEA minibodies and diabodies allow high-contrast, antigen-specific small-animal PET imaging of xenografts in athymic mice. Journal of nuclear medicine : official publication, Society of Nuclear Medicine. 2003;44:1962-9.

9. Robinson MK, Doss M, Shaller C, Narayanan D, Marks JD, Adler LP, et al. Quantitative immuno-positron emission tomography imaging of HER2-positive tumor xenografts with an iodine-124 labeled anti-HER2 diabody. Cancer Res. 2005;65:1471-8.

10. McCabe KE, Liu B, Marks JD, Tomlinson JS, Wu H, Wu AM. An engineered cysteine-modified diabody for imaging activated leukocyte cell adhesion molecule (ALCAM)-positive tumors. Molecular imaging and biology : MIB : the official publication of the Academy of Molecular Imaging. 2012;14:336-47.

11. Fu M, Brewer S, Olafsen T, Wu AM, Gordon LK, Said J, et al. Positron emission tomography imaging of endometrial cancer using engineered anti-EMP2 antibody fragments. Molecular imaging and biology : MIB : the official publication of the Academy of Molecular Imaging. 2013;15:68-78.

Chapter 4: Construction of novel human scFv phage display libraries

4.1 Introduction

As discussed and demonstrated in the previous chapters, phage display technology is a reliable tool to rapidly provide fully human antibody fragments for protein engineering and immunoPET imaging probe development. On the other hand, such tool can be further optimized to better accommodate specific needs for different applications.

Diabodies are promising, universal candidates for immunoPET imaging probe development. They exhibit fast blood clearance because of their small sizes and the lack of FcRn interaction. Diabodies represent the smallest bivalent antibody fragments, so they also benefit from the avidity effect to achieve higher accumulation in the target tissue. Therefore, by using diabody based imaging probes, investigators can achieve very low blood background while still attaining satisfactory tumor uptake in just a few hours (1-7). Unlike other larger bivalent fragments, such as minibodies and scFv-Fcs, diabodies can be easily produced in bacteria, which is a favorable feature for early stage development, when multiple lead candidates need to be produced and tested.

While most scFv phage display libraries have built-in restriction sites that one can use to conveniently sub-clone selected scFvs into separate vectors to make scFv-Fc or minibody constructs, reformatting those scFvs into diabodies usually requires overlap extension PCRs which are laborious and sometimes technically challenging (Figure 4.1), hindering the development of diabodies for various applications. This calls for a further optimization of this valuable tool for easier antibody engineering.

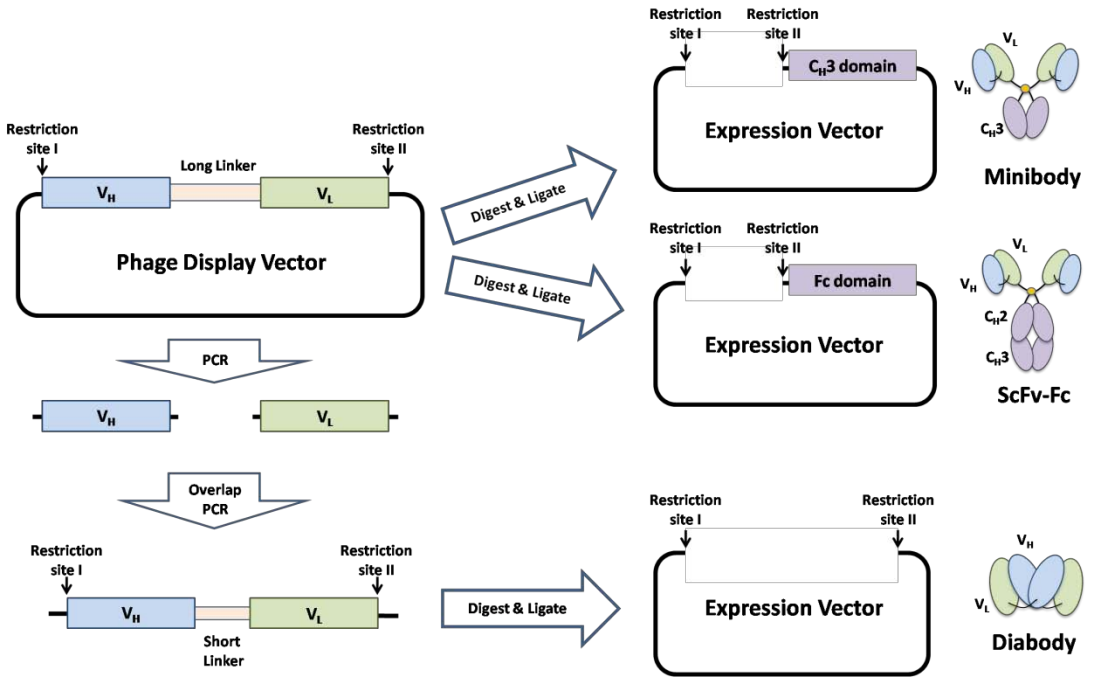

Figure 4.1: Reformatting selected scFvs from common phage libraries.
In most conventional scFv phage display libraries, the flanking restriction sites (I & II as shown here) can be utilized to rapidly make minbody and scFv-Fc constructs. However, to reformat a scFv into a diabody, the long linker in a scFv has to be shortened in order to induce dimerization. It is usually done by a series of PCRs, which is far more complicated and time consuming, requiring careful design of multiple pairs of primers.

Using a similar principle, restriction sites can also be incorporated into the linker region to simplify the linker length reduction process. By incorporating either two identical restriction sites or two different sites for a pair of restriction enzymes that generate the same cohesive ends, researchers can simply digest the DNA with the corresponding enzymes, and then use self-ligation to create a shorter linker, eliminating the need for the traditional overlap PCR.

Here is presented the construction of two fully human scFv phage display libraries with different linker designs. The first library features a 17-residue linker containing two SalI restriction sites and one AscI site, called “17aa-SSA linker”. The AscI site was used for V gene shuffling during the library construction, and the two SalI sites can be used to rapidly reduce the linker length from 17 residues to 7 residues. The second library has an 18-residue linker with one SalI site and one XhoI site named “18aa-SX linker”, which can be used for both library construction and also linker length reduction, because the restriction enzymes SalI and XhoI generate the same cohesive ends after digestion. Preexisting V_H and V_L libraries from Dr. James D. Marks’ laboratory were used as the V gene source; these are the same libraries that were used to generate the Sheets library (8) which we used for the anti-MET selection in Chapter 2. By using the two-step method described below, two fully human scFv phage display library with 1.8×10^{10} and 4.1×10^{9} transformants respectively were successfully produced.

4.2 Materials and methods

4.2.1 Incorporating the new linkers into pHEN1 vector

The V genes were cloned from the preexisting fully human V_H and V_L libraries via PCR and incorporated to pHEN1 phage display vectors (8), containing the customized 17aa-SSA linker or the 18aa-SX linker. Figure 4.2 shows the pHEN1 map and the sequences of the traditional (G4S)3 linker (8, 9), the 17aa-SSA linker (GGSTGGGSG-GGGSTGAP) and the 18aa-SX linker (GGSTGGGSGGGSGGGSSG).

To first build a pHEN1 vector containing the 17aa-SSA linker, The new linker was introduced to replace the original (G4S)3 linker in an anti-EpCAM phage clone via traditional overlap extension PCR. The 17aa-SSA linker DNA fused with the flanking overlap sequences was produced by direct annealing and amplification using the RJH12-LSSA primer and the RVλ2-LSSA primer (See sequences in Table 4.1). The VH and VL genes were separately PCR-amplified using the corresponding V gene PCR primers (Table 4.1). Then the three fragments (V_H, V_L and linker) were gel-purified and then joined together using overlap extension PCR using the V gene PCR primers. For overlap extension PCR, all the DNA fragments must have blunt ends, and anneal to each other perfectly at the overlapping region. Therefore, the high-fidelity, proofreading DNA polymerase KOD Xtreme (Novagen) was used for the PCR amplifications. This is also the polymerase used for all the PCR reactions in this

chapter. The reactions were cycled 30 times (98°C for 10 seconds, 60 °C for 30 seconds, and 68 °C for 1 min/kbp).

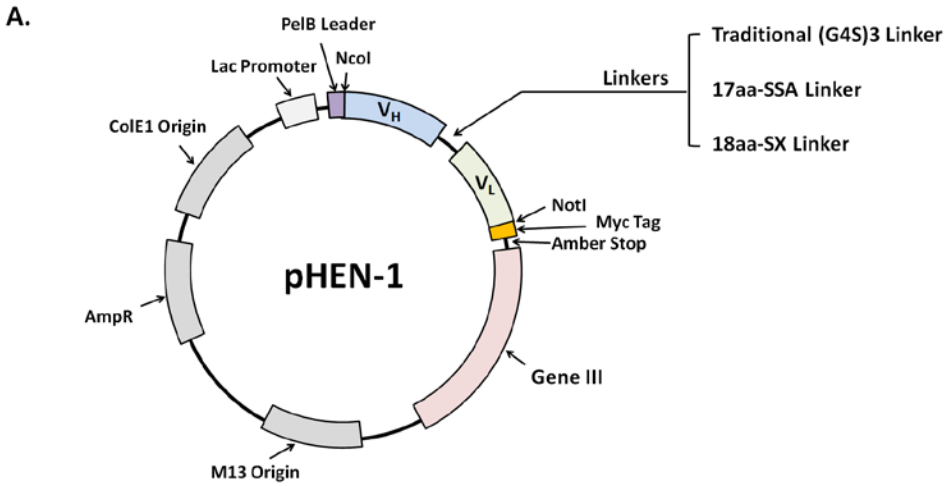

B.

Traditional (G4S)3 Linker:
DNA sequence: GGTGGAGGCGGTTCAGGCGGAGGTGGCTCTGGCGGTGGCGGATCG

Protein sequence: GGGGSGGGGSGGGGS

17aa-SSA Linker:
DNA sequence: GGAGGGTCGACAGGAGGTGGTTCTGGCGGTGGCGGGTCGACTGGCGCGCCA
SalI SalI AscI

Protein sequence: GGSTGGGSGGGGSTGAP

18aa-SX Linker:
DNA sequence: GGAGGGTCGACAGGAGGCGGTTCTGGCGGAGGTTCAGGTGGAGGCTCGAGTGGT
SalI XhoI

Protein sequence: GGSTGGGSGGGSGGGSSG

Figure 4.2: pHEN1 phagemid vector and different linkers.

A. The map of major components of the pHEN1 phagemid vector. V_H and V_L genes are in the same reading frame with the PelB leader, the linker, the Myc tag, the amber stop codon and the phage minor coat protein gene III. The amber stop codon can be read through in the suppressor strains such as TG1, yielding the scFv-protein III fusion. The transcription of the scFv-protein III fusion is driven by the lac promoter. The phagemid also contains the ColE1 origin and M13 origin which are required for the DNA replication, and the ampicillin resistance gene (AmpR) as a selection marker. Restriction sites NcoI and NotI can be used for subcloning of the scFv gene. **B.** DNA and Protein sequences of the linkers. Additional restriction sites are engineered into the 17aa-SSA linker and 18aa-SX linker for easier linker length reduction and library construction.

The assembled scFv with the 17aa-SSA linker was then gel purified and cloned into the pHEN1 vector using the NcoI and NotI sites. The construct was then transformed into chemically competent TG1 bacteria (Zymo Research) according to the recommended protocol. The 18aa-SX-linker-pHEN1 vector was built after the 17aa-SSA-scFv library construction. The 18aa-SX-linker was produced by direct annealing and amplification using the primer SXlinker-up and the primer SXlinker-down (Table 4.1). It was then fused to a random V_L gene via overlap PCR. This 18aa-SX-linker-V_L fusion was cloned into a random 17aa-SSA-scFv-pHEN1 clone to replace the original V_L and most part of the linker via SalI and NotI sites to build a new 18aa-SX-linker-pHEN1 vector. The V_H, V_L and scFv libraries were then constructed using the scheme outlined in Figure 4.3. All the primers used for the library construction were summarized in Table 4.1.

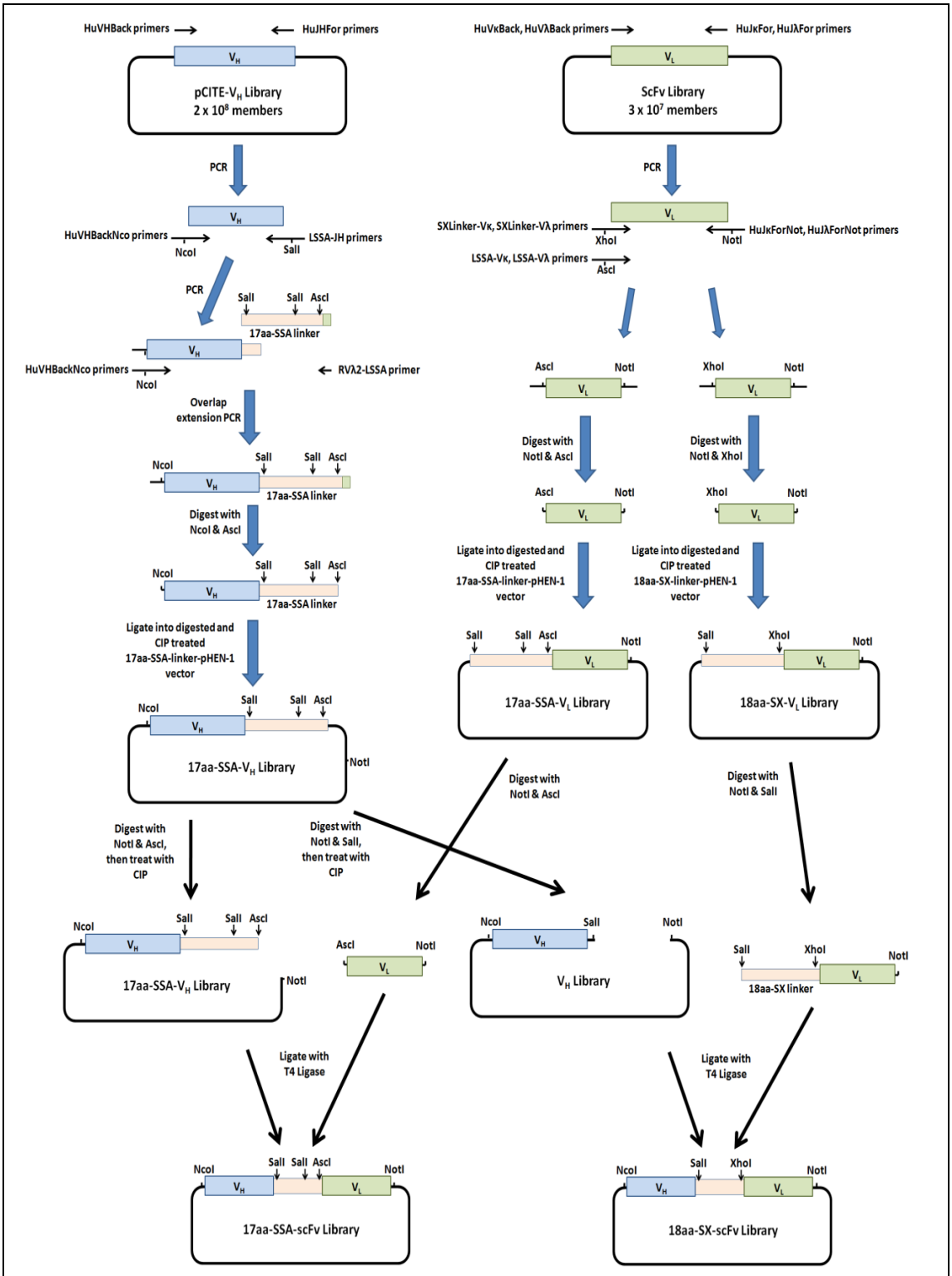

Figure 4.3: Schematic outline of the library construction.

The library construction begins with two existing V gene libraries that were created by James D. Marks' laboratory (8). The V genes were PCR-amplified and cloned into 17aa-SSA-linker-pHEN1 and 18aa-SX-linker-pHEN1 vectors to build the VH and VL libraries. To build the final scFv libraries, the VL gene repertoire was cut out from the VL libraries using the proper restriction enzymes and then ligated into the VH library. CIP stands for calf intestinal alkaline phosphatase.

4.2.2 Construction of the V_H and V_L libraries containing the new linkers

The V_H gene repertoire was cloned into the 17aa-SSA-linker-pHEN1 vector to build the 17aa-SSA-V_H library. A preexisting pCITE-V_H library with 2 x 10^8 members (8) was used as the V_H gene source (100 ng plasmid for every 50 µL of PCR reaction). The V_H gene repertoire was PCR-amplified with the human V_H back primers and J_H forward primers modified from James D. Marks *et al.*, 1991 (10), as shown in Table 4.1. The amplified V_H DNA fragments were amplified again with HuVHBackNco primers and LSSA-JH primers (Table 4.1) to add the NcoI restriction site and the sequence overlapping the linker region. The 17aa-SSA linker was amplified from the 17aa-SSA-scFv-pHEN1 vector using LSSA-up primer and the RVλ2-LSSA primer (Table 4.1). The gel-purified V gene repertoire was joined to the 17aa-SSA linker via overlap extension PCR (80 ng VH PCR product and 10 ng of 17aa-SSA linker for every 50 µL of PCR reaction) using the HuVHBackNco primers and the RVλ2-LSSA primer (Table 4.1). The PCR product was then directly purified using a spin column without agarose gel electrophoresis (Qiagen, QIAquick Gel Extraction Kit, cat#: 28704). The purified DNA was digested with NcoI and AscI restriction enzymes (New England Biolabs). In every 1000 µL reaction buffered with NEBuffer 4, 20 µg V_H-linker DNA was digested with 100 units of NcoI and AscI overnight at 37 °C. The 17aa-SSA-linker-pHEN1 vector DNA was extracted from the bacteria with the QIAprep Spin Miniprep Kit (Qiagen, cat#: 27106). 40 µg of the 17aa-SSA-linker-pHEN1 vector DNA was digested in every 1000 µL reaction with 100 units of NcoI and AscI for 6 hours, and 20 units of calf intestinal alkaline phosphatase (CIP, New

England Biolabs) was then added for another hour of incubation at 37°C. (Prolonged incubation for the vector digestion was avoided to reduce star activity.) The gel-purified V_H and vector DNA was ligated with T4 ligase (New England Biolabs) at 16 °C overnight (1.5 µg digested VH and 5 µg digested vector in every 100 µL reaction with 2000 units of T4 ligase) . The ligated DNA was gel purified and electroporated into electrocompetent TG1 bacteria (Lucigen). The electroporations were performed at 1.8 kV for 5 ms, using cuvettes with 1 mm gaps (Eppendorf), filled with 1.5 µg of purified DNA and 50 µL of TG1 electrocompetent cells. (**Important:** the ligated DNA should be eluted with water only. Limit the volume of elution to increase the concentration. The volume of the DNA added to the electrocompetent cells should not exceed 1/10 of the total volume. These rules were followed for all the electroporations in the following steps.) The electroporated cells were immediately rescued with the supplied recovery media according to recommended protocol. The electroporated cells were plated on 2YT/amp/glucose plates (2YT media, 100 µg/mL ampicillin, 2% glucose and 1.5% agar). After overnight culture at 37 °C, the bacteria were scraped from the plates and mixed with autoclaved glycerol to make 15%-glycerol stocks to be stored at -80 °C.

The V_L gene repertoire was cloned into the 17aa-SSA-linker-pHEN1 vector and the 18aa-SX-linker-pHEN1 vector to build the 17aa-SSA-V_L and the 18aa-SX-V_L libraries. V_L genes were PCR amplified from a small previous scFv library with 3×10^7 members using human V_κ, V_λ back primers and J_κ, J_λ forward primers. The restriction sites were

then added to V_L genes by PCR with HuJκForNot and HuJλForNot primers in combination with LSSA-Vκ and LSSA-Vλ primers for the 17aa-SSA-V_L library construction, or in combination with SXLinker-Vκ and SXLinker-Vλ for the 18aa-SX-V_L library construction (See primer sequences in Table 4.1). The V_L genes and vectors were digested, ligated and electroporated into TG1 bacteria using the similar method as in the V_H library construction.

4.2.3 Construction of the scFv libraries containing the new linkers

The 17aa-SSA-scFv phage display library and the 18aa-SX-scFv phage display library were constructed via V gene shuffling of the V_H and V_L libraries. The plasmids of the V_H and V_L libraries were extracted from the bacteria stock with the QIAprep Spin Miniprep Kit. The plasmids were digested with the enzymes as described in Figure 4.3. For the V_H library, 20 µg of plasmid is digested with 60 units of each of the restriction enzymes in every 350 µL reaction for 5 hours, and then treated with CIP for one more hour before gel purification. For the V_L libraries, 20 µg of plasmid is digested with 60 units of each of the restriction enzymes in every 350 µL reaction for 8 hours, and then the VL gene repertoire is gel purified and ligated into the digested pHEN1-V_H vector (1.5 µg digested V_L and 5 µg digested vector in every 100 µL reaction with 2000 units of T4 ligase, incubate at 16 °C overnight). The ligated DNA is then gel purified for electroporations. Due to the large amount of DNA and electrocompetent TG1 cells, cuvettes with 2 mm gaps were used for this step. 5 µg of purified DNA was mixed with

150 µL of electrocompetent TG1 cells and then transferred to each cuvette. The electroporations were performed at 2.5 kV for 5 ms. The electroporated TG1 cells are then rescued and plated using a method similar to that used in the V_H library construction. Random scFv clones from the final transformation were sequenced with M13R primer (5'-CAGGAAACAGCTATGACCATG-3', priming to the upstream of the scFv gene) and fdseq primer (5'-GAATTTTCTGTATGAGG-3', priming to the gene III region) from both directions to determine the percentage of functional clones.

4.2.4 Phage production from the new libraries

Phage production was performed according to a previously published method (11). The glycerol bacteria stocks were inoculated into 2YT/amp/glucose media (2YT media with 100 µg/mL ampicillin and 2% glucose). The inoculated cell number should be more than five times of the library size (typical cell number is 10^9/mL when A_{600} = 1), and the initial A_{600} should be less than 0.05 to allow multiple doubling times before adding helper phage. (Because there are multiple bacteria stocks from multiple transformations, the inoculated amount of different bacteria stocks should be determined by the stock concentrations and the number of transformants for each transformation to make sure the number of inoculated cells from one stock is proportional to the number of transformants for that transformation.) The culture was grown at 37 °C with shaking (300 rpm) until the A_{600} = 0.5. The M13KO7 helper phage (New England Biolabs) was then added to the culture at a helper phage : bacteria

ratio of 10-20 : 1. The culture was incubated in a 37 °C water bath with occasional mixing for 30 min, then shaken at 37 °C for another 30 min. (Optional: the infection efficiency can be evaluated by checking the titer of kanamycin-resistant bacteria and the ampicillin-resistant bacteria on 2YT/kan/glucose and 2YT/amp/glucose plates respectively. All the bacteria cells are ampicillin-resistant because of the pHEN1 vector, and the helper phage infected bacteria will also acquire the kanamycin-resistance.) The bacteria cells were spun down at 2800 g, and then resuspended in the same volume of 2YT/am/kan media (2YT media with 100 μg/mL ampicillin and 25 μg/mL kanamycin). The culture was grown at 30 °C with shaking overnight. Next day, the culture was centrifuged at 6000 g for 30 min, and then the supernatant was transferred to new containers. 1/10 to 1/5 volume of PEG/NaCl solution (20% polyethylene glycol 6000, 2.5M NaCl) was added to the supernatant to precipitate the phage on ice for 1 hour. The phage were then spun down and resuspended in 1/10 to 1/5 of the original volume of PBS. Then another 15 min of 6000 g centrifugation was performed to remove bacterial debris. This process was repeated to further concentrate the phage into 1/100 to 1/50 volume of PBS. The concentrated phage were then aliquoted and stored at -80 °C for future selections.

Table 4.1: Primers used for the library construction.

Primers to build the 17aa-SSA linker	
RJH12-LSSA	5’- GCACCCTGGTCACCGTCTCCTCAGGAGGGTCGACAGGAGGTGGTTCTGGCGGTGGCGG-3’
RVλ2-LSSA	5’- GCAGGCTGAGTCAGGGCAGACTGTGGCGCGCCAGTCGACCCGCCACCGCCAGAACCACC-3’
LSSA-up	5’-GGAGGGTCGACAGGAGGTGGTTCTGG-3’
Primers to build the 18aa-SX linker	
SXlinker-up	5’-GGAGGGTCGACAGGAGGCGGTTCTGGCGGAGGTTCAGG-3’
SXlinker-down	5’-ACCACTCGAGCCTCCACCTGAACCTCCGCCAGAACCGC-3’
Human VH back primers	
HuVH1aBack	5’-CAGGTGCAGCTGGTGCAGTCTGG-3’
HuVH2aBack	5’-CAGGTCACCTTGAAGGAGTCTGG-3’
HuVH3aBack	5’-GAGGTGCAGCTGGTGGAGTCTGG-3’
HuVH4aBack	5’-CAGGTGCAGCTGCAGGAGTCGGG-3’
HuVH5aBack	5’-GAGGTGCAGCTGGTGCAGTCTGG-3’
HuVH6aBack	5’-GAAATTGTGCTGACTCAGTCTCC-3’
Human JH forward primers	
HuJH1-2For	5’-TGAGGAGACGGTGACCAGGGTGCC-3’
HuJH3For	5’-TGAAGAGACGGTGACCATTGTCCC-3’
HuJH4-5For	5’-TGAGGAGACGGTGACCAGGGTTCC-3’
HuJH6For	5’-TGAGGAGACGGTGACCGTGGTCCC-3’
Human Vκ back primers	
HuVκ1aBack	5’-GACATCCAGATGACCCAGTCTCC-3’
HuVκ2aBack	5’-GATGTTGTGATGACTCAGTCTCC-3’
HuVκ3aBack	5’-GAAATTGTGTTGACGCAGTCTCC-3’
HuVκ4aBack	5’-GACATCGTGATGACCCAGTCTCC-3’
HuVκ5aBack	5’-GAAACGACACTCACGCAGTCTCC-3’
HuVκ6aBack	5’-GAAATTGTGCTGACTCAGTCTCC-3’
Human Jκ forward primers	
HuJκ1For	5’-ACGTTTGATTTCCACCTTGGTCCC-3’
HuJκ2For	5’-ACGTTTGATCTCCAGCTTGGTCCC-3’
HuJκ3For	5’-ACGTTTGATATCCACTTTGGTCCC-3’
HuJκ4For	5’-ACGTTTGATCTCCACCTTGGTCCC-3’
HuJκ5For	5’-ACGTTTAATCTCCAGTCGTGTCCC-3’
Human Vλ back primers	
HuVλ1Back	5’-CAGTCTGTGTTGACGCAGCCGCC-3’
HuVλ2Back	5’-CAGTCTGCCCTGACTCAGCCTGC-3’
HuVλ3aBack	5’-TCCTATGTGCTGACTCAGCCACC-3’
HuVλ3bBack	5’-TCTTCTGAGCTGACTCAGGACCC-3’
HuVλ4Back	5’-CACGTTATACTGACTCAACCGCC-3’
HuVλ5Back	5’-CAGGCTGTGCTCACTCAGCCGTC-3’
HuVλ6Back	5’-AATTTTATGCTGACTCAGCCCCA-3’

Human Jλ forward primers	
HuJλ1For	5′-ACCTAGGACGGTGACCTTGGTCCC-3′
HuJλ2-3For	5′-ACCTAGGACGGTCAGCTTGGTCCC-3′
HuJλ4-5For	5′-ACCTAAAACGGTGAGCTGGGTCCC-3′
HuVHBackNco primers to add NcoI restriction site	
HuVH1aBackNco	5′-GTCCTCGCAACTGCCATGGCCCAGGTGCAGCTGGTGCAGTCTGG-3′
HuVH2aBackNco	5′-GTCCTCGCAACTGCCATGGCCCAGGTCACCTTGAAGGAGTCTGG-3′
HuVH3aBackNco	5′-GTCCTCGCAACTGCCATGGCCGAGGTGCAGCTGGTGGAGTCTGG-3′
HuVH4aBackNco	5′-GTCCTCGCAACTGCCATGGCCCAGGTGCAGCTGCAGGAGTCGGG-3′
HuVH5aBackNco	5′-GTCCTCGCAACTGCCATGGCCGAGGTGCAGCTGGTGCAGTCTGG-3′
HuVH6aBackNco	5′-GTCCTCGCAACTGCCATGGCCCAGGTACAGCTGCAGCAGTCAGG-3′
HuJκForNot primers to add NotI restriction site	
HuJκ1ForNot	5′-GAGTCATTCTCGACTTGCGGCCGCACGTTTGATTTCCACCTTGGTCCC-3′
HuJκ2ForNot	5′-GAGTCATTCTCGACTTGCGGCCGCACGTTTGATCTCCAGCTTGGTCCC-3′
HuJκ3ForNot	5′-GAGTCATTCTCGACTTGCGGCCGCACGTTTGATATCCACTTTGGTCCC-3′
HuJκ4ForNot	5′-GAGTCATTCTCGACTTGCGGCCGCACGTTTGATCTCCACCTTGGTCCC-3′
HuJκ5ForNot	5′-GAGTCATTCTCGACTTGCGGCCGCACGTTTAATCTCCAGTCGTGTCCC-3′
HuJλForNot primers to add NotI restriction site	
HuJλ1ForNot	5′-GAGTCATTCTCGACTTGCGGCCGCACCTAGGACGGTGACCTTGGTCCC-3′
HuJλ2-3ForNot	5′-GAGTCATTCTCGACTTGCGGCCGCACCTAGGACGGTCAGCTTGGTCCC-3′
HuJλ4-5ForNot	5′-GAGTCATTCTCGACTTGCGGCCGCACCTAAAACGGTGAGCTGGGTCCC -3′
LSSA-JH primers to add DNA sequence overlapping the 17aa-SSA linker region	
LSSA-JH1-2F	5′-CCAGAACCACCTCCTGTCGACCCTCCTGAGGAGACGGTGACCAGGGTGCC-3′
LSSA-JH3F	5′-CCAGAACCACCTCCTGTCGACCCTCCTGAAGAGACGGTGACCATTGTCCC-3′
LSSA-JH4-5F	5′-CCAGAACCACCTCCTGTCGACCCTCCTGAGGAGACGGTGACCAGGGTTCC-3′
LSSA-JH6F	5′-CCAGAACCACCTCCTGTCGACCCTCCTGAGGAGACGGTGACCGTGGTCCC-3′
LSSA-Vκ primers to add AscI restriction site	
LSSA-Vκ1aB	5′-GGCGGGTCGACTGGCGCGCCAGACATCCAGATGACCCAGTCTCC-3′
LSSA-Vκ2aB	5′-GGCGGGTCGACTGGCGCGCCAGATGTTGTGATGACTCAGTCTCC-3′
LSSA-Vκ3aB	5′-GGCGGGTCGACTGGCGCGCCAGAAATTGTGTTGACGCAGTCTCC-3′
LSSA-Vκ4aB	5′-GGCGGGTCGACTGGCGCGCCAGACATCGTGATGACCCAGTCTCC-3′
LSSA-Vκ5aB	5′-GGCGGGTCGACTGGCGCGCCAGAAACGACACTCACGCAGTCTCC-3′
LSSA-Vκ6aB	5′-GGCGGGTCGACTGGCGCGCCAGAAATTGTGCTGACTCAGTCTCC-3′
LSSA-Vλ primers to add AscI restriction site	
LSSA-Vλ1B	5′-GGCGGGTCGACTGGCGCGCCACAGTCTGTGTTGACGCAGCCGCC-3′
LSSA-Vλ2B	5′-GGCGGGTCGACTGGCGCGCCACAGTCTGCCCTGACTCAGCCTGC-3′
LSSA-Vλ3aB	5′-GGCGGGTCGACTGGCGCGCCATCCTATGTGCTGACTCAGCCACC-3′
LSSA-Vλ3bB	5′-GGCGGGTCGACTGGCGCGCCATCTTCTGAGCTGACTCAGGACCC-3′
LSSA-Vλ4B	5′-GGCGGGTCGACTGGCGCGCCACACGTTATACTGACTCAACCGCC-3′
LSSA-Vλ5B	5′-GGCGGGTCGACTGGCGCGCCACAGGCTGTGCTCACTCAGCCGTC-3′
LSSA-Vλ6B	5′-GGCGGGTCGACTGGCGCGCCAAATTTTATGCTGACTCAGCCCCA-3′

SXLinker-Vκ primers to add XhoI restriction site	
SXLinker-Vκ1aB	5′-GGTGGAGGCTCGAGTGGTGACATCCAGATGACCCAGTCTCC-3′
SXLinker-Vκ2aB	5′-GGTGGAGGCTCGAGTGGTGATGTTGTGATGACTCAGTCTCC-3′
SXLinker-Vκ3aB	5′-GGTGGAGGCTCGAGTGGTGAAATTGTGTTGACGCAGTCTCC-3′
SXLinker-Vκ4aB	5′-GGTGGAGGCTCGAGTGGTGACATCGTGATGACCCAGTCTCC-3′
SXLinker-Vκ5aB	5′-GGTGGAGGCTCGAGTGGTGAAACGACACTCACGCAGTCTCC-3′
SXLinker-Vκ6aB	5′-GGTGGAGGCTCGAGTGGTGAAATTGTGCTGACTCAGTCTCC-3′
SXLinker-Vλ primers to add XhoI restriction site	
SXLinker-Vλ1B	5′-GGTGGAGGCTCGAGTGGTCAGTCTGTGTTGACGCAGCCGCC-3′
SXLinker-Vλ2B	5′-GGTGGAGGCTCGAGTGGTCAGTCTGCCCTGACTCAGCCTGC-3′
SXLinker-Vλ3aB	5′-GGTGGAGGCTCGAGTGGTTCCTATGTGCTGACTCAGCCACC-3′
SXLinker-Vλ3bB	5′-GGTGGAGGCTCGAGTGGTTCTTCTGAGCTGACTCAGGACCC-3′
SXLinker-Vλ4B	5′-GGTGGAGGCTCGAGTGGTCACGTTATACTGACTCAACCGCC-3′
SXLinker-Vλ5B	5′-GGTGGAGGCTCGAGTGGTCAGGCTGTGCTCACTCAGCCGTC-3′
SXLinker-Vλ6B	5′-GGTGGAGGCTCGAGTGGTAATTTTATGCTGACTCAGCCCCA-3′

4.3 Results

4.3.1 Construction of the V_H and V_L libraries

The 17aa-SSA-V_H library was constructed with 9 ligations and electroporated into TG1 bacteria at different dates. The amount of DNA and number of transformants were summarized in Table 4.2.The 17aa-SSA-V_L library and 18aa-SX-VL library were constructed with 6 ligations and 1 ligation respectively, as summarized in Table 4.3 and Table 4.4. The transformation efficiency ranged from 2.7 x 10^6 – 3.2 x 10^7 per microgram of ligated DNA (average efficiencies for 17aa-SSA-V_H library, 17aa-SSA-V_L library and 18aa-SX-V_L library construction were 6.9 x 10^6 /μg, 1.9 x 10^7 /μg and 7.1 x 10^6 /μg, respectively).

Table 4.2: Summary of transformations for 17aa-SSA-V_H library construction.

Batch	Date	Amount of DNA	Number of transformants	Transformation efficiency	Stock concentration
1	Jan 18, 2012	9.3 μg	4.3×10^7	4.6×10^6 /μg	A_{600}=100
2	Jan 21, 2012	3.1 μg	3.1×10^7	1.0×10^7 /μg	A_{600}=100
3	Jan 23, 2012	2.2 μg	5.1×10^7	2.4×10^7 /μg	A_{600}=100
4	Jan 23, 2012	3.7 μg	1.1×10^8	3.0×10^7 /μg	A_{600}=70
5	Jan 24, 2012	13.5 μg	3.6×10^7	2.7×10^6 /μg	A_{600}=150
6	Jan 30, 2012	8.4 μg	5.1×10^7	6.1×10^6 /μg	A_{600}=75
7	Jan 31 2012	18.9 μg	5.1×10^7	2.7×10^6 /μg	A_{600}=100
8	Feb 4, 2012	8.5 μg	3.8×10^7	4.5×10^6 /μg	A_{600}=125
9	Feb 4, 2012	9.2 μg	1.2×10^8	1.3×10^7 /μg	A_{600}=100
Total	N. A.	76.7 μg	5.3×10^8	6.9×10^6 /μg	N. A.

Table 4.3: Summary of transformations for 17aa-SSA-V_L library construction.

Batch	Date	Amount of DNA	Number of transformants	Transformation efficiency	Stock concentration
1	Jan 12, 2012	0.8 μg	1.1×10^7	1.4×10^7 /μg	A_{600}=100
2	Jan 12, 2012	0.7 μg	2.8×10^6	3.9×10^6 /μg	A_{600}=100
3	Jan 14, 2012	0.4 μg	2.0×10^6	4.6×10^6 /μg	A_{600}=100
4	Jan 16, 2012	1.7 μg	5.4×10^7	3.2×10^7 /μg	A_{600}=70
5	Jan 17, 2012	0.6 μg	1.4×10^7	2.3×10^7 /μg	A_{600}=150
6	Jan 17, 2012	0.6 μg	1.0×10^7	1.6×10^7 /μg	A_{600}=75
Total	N. A.	4.9 μg	9.4×10^7	1.9×10^7 /μg	N. A.

Table 4.4: Summary of transformations for 18aa-SX-V_L library construction.

Batch	Date	Amount of DNA	Number of transformants	Transformation efficiency	Stock concentration
1	Nov 18, 2013	10.0 μg	7.1×10^7	7.1×10^6 /μg	A_{600}=47

4.3.2 Construction of the 17aa-SSA-scFv library and the 18aa-SX-scFv library

The 17aa-SSA-scFv and 18aa-SX-scFv libraries were built through shuffling of the plasmid fragments of the V_H and V_L libraries. The numbers of transformants in the final 17aa-SSA-scFv library and 18aa-SX-scFv library were 1.8×10^{10} and 4.1×10^9 respectively, and the average transformation efficiencies were 2.8×10^8 /μg and 4.9 x

10^7 /μg respectively. The details are summarized in Table 4.5 and Table 4.6. However, sequencing results of the random clones from the 17aa-SSA-scFv library and 18aa-SX-scFv library show both libraries have about half of the clones with functional scFv sequences, with the other half showing either no sequencing signal, no scFv insert, or non-functional sequences with premature stop codons. Therefore, the effective library sizes should be about 9 x 10^9 and 2 x 10^9 respectively.

Table 4.5: Summary of transformations for 17aa-SAA-scFv library construction.

Batch	Date	Amount of DNA	Number of transformants	Transformation efficiency	Stock concentration
1	Feb 11, 2012	11.6 μg	1.3 x 10^9	1.1 x 10^8 /μg	A_{600}=85
2	Feb 16, 2012	7.1 μg	4.8 x 10^8	6.7 x 10^7 /μg	A_{600}=85
3	Feb 16, 2012	6.6 μg	6.4 x 10^8	9.8 x 10^7 /μg	A_{600}=110
4	Feb 20, 2012	3.6 μg	3.4 x 10^8	9.4 x 10^7 /μg	A_{600}=100
5	Feb 20, 2012	3.7 μg	4.2 x 10^8	1.1 x 10^8 /μg	A_{600}=85
6	Feb 25, 2012	32.0 μg	1.5 x 10^{10}	4.7 x 10^8 /μg	A_{600}=130
Total	N. A.	64.7 μg	1.8 x 10^{10}	2.8 x 10^8 /μg	N. A.

Table 4.6: Summary of transformations for 18aa-SX-scFv library construction.

Batch	Date	Amount of DNA	Number of transformants	Transformation efficiency	Stock concentration
1	Jan 12, 2014	1.0 μg	1.8 x 10^8	1.8 x 10^8 /μg	A_{600}=38
2	Jan 15, 2014	6.0 μg	4.4 x 10^8	7.4 x 10^7 /μg	A_{600}=79
3	Jan 16, 2014	1.0 μg	7.9 x 10^7	7.9 x 10^7 /μg	A_{600}=60
4	Jan 20, 2014	1.0 μg	7.9 x 10^7	7.9 x 10^7 /μg	A_{600}=77
5	Jan 21, 2014	12.0 μg	8.1 x 10^8	6.8 x 10^7 /μg	A_{600}=91
6	Jan 27, 2014	1.0 μg	6.5 x 10^7	6.5 x 10^7 /μg	A_{600}=70
7	Jan 28, 2014	13.8 μg	6.8 x 10^8	4.9 x 10^7 /μg	A_{600}=77
8	Feb 1, 2014	11.0 μg	6.7 x 10^8	6.1 x 10^7 /μg	A_{600}=78
9	Feb 5, 2014	13.2 μg	6.6 x 10^8	5.0 x 10^7 /μg	A_{600}=34
10	Feb 8, 2014	8.4 μg	2.1 x 10^8	2.5 x 10^7 /μg	A_{600}=68
11	Feb 11, 2014	14.9 μg	2.0 x 10^8	1.3 x 10^7 /μg	A_{600}=48
Total	N. A.	83.3 μg	4.1 x 10^9	4.9 x 10^7 /μg	N. A.

4.3.3 Phage production from the new libraries

Large batches of phage displaying fully human 17aa-SSA-scFv or 18aa-SX-scFv were produced and stored at -80 °C to be used for future selection. According to the stock concentrations and transformant numbers, different amount of bacteria from different batch of glycerol stocks were used for the phage production. For the 17aa-SSA-scFv library, the phage was produced from a total of 3 L overnight culture and concentrated into 40 mL PBS, with the final titer of 4.3 x 10^{13} colony-forming units/mL (cfu/mL). The 18aa-SX-scFv phage was produced from 2 L of overnight culture and concentrated into 40 mL PBS, and the titer was 7 x 10^{12} cfu/mL. The phage were stored at -80 °C in 1 mL aliquots.

4.4 Discussion

Presented in this chapter is the detailed strategy and process of the construction of two novel fully human scFv libraries with two different customized linkers. Unlike the traditional 15-residue (G4S)3 scFv linker introduced by Huston *et al.*(9), which is used in many scFv phage display libraries(8, 12-14), these customized linkers have various restriction sites incorporated into the DNA sequences to be employed for rapid linker length reduction via restriction digest and ligation. The multimerization of scFvs depends on the different lengths of the linkers. Generally, long flexible linkers allow self-pairing to form scFv monomers, and shorter linkers will induce the formation of multimers. In one example, Kortt, Atwell and their colleagues studied the effect of the

linker length on the anti-neuraminidase antibody NC10 scFv. While NC10 scFv with 15-residue linker forms a monomer, the 3 to 10-residue linkers induced dimerization, and the 0 to 2-residue linkers resulted in trimers (15, 16). Whitlow *et al.* also reported a scFv dimer with a 12-residue linker (17). However, such requirement on linker length is not universal. The multimerization is also dependent on the different structures of individual scFv clones and the properties of different linkers. In one study by Le Gall *et al.*, an anti-CD19 scFv, HD37, formed a mixture of monomer, dimer and tetramer, even with a 18-residue linker (18). The linker length requirement also changes when the orientation of the V domains changes from V_H-V_L to V_L-V_H, because the distance between the C-terminus of V_L and the N-terminus of V_H is larger than the one between the C-terminus of VH and the N-terminus of VL (19-22). According to practices in our lab, 15 to 18-residue linkers with small, hydrophilic amino acids such as glycine, serine and threonine work well for scFv monomers in most cases, and 5 to 8-residue linker can usually induce successful dimerizations(2, 5, 6, 23, 24). We expect a scFv phage display library with a flexible linker that can facilitate easy linker length change in this range can accommodate the needs of most of the monomers and dimers. However, considering the enormous number of different scFv clones in one library, it will be difficult to say whether such linker length change will be perfect for every clone.

In order to keep the maximal diversity during V gene cloning and shuffling, I chose to incorporate the recognition site of a rare-cutter enzyme AscI into the 17aa-SSA linker

for cloning purpose. AscI has no known cuts in the germline V genes, and its 8-bp recognition site is less likely to be found in the mature antibody DNA. However, this leads to some less common residues in the protein sequence (GGSTGGGSGGGGS-TGAP). In order to provide enough flexibility to allow self-pairing, people usually choose small, hydrophilic amino acids such as glycine, serine and threonine for scFv linkers. (G4S)3 linker is an example of such principle. On the other hand, due to its unique structure, prolines are usually used in more rigid linkers where the inter domain interactions are to be avoided(25). Proline-rich sequences such as $(XP)_n$ are commonly seen in natural peptides displaying relatively elongated and rigid conformations (26). Considering the possible stiffness caused by the proline, I set the linker length to the longer side, using a 17-residue linker (GGSTGGGSGGGGSTGAP) for monomers and a 7-residue linker (GGSTGAP) for dimers. In the 18aa-SX linker, I adopted a more traditional design, using only glycines, serines and threonines. It also has a bigger difference in the designed linker lengths for monomers (18-residue: GGSTGGGSGGGSGGGSSG) and dimers (5-residue: GGSSG). The evaluation of the effectiveness of the linker length dependent multimerization is to be demonstrated in the next chapter.

Because of the high diversity of the V gene repertoires, it is very difficult to get clean, high quality PCR products. Any error or complication in the PCR process can lead to difficulties in the subsequent digest, ligation, and transformation. Although I managed to PCR the V_H and V_L gene repertoires, I observed the trend of decreasing

transformation efficiencies as the complexity of PCR goes up. In the process of 17aa-SSA-scFv library construction, the highest transformation efficiency was observed in the final shuffling of plasmid fragments (average transformation efficiency: 2.8 x 10^8 /μg), when no PCR was involved. The construction of the 17aa-SSA-V_L library was performed by the digestion and ligation of the PCR products of the V_L genes, so the transformation efficiency is lower (average transformation efficiency: 1.9 x 10^7 /μg). The lowest transformation efficiency is seen in the V_H library construction, when the more complicated overlap extension PCR was employed. The variation in transformation efficiency can also be caused by the quality variation between different batches of electrocompetent cells. This is probably the reason for the relatively lower transformation efficiency when building the 18aa-SX-V_L and 18aa-SX-scFv libraries (average efficiencies: 7.1 x 10^6 /μg and 4.9 x 10^7 /μg). Using these libraries with restriction sites designed for V gene shuffling, one can easily build even larger scFv libraries with high transformation efficiency using digested plasmid fragments. People can also easily perform V gene shuffling on selected scFvs in order to tune up affinity or achieve better expression levels. The further validation of these new scFv libraries are discussed in the next chapter.

4.5 Bibliography

1. Wu AM, Chen W, Raubitschek A, Williams LE, Neumaier M, Fischer R, et al. Tumor localization of anti-CEA single-chain Fvs: improved targeting by non-covalent dimers. Immunotechnology : an international journal of immunological engineering. 1996;2:21-36.

2. Sundaresan G, Yazaki PJ, Shively JE, Finn RD, Larson SM, Raubitschek AA, et al. 124I-labeled engineered anti-CEA minibodies and diabodies allow high-contrast, antigen-specific small-animal PET imaging of xenografts in athymic mice. Journal of nuclear medicine : official publication, Society of Nuclear Medicine. 2003;44:1962-9.

3. Robinson MK, Doss M, Shaller C, Narayanan D, Marks JD, Adler LP, et al. Quantitative immuno-positron emission tomography imaging of HER2-positive tumor xenografts with an iodine-124 labeled anti-HER2 diabody. Cancer Res. 2005;65:1471-8.

4. Cai W, Olafsen T, Zhang X, Cao Q, Gambhir SS, Williams LE, et al. PET imaging of colorectal cancer in xenograft-bearing mice by use of an 18F-labeled T84.66 anti-carcinoembryonic antigen diabody. Journal of nuclear medicine : official publication, Society of Nuclear Medicine. 2007;48:304-10.

5. Sirk SJ, Olafsen T, Barat B, Bauer KB, Wu AM. Site-specific, thiol-mediated conjugation of fluorescent probes to cysteine-modified diabodies targeting CD20 or HER2. Bioconjugate chemistry. 2008;19:2527-34.

6. Girgis MD, Kenanova V, Olafsen T, McCabe KE, Wu AM, Tomlinson JS. Anti-CA19-9 diabody as a PET imaging probe for pancreas cancer. The Journal of surgical research. 2011;170:169-78.

7. Olafsen T, Sirk SJ, Olma S, Shen CK, Wu AM. ImmunoPET using engineered antibody fragments: fluorine-18 labeled diabodies for same-day imaging. Tumour biology : the journal of the International Society for Oncodevelopmental Biology and Medicine. 2012;33:669-77.

8. Sheets MD, Amersdorfer P, Finnern R, Sargent P, Lindquist E, Schier R, et al. Efficient construction of a large nonimmune phage antibody library: the production of high-affinity human single-chain antibodies to protein antigens. Proceedings of the National Academy of Sciences of the United States of America. 1998;95:6157-62.

9. Huston JS, Levinson D, Mudgett-Hunter M, Tai MS, Novotny J, Margolies MN, et al. Protein engineering of antibody binding sites: recovery of specific activity in an anti-digoxin single-chain Fv analogue produced in Escherichia coli. Proceedings of the National Academy of Sciences of the United States of America. 1988;85:5879-83.

10. Marks JD, Hoogenboom HR, Bonnert TP, McCafferty J, Griffiths AD, Winter G. By-passing immunization. Human antibodies from V-gene libraries displayed on phage. Journal of molecular biology. 1991;222:581-97.

11. Marks JD, Bradbury A. Selection of Human Antibodies from Phage Display Libraries. In: Lo BKC, editor. Antibody engineering : methods and protocols. Totowa, N.J.: Humana Press; 2004. p. 161 p.

12. Wajanarogana S, Prasomrothanakul T, Udomsangpetch R, Tungpradabkul S. Construction of a human functional single-chain variable fragment (scFv) antibody recognizing the malaria parasite Plasmodium falciparum. Biotechnology and applied biochemistry. 2006;44:55-61.

13. de Kruif J, Boel E, Logtenberg T. Selection and application of human single chain Fv antibody fragments from a semi-synthetic phage antibody display library with designed CDR3 regions. Journal of molecular biology. 1995;248:97-105.

14. Okamoto T, Mukai Y, Yoshioka Y, Shibata H, Kawamura M, Yamamoto Y, et al. Optimal construction of non-immune scFv phage display libraries from mouse bone marrow and spleen established to select specific scFvs efficiently binding to antigen. Biochemical and biophysical research communications. 2004;323:583-91.

15. Kortt AA, Lah M, Oddie GW, Gruen CL, Burns JE, Pearce LA, et al. Single-chain Fv fragments of anti-neuraminidase antibody NC10 containing five- and ten-residue linkers form dimers and with zero-residue linker a trimer. Protein engineering. 1997;10:423-33.

16. Atwell JL, Breheney KA, Lawrence LJ, McCoy AJ, Kortt AA, Hudson PJ. scFv multimers of the anti-neuraminidase antibody NC10: length of the linker between VH and VL domains dictates precisely the transition between diabodies and triabodies. Protein engineering. 1999;12:597-604.

17. Whitlow M, Filpula D, Rollence ML, Feng SL, Wood JF. Multivalent Fvs: characterization of single-chain Fv oligomers and preparation of a bispecific Fv. Protein engineering. 1994;7:1017-26.

18. Le Gall F, Kipriyanov SM, Moldenhauer G, Little M. Di-, tri- and tetrameric single chain Fv antibody fragments against human CD19: effect of valency on cell binding. FEBS letters. 1999;453:164-8.

19. Dolezal O, Pearce LA, Lawrence LJ, McCoy AJ, Hudson PJ, Kortt AA. ScFv multimers of the anti-neuraminidase antibody NC10: shortening of the linker in single-chain Fv fragment assembled in V(L) to V(H) orientation drives the formation of dimers, trimers, tetramers and higher molecular mass multimers. Protein engineering. 2000;13:565-74.

20. Kortt AA, Dolezal O, Power BE, Hudson PJ. Dimeric and trimeric antibodies: high avidity scFvs for cancer targeting. Biomolecular engineering. 2001;18:95-108.

21. Arndt KM, Muller KM, Pluckthun A. Factors influencing the dimer to monomer transition of an antibody single-chain Fv fragment. Biochemistry. 1998;37:12918-26.

22. Huston JS, Mudgett-Hunter M, Tai MS, McCartney J, Warren F, Haber E, et al. Protein engineering of single-chain Fv analogs and fusion proteins. Methods in enzymology. 1991;203:46-88.

23. Shimazaki K, Lepin EJ, Wei B, Nagy AK, Coulam CP, Mareninov S, et al. Diabodies targeting epithelial membrane protein 2 reduce tumorigenicity of human endometrial cancer cell lines. Clin Cancer Res. 2008;14:7367-77.

24. Leyton JV, Olafsen T, Sherman MA, Bauer KB, Aghajanian P, Reiter RE, et al. Engineered

humanized diabodies for microPET imaging of prostate stem cell antigen-expressing tumors. Protein engineering, design & selection : PEDS. 2009;22:209-16.

25. Zhao HL, Yao XQ, Xue C, Wang Y, Xiong XH, Liu ZM. Increasing the homogeneity, stability and activity of human serum albumin and interferon-alpha2b fusion protein by linker engineering. Protein expression and purification. 2008;61:73-7.

26. Chen X, Zaro JL, Shen WC. Fusion protein linkers: property, design and functionality. Advanced drug delivery reviews. 2013;65:1357-69.

Chapter 5: Reformatting and analysis of antibody fragments from the new libraries

5.1 Introduction

As shown in chapter 4, two novel fully human scFv libraries were successfully constructed for rapid antibody reformatting. The 17-residue linker in the 17aa-SSA-scFv library can be rapidly shortened to a 7-residue linker by SalI digestion and re-ligation. The18-residue linker in the 18aa-SX-scFv library can be shortened to 5 residues by SalI, XhoI double digestion and re-ligation. This makes it much easier to reformat the selected scFvs into diabodies compared to the traditional overlap extension PCR method. Using the upstream NcoI site and the downstream NotI site, the scFvs can also be easily transferred to other vectors to generate minibody or scFv-Fc clones. In order to validate the two new libraries, they were used for selections against multiple antigens, and both libraries have provided positive clones, proving their diversity. Four anti-Ncad scFvs from the 17aa-SSA-scFv library were cloned into the pSYN1 vector and successfully produced in bacteria. Their affinities were estimated to be 1.5 to 28 nM by ELISA using recombinant Ncad protein. The corresponding diabodies with 7-residue linkers were also constructed using the built-in SalI sites. Two random clones from the 18aa-SX-scFv library were also cloned into the pSYN1 vector and then reformatted into diabodies with 5-residue linkers. The

bacteria produced scFvs and diabodies were analyzed by size exclusion chromatography to evaluate the linker length dependent dimerizations.

5.2 Materials and methods

5.2.1 Phage library selection and phage ELISA

The phage selections and the phage ELISA were performed according to the methods described in chapter 2. The 17aa-SSA-scFv library was used for the selections against the human Ncad protein (extracellular domain fused to C-terminal polyhistidine tag, Sino Biological, cat#: 11039-H08H), human Trop-2 protein (T88-T274, fused to human IgG1 Fc and polyhistidine tag, R&D Systems, cat#: 650-T2) and two phosphopeptides named PEP1-P and PEP2-P. The 18aa-SX-scFv library was used for the anti-human CD4 (extracellular domain fused to C-terminal polyhistidine tag, Sino Biological, cat#: 10400-H08H) selection. For the anti-Trop-2 selection, 200 µg of total human IgG (provided by Dr. Mireille Riedinger) was added to the immunotube during phage incubation for counter selection, in order to prevent the enrichment of anti-Fc phage (see Figure 5.1 for the principles). Bovine serum albumin (BSA) was used as a carrier protein for the anti-phosphopeptide selections. BSA conjugated phosphopeptides (BSA-PEP1-P and BSA-PEP2-P) and BSA conjugated non-phosphorylated peptides (BSA-PEP1 and BSA-PEP2) were purchase from ELIM Biopharm. 500 µg of BSA conjugated non-phosphorylated peptides were used for counter selections in each round, in order to enrich only the phages that bind to the

phosphorylation sites. The detailed information about the amount of antigens and washing conditions for the selections are summarized in Table 5.1 to Table 5.5. After 3 to 4 rounds of selections, random clones were picked and sequenced to identify distinct clones, and their binding to the recombinant antigens were evaluated by phage ELISA.

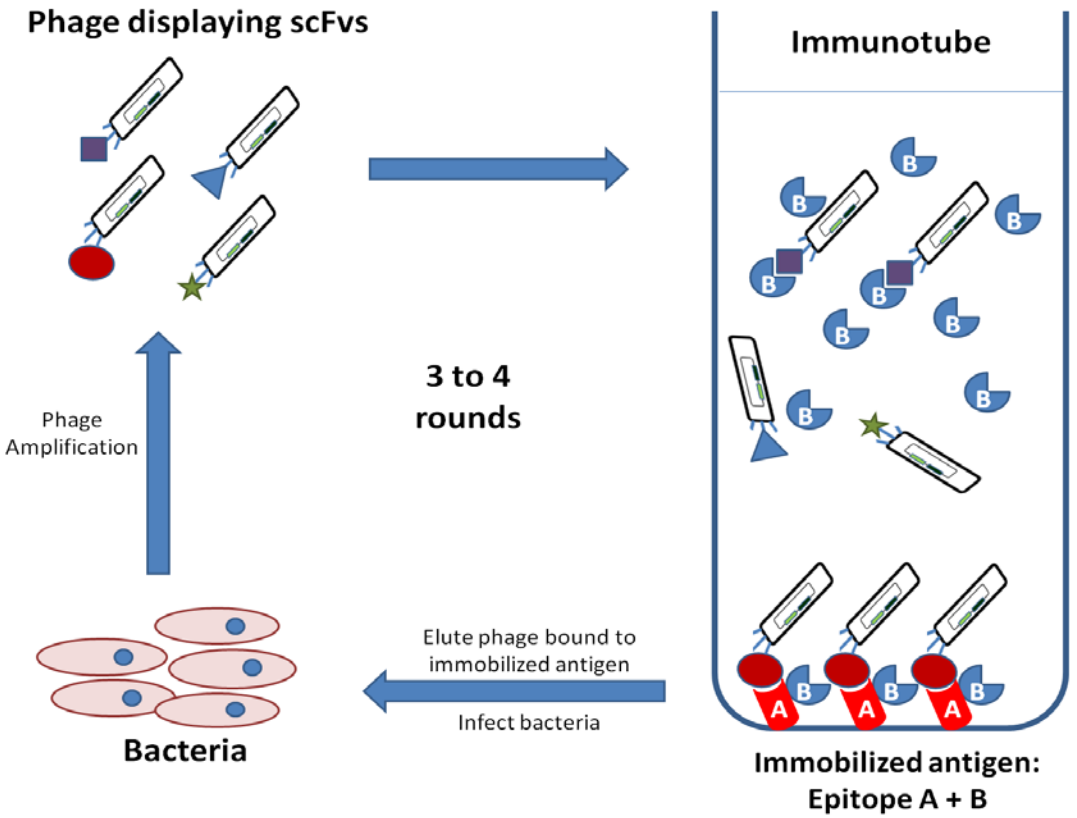

Figure 5.1: Counter selection to avoid unwanted phage clones.
To avoid the enrichment of phage clones that bind to certain epitopes on the antigen, a different protein with these epitopes is included in the liquid phage during phage incubation for counter selection. The target antigen containing epitope A and B is immobilized on the immunotube. Excess amount of a different protein with epitope B in the liquid phage will compete for the phage clones that bind to epitope B. The phage clones binding epitope A can bind to immobilized antigen and get enriched.

5.2.2 ScFv subcloning and reformatting

Four anti-Ncad 17aa-SSA-scFvs and two random 18aa-SX-scFvs were subcloned into the expression vector pSYN1(1, 2)via NcoI and NotI site to fuse to a C-terminal sequence containing a Myc tag and a 6-his tag (AAAEQKLISEEDLNGAAHHHHHH, "AAA" is the NotI site), and then transformed into chemically competent TG1 bacteria (Zymo Research) for protein production. To reformat the scFvs into diabodies, the pSYN1-17aa-scFv and pSYN1-18aa-scFv plasmids were digested either with SalI alone (for 17aa-SSA linker) or with SalI and XhoI (for 18aa-SX linker). The digested plasmids were purified using a spin column without agarose gel electrophoresis (Qiagen, QIAquick Gel Extraction Kit, cat#: 28704), and then re-ligated with T4 ligase (New England Biolab). After the digestion and re-ligation, the 17-residue or 18-residue linkers were shortened to 7-residue or 5-residue linkers, respectively. These pSYN1-7aa-diabody and pSYN1-8aa-diabody plasmids were also transformed into TG1 bacteria.

5.2.3 Expression and purification of scFvs and diabodies

The overnight bacteria culture was inoculated into 2YT media with 100 μg/mL ampicillin and 0.1% glucose, and then grown at 37 °C with shaking (300 rpm) until A_{600}=0.9. IPTG (Isopropyl β-D-1-thiogalactopyranoside) was then added to the culture to the final concentration of 0.5 mM. The bacteria culture was then cultured at room temperature with shaking (300 rpm) overnight for induction. Next day, the bacteria

cells were pelleted and lysed with BugBuster Master Mix (Novagen) to release the protein according to recommended protocol. After lysis, the bacteria debris was spun down, and the supernatant containing the antibody fragment was loaded to the HisTrap HP column (GE Healthcare). (To avoid protein precipitation, the column was pre-equilibrated with the BugBuster Master Mix before loading the supernatant.) The column was then washed with the washing buffer (30 mM imidazole, 500 mM NaCl, 50 mM sodium phosphate buffer, pH = 7.4), and the gradient elution was carried out to recover the bound antibody fragments. The fractions containing the antibody fragments were combined and dialyzed to PBS.

5.2.4 Affinity determination by ELISA

The affinities of the anti-Ncad 17aa-SSA-scFvs were determined by ELISA. The human Ncad protein (Sino Biological, cat#: 11039-H08H) was coated to a 96-well ELISA plate (3 μg/mL, 100 μL/well, overnight incubation at 4 °C). After washing and blocking with 2% milk-PBS, the plate was incubated with serial diluted scFvs (100 μL/well, the scFvs were diluted in 2% milk-PBS). After equilibrium, the un-bound scFvs were washed of with PBS and the bound scFvs were detected by a 1:1000 diluted rabbit anti-Myc antibody incubation followed by a 1:1000 diluted alkaline phosphatase (AP) conjugated goat anti-rabbit antibody incubation. The final development was performed using the PNPP substrate (Thermo Scientific) according to recommended protocol. Each concentration was done in duplicates. A_{405} of each

well was read and the binding curves were analyzed using Graphpad Prism to calculate dissociation constants using the “one site-specific binding” model.

5.2.5 Size exclusion chromatography

In order to evaluate the linker length dependent dimerization, the native structural sizes of the antibody fragments were determined by size exclusion chromatography. Approximately 20 to 40 µg of the purified antibody fragments were analyzed on a Superdex 75 column (GE Healthcare) using PBS as the running buffer at the flow rate of 0.5 mL/min. The curves were exported and analyzed using Graphpad Prism.

5.3 Results

5.3.1 Phage selections

The 17aa-SSA-scFv library has been used for selections against multiple targets, including human Ncad, human Trop-2 and two phosphopeptides (PEP1-P and PEP2-P). The detailed conditions and results of each round of these selections are summarized in Table 5.1 to Table 5.4. The 18aa-SX-scFv library was used for the selection against human CD4 (performed by Keyu Li and Amanda Freise), as summarized in Table 5.5.

Table 5.1: Results of anti-human Ncad selection using the 17aa-SSA-scFv library.

	Round 1	Round 2	Round 3
Antigen used to coat the immunotube	40 µg Ncad (Sino Bio)	20 µg Ncad (Sino Bio)	20 µg Ncad (Sino Bio)
Washing Condition	3 PBS washes	5 PBS-Tween washes and 5 PBS washes	5 PBS-Tween washes and 10 PBS washes
Phage input	4.3×10^{13}	3.6×10^{12}	6.0×10^{13}
Phage output	2.8×10^{9}	7.3×10^{4}	2.0×10^{8}
Output / input ratio	6.5×10^{-5}	2.0×10^{-8}	3.3×10^{-6}

Table 5.2: Results of anti-human Trop-2 selection using the 17aa-SSA-scFv library.

	Round 1	Round 2	Round 3
Antigen used to coat the immunotube	40 µg Trop-2-human IgG1 Fc (R&D)	20 µg Trop-2-human IgG1 Fc (R&D)	20 µg Trop-2-human IgG1 Fc (R&D)
Protein used for counter selection	200 µg total human IgG	200 µg total human IgG	200 µg total human IgG
Washing Condition	3 PBS washes	5 PBS-Tween washes and 5 PBS washes	6 PBS-Tween washes and 10 PBS washes
Phage input	4.3×10^{13}	2.3×10^{13}	5.0×10^{13}
Phage output	2.0×10^{9}	2.5×10^{6}	1.4×10^{8}
Output / input ratio	4.7×10^{-5}	1.1×10^{-7}	2.8×10^{-6}

Table 5.3: Results of anti-PEP1-P selection using the 17aa-SSA-scFv library.

	Round 1	Round 2	Round 3
Antigen used to coat the immunotube	150 µg BSA-PEP1-P	100 µg BSA-PEP1-P	100 µg BSA-PEP1-P
Protein used for counter selection	500 µg BSA-PEP1	500 µg BSA-PEP1	500 µg BSA-PEP1
Washing Condition	3 PBS washes	5 PBS-Tween washes and 5 PBS washes	5 PBS-Tween washes and 5 PBS washes
Phage input	2.1×10^{13}	2.0×10^{12}	6.4×10^{13}
Phage output	5.3×10^{8}	1.8×10^{5}	2.3×10^{8}
Output / input ratio	2.5×10^{-5}	9.0×10^{-8}	3.6×10^{-6}

Table 5.4: Results of anti-PEP2-P selection using the 17aa-SSA-scFv library.

	Round 1	Round 2	Round 3	Round 4
Antigen used to coat the immunotube	150 μg BSA-PEP2-P	100 μg BSA-PEP2-P	100 μg BSA-PEP2-P	100 μg BSA-PEP2-P
Protein used for counter selection	500μg BSA-PEP2	500μg BSA-PEP2	500μg BSA-PEP2	500μg BSA-PEP2
Washing Condition	3 PBS washes	5 PBS-Tween washes and 5 PBS washes	10 PBS-Tween washes and 10 PBS washes	10 PBS-Tween washes and 10 PBS washes
Phage input	2.1×10^{13}	1.0×10^{12}	1.3×10^{13}	3.1×10^{13}
Phage output	7.3×10^{8}	1.3×10^{5}	2.9×10^{5}	2.0×10^{7}
Output / input ratio	3.5×10^{-5}	1.3×10^{-7}	2.2×10^{-8}	6.5×10^{-7}

Table 5.5: Results of anti-human CD4 selection using the 18aa-SX-scFv library.

	Round 1	Round 2	Round 3	Round 4
Antigen used to coat the immunotube	40 μg CD4 (Sino Bio)	20 μg CD4 (Sino Bio)	20 μg CD4 (Sino Bio)	20 μg CD4 (Sino Bio)
Washing Condition	2 PBS washes	5 PBS-Tween washes and 10 PBS washes	10 PBS-Tween washes and 10 PBS washes	10 PBS-Tween washes and 10 PBS washes
Phage input	7.0×10^{12}	1.2×10^{13}	2.7×10^{13}	1.2×10^{13}
Phage output	2.5×10^{8}	8.0×10^{3}	7.4×10^{5}	1.5×10^{6}
Output / input ratio	3.6×10^{-5}	6.7×10^{-10}	2.7×10^{-8}	1.3×10^{-7}

5.3.2 Phage ELISA

For the anti-Ncad selection, sequencing results of 96 random clones from the round 3 output revealed 37 distinct functional sequences, 15 of which have two or more duplicates. (There were 7 clones showing either no sequencing signal or non-functional sequences.) Because of limited amount of antigen at the time, only 1 representative clone for each functional sequence was used for the phage ELISA. The results of the phage ELISA are summarized in Table 5.6. The clones are ranked

according to the numbers of duplicates, and the A_{405} values are color coded according to the signal strength. (NC 1-3 are the negative controls, using only helper phage that displays no scFv.) These clones were also used for anti-Ecad phage ELISA to test specificity, and all clones showed negative results (A_{405}≤ 0.058).

Table 5.6: Results of anti-human Ncad phage ELISA.

Clone name	A6	B3	G6	A1	D6	H3	B6	D3	C8	D10
Number of duplicates	12	9	9	7	5	4	4	3	2	2
A_{405}	0.1715	0.2198	0.1606	0.2096	0.1657	0.2231	0.2033	0.1354	0.1847	0.1811
Clone name	**B5**	**D11**	**F12**	**B11**	**D2**	**D12**	**B7**	**G12**	**F8**	**C2**
Number of duplicates	2	2	2	2	2	1	1	1	1	1
A_{405}	0.1682	0.1669	0.1482	0.1426	0.1422	0.2599	0.2122	0.2063	0.2049	0.1882
Clone name	**H4**	**B12**	**E5**	**A11**	**H8**	**H2**	**C4**	**E7**	**C10**	**E11**
Number of duplicates	1	1	1	1	1	1	1	1	1	1
A_{405}	0.1787	0.1744	0.1722	0.1713	0.1693	0.1569	0.1433	0.1415	0.133	0.1285
Clone name	**C7**	**A5**	**F6**	**E3**	**F1**	**H5**	**G11**	**NC 1**	**NC 2**	**NC 3**
Number of duplicates	1	1	1	1	1	1	1	-	-	-
A_{405}	0.101	0.0847	0.0816	0.0728	0.0722	0.0592	0.0555	0.0545	0.0496	0.0508

For the anti-Trop-2 selection, 96 random clones from the round 3 output were used for phage ELISA, and the results were summarized in Table 5.7 (numbers stand for the A_{405} values of each clone). To exclude the phage clones that bind to the Fc region, all the clones were also tested in phage ELISA using total human IgG, and the results were all negative (A_{405}≤ 0.064). The sequencing results revealed 27 distinct functional sequences, 12 of which have two or more duplicates. (There were 34 clones showing either no sequencing signal or non-functional sequences.) The number of duplicates and average A_{405} value for each distinct sequence were summarized in Table 5.8. According to these results, A7, B7 and F10 clones are probably false positive clones.

Table 5.7: Results of anti-human Trop-2 phage ELISA.

<>	1	2	3	4	5	6	7	8	9	10	11	12
A	0.2369	0.2429	0.2092	0.0579	0.1425	0.1653	0.0560	0.0795	0.1321	0.0916	0.1569	0.2064
B	0.3025	0.1370	0.1023	0.1184	0.2024	0.1852	0.0633	0.1234	0.2460	0.1114	0.1807	0.1123
C	0.3034	0.0821	0.1114	0.0603	0.1283	0.1619	0.0676	0.1349	0.1718	0.1367	0.1320	0.1239
D	0.3550	0.2181	0.1219	0.0562	0.1645	0.1340	0.1114	0.0612	0.0568	0.1203	0.0674	0.0709
E	0.1245	0.2143	0.1472	0.1474	0.1241	0.0959	0.0877	0.1253	0.1637	0.0857	0.1526	0.1468
F	0.2739	0.1270	0.0624	0.1140	0.1236	0.1444	0.1095	0.1734	0.1315	0.0633	0.1300	0.0553
G	0.1789	0.1774	0.1978	0.0577	0.0614	0.1129	0.0702	0.1583	0.1727	0.1298	0.1578	0.0720
H	0.2638	0.0548	0.0557	0.0868	0.2180	0.3410	0.0614	0.2011	0.1284	0.1029	0.1552	0.1125

Table 5.8: Summary of the anti-human Trop-2 phage ELISA for the functional clones.

Clone name	**A1**	**A7**	**B4**	**C9**	**C10**	**E5**	**B11**	**E10**	**E8**	**A3**
Number of duplicates	13	7	4	3	3	3	3	3	2	2
Average A_{405}	0.1987	0.0646	0.1276	0.2138	0.1620	0.1443	0.1427	0.0990	0.1946	0.1664
Clone name	**B2**	**B10**	**C1**	**A2**	**A12**	**F8**	**E9**	**H11**	**A9**	**F9**
Number of duplicates	2	2	1	1	1	1	1	1	1	1
Average A_{405}	0.1233	0.1127	0.3034	0.2429	0.2064	0.1734	0.1637	0.1552	0.1321	0.1315
Clone name	**B8**	**B12**	**D7**	**C3**	**C2**	**B7**	**F10**			
Number of duplicates	1	1	1	1	1	1	1			
Average A_{405}	0.1234	0.1123	0.1114	0.1114	0.0821	0.0633	0.0633			

The selections against the phosphopeptides were more difficult because the target epitopes were much smaller compared to the other selections. We tried 3 rounds of selection on PEP1-P using relatively mild washing conditions, and 4 rounds of selection on PEP2-P using more stringent washes. To make sure the enriched clones bind only to the phosphorylated peptide, we compared the phage ELISA results on both the phosphorylated peptides (BSA-PEP1-P or BSA-PEP2-P) and the non-phosphorylated peptides (BSA-PEP1 or BSA-PEP2). The signals are called A_{405}(+) and A_{405}(-) respectively. According to the sequencing results, we identified 9 distinct functional sequences from 96 anti-PEP1-P clones, but only 2 distinct

functional sequences from 96 anti-PEP2-P clones. The number of duplicates and average $A_{405}(+)$ / $A_{405}(-)$ ratio for each distinct sequence were summarized in Table 5.9 and Table 5.10. Many of these clones showed poor distinction between the phosphorylated and non-phosphorylated peptides. Five of the anti-PEP1-P clones (A1, C7, A7, C10, H2) showed at least 30% higher signal for the phosphorylated peptide. One of the anti-PEP2-P clones (F3) showed 128% higher signal for the phosphorylated peptide. Other clones are probably false positive clones.

Table 5.9: Summary of the phage ELISA results for the anti-PEP1-P functional clones.

Clone name	A1	C7	D12	A7	C10	H2	G12	C2	C12
Number of duplicates	42	9	7	6	4	3	1	1	1
Average $A_{405}(+)$ / $A_{405}(-)$ ratio	1.413	1.333	1.015	1.840	1.769	1.428	1.079	1.039	0.710

Table 5.10: Summary of the phage ELISA results for the anti-PEP2-P functional clones.

Clone name	F3	F1
Number of duplicates	34	1
Average $A_{405}(+)$ / $A_{405}(-)$ ratio	2.279	0.973

The 18aa-SX-scFv library has been used for only one target, the extracellular domain of human CD4. Six distinct functional sequences were identified according to the sequencing results of 96 random clones after 4 rounds of selections. One of these clone, A1, has the 17aa-SSA linker instead of the 18aa-SX linker, probably because of incomplete digestion during the scFv library construction. The preliminary phage ELISA was performed in duplicated wells for each of the six representative clones and the helper phage control (NC). The results are summarized in Table 5.11. (The

sequence analysis and phage ELISA of the anti-human CD4 clones were performed by Amanda Freise.)

Table 5.11: Summary of the phage ELISA results for the anti-human CD4 functional clones

Clone name	A1	A3	A12	A2	A4	C1	NC
Number of duplicates	23	21	13	9	5	4	-
A_{405} (1st well)	0.164	0.101	0.11	0.077	0.075	0.078	0.073
A_{405} (2nd well)	0.151	0.097	0.099	0.084	0.073	0.071	0.07

5.3.3 *In vitro* characterization of anti-Ncad 17aa-SSA-scFvs

Among the anti-Ncad 17aa-SSA-scFv phage clones that showed positive phage ELISA signals, four clones (A1, A6, D6, G6) were randomly picked and subcloned to pSYN1 vector. These scFv proteins were successfully produced and purified. Julia Lipianskaya and Dr. Kirstin Anja Zettlitz tested their affinities by ELISA. The preliminary results are summarized in Figure 5.2. A1, A6 and D6 scFvs have low nanomolar affinities ranging from 1.5 nM to 28 nM. The G6 scFv did not show significant binding. Our collaborator Joyce Yamashiro (Dr. Robert Reiter's laboratory) also tested these scFvs in flow cytometry experiments, and got similar results. A1, A6 and D6 scFvs can bind to the Ncad positive cells, but G6 scFv showed no binding.

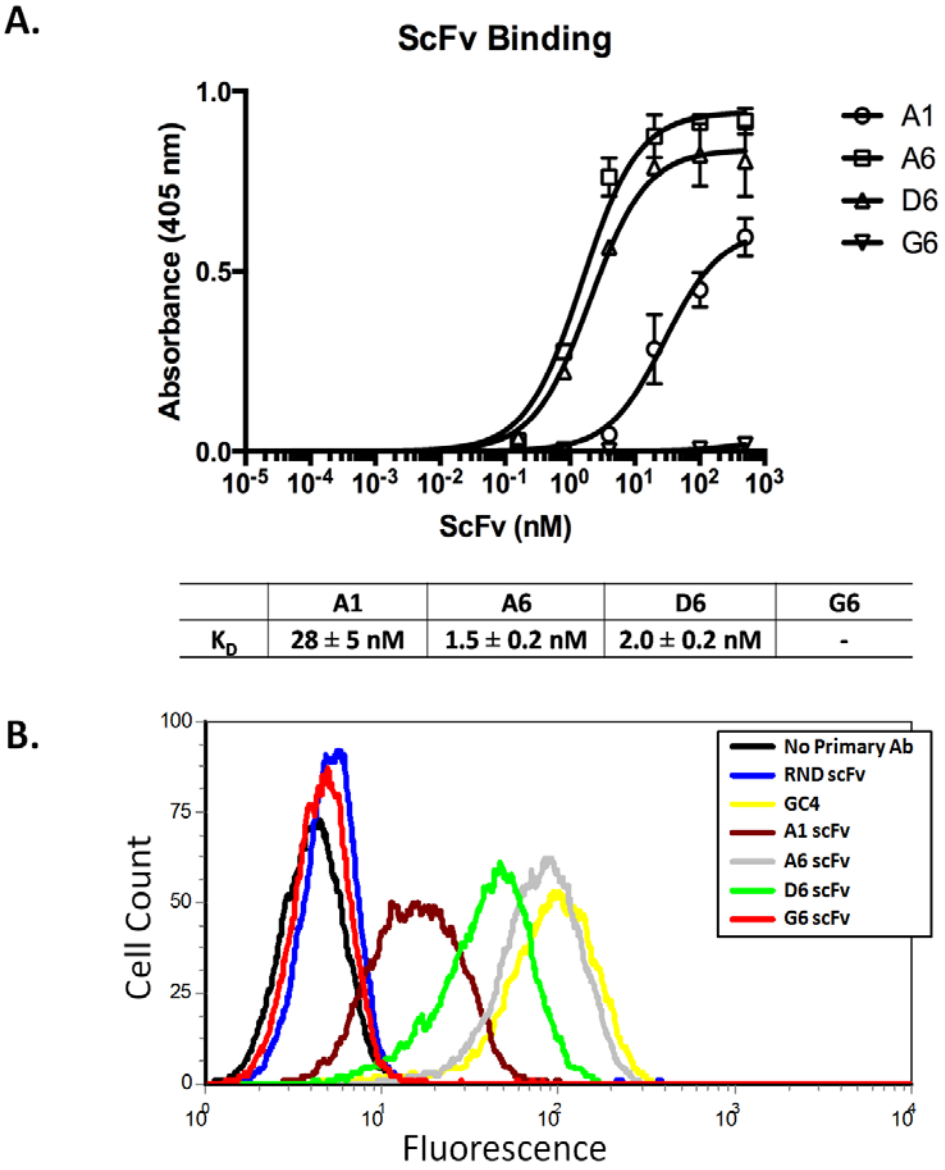

	A1	A6	D6	G6
K_D	28 ± 5 nM	1.5 ± 0.2 nM	2.0 ± 0.2 nM	-

Figure 5.2: *In vitro* characterization of anti-Ncad 17aa-SSA scFvs.

A. The affinities of the anti-Ncad scFvs were estimated by ELISA on immobilized Ncad recombinant protein. Each concentration was done in duplicates. The binding curves were analyzed in Graphpad Prism to calculate dissociation constants using the "one site-specific binding" model. **B.** Flow cytometry experiments using Ncad positive PC3 cells. A1, A6 and D6 scFvs all show binding to the Ncad positive PC3 cells. G6 scFv did not show binding to PC3. (RND scFv: a random scFv from the 18aa-SX-scFv library, used as a negative control; GC4: a commercial Ncad antibody, used as a positive control.)

5.3.4 Linker length dependent dimerizations

Four pairs of anti-Ncad 17aa-linker scFvs and 7aa-linker diabodies were analyzed by size exclusion chromatography (SEC) using a superdex 75 column. As shown in Figure 5.3, the linkers worked well for the A1 and G6 clones. The 17aa-linker A1 scFv and G6 scFv formed mostly monomers, while the 7aa-linker diabodies formed mostly dimers. However, this is not the case for the A6 and D6 clones. The 7aa-linker A6 diabody formed both monomer and dimer, indicating the linker length was not short enough to induce complete dimerization. On the other hand, the 17aa-linker D6 scFv also formed a mixture, showing the D6 clone has a strong tendency to dimerize even with a long 17-residue linker.

Two random clones (A1 and A2) from the 18aa-SX-scFv library were also successfully reformatted expressed and purified. The superdex 75 SEC analysis of these antibody fragments showed expected results . Both 18aa-linker scFvs were monomers and both 5aa-linker diabodies were dimers.

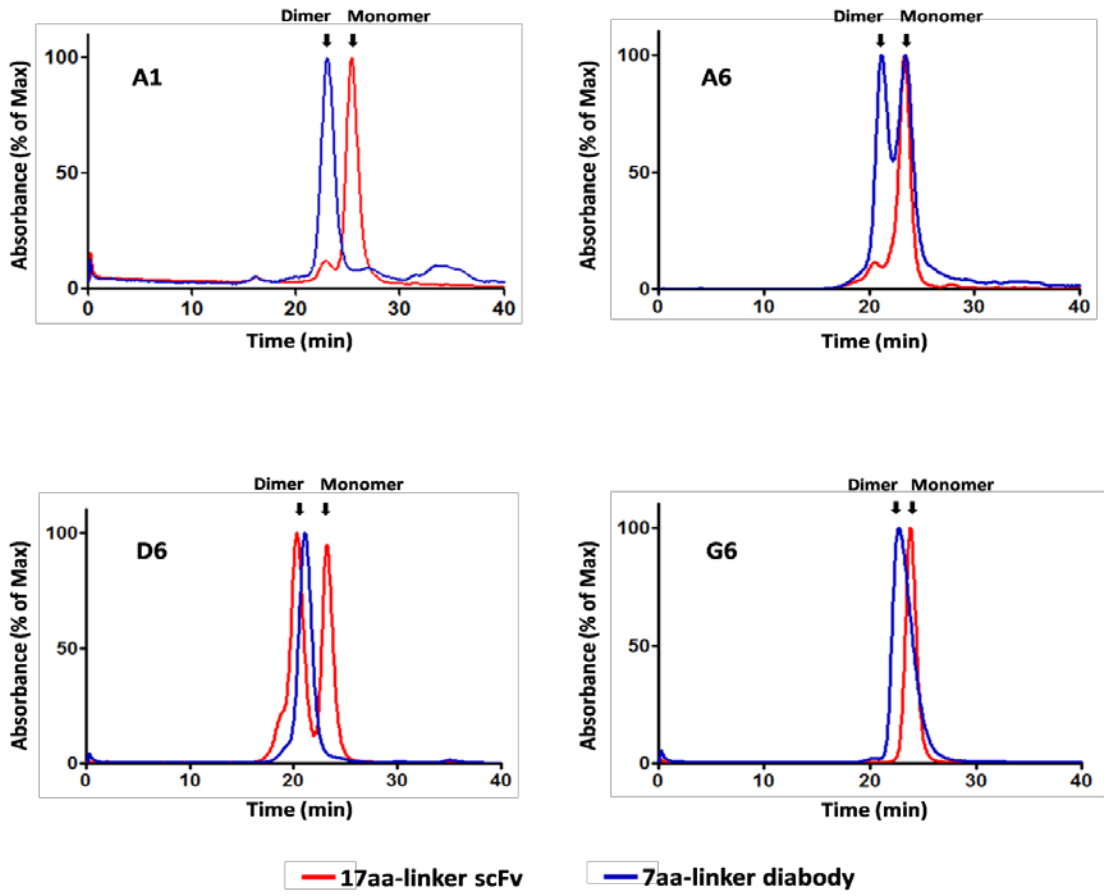

Figure 5.3: SEC analysis of anti-Ncad 17aa-linker scFvs and 7aa-linker diabodies.

Four pairs of anti-Ncad antibody fragments were analysed by superdex 75 size exclusion chromatography. The 17aa-linker and the 7aa-linker worked best for the A1 and G6 clones. For the A6 clone, the 7aa-linker diabody formed a mixture of monomer and dimer. For the D6 clone, the 17aa-linker scFv formed a mixture of monomer and dimer.

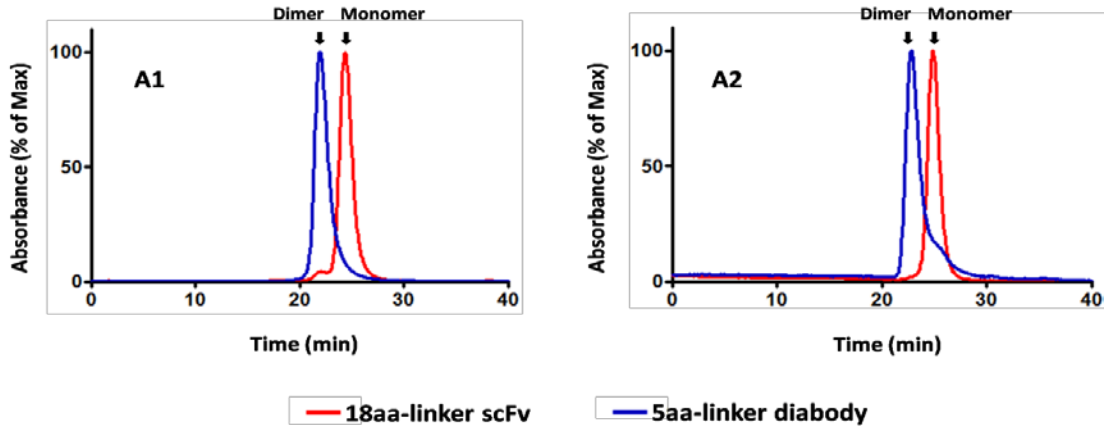

Figure 5.4: SEC analysis of 18aa-linker scFvs and 5aa-linker diabodies.

Two random clones (A1 and A2) from the 18aa-SX-scFv library were reformatted, expressed and purified. The 5aa-linker successfully induced dimerization for both clones.

5.4 Discussion

In order to validate the new fully human scFv phage display libraries, they were used for selections against multiple targets. The 17aa-SSA-scFv library has been used for selections against four different targets, including two larger protein targets (human Ncad and Trop-2) and two phosphopeptides (PEP1-P and PEP2-P). The selection against the human Ncad produced the largest number of positive antibody clones (37 distinct sequences, 35 of which showed average A_{405} over 0.07, while the average background signal was about 0.05), probably because it is the largest one in the four antigens (about 700 amino acids). The selection against the human Trop-2 also produced over 20 distinct positive clones. The 187-residue Trop-2 sequence (T88-T274) was fused to the human IgG1 Fc domain for better production and stability. To avoid enriching the phage clones that bind to the Fc domain, excess total human IgG proteins were included in the liquid phase during phage incubation for counter selection. The negative phage ELISA results of all 96 random clones on the total human IgG protein proved the effectiveness of the counter selection. The preliminary affinity test of the four anti-Ncad scFvs showed three of them had low nanomolar affinities ranging from 1.5 nM to 28 nM, which is comparable to the scFv clones obtained from the Sheets library (3) that we used for the anti-MET selection. The successful generation of high affinity scFv clones against these larger protein targets proved the high diversity of the 17aa-SSA-scFv library.

On the other hand, it is much more difficult to produce the phosphopeptide specific scFv clones, considering the limited epitope size and the requirement of extremely high specificity. Two different selection strategies were adopted for the two phosphopeptides. For the PEP1-P, the washing stringency was relatively mild, in the hope of keeping maximal diversity of the phage pool. More stringent washing conditions were applied in the anti-PEP2-P selection, in order to onlyenrich the clones with high affinity and specificity. The results also reflected the effects of these different strategies. With the mild washing conditions, the anti-PEP1-P selection produced 9 distinct scFv clones, but only 5 clones showed more than 30% higher phage ELISA signals on the phosphopeptide than on the non-phosphorylated counterpart. The most populated phage clone, A1 (42 duplicates among 74 functional clones), had an average $A_{405}(+)$ / $A_{405}(-)$ ratio of 1.41. However, the $A_{405}(+)$ / $A_{405}(-)$ ratios showed considerable variations between the duplicates. The ratios for the top 4 duplicates are all higher than 2.0 (A1: 3.05, G8: 2.23, B1: 2.22, A5: 2.05), while the bottom 4 duplicates have ratios lower than 1.2 (F11: 1.15, E5: 1.15, H4: 1.14, H6: 1.01), despite the exactly same sequence they all share. This is most likely caused by the variation in the expression level during the phage production because some of the duplicates may have not reached the optimized optical density when the helper phage was added. Therefore, the low phage ELISA signals do not necessarily indicate low binding affinity of the scFv, because they could likely be a result of failed phage production. As only a qualitative indication, the importance of the high phage ELISA signals of the top duplicates should outweigh the low signals of some of the duplicated

clones. One clone should only be rejected when most of the duplicates show uniformly low signals, as in the case of the A7 clone in the anti-Trop-2 selection. Clones with mixed results should still be considered as candidates for further characterizations. More quantitative conclusions should only be drawn according to characterizations using the purified scFv proteins.

For the PEP2-P phosphopeptide, the more stringent washes led to only two functional sequences, with one having 34 duplicates and the other having only 1 copy. The single copy F1 clone showed no distinction between the phosphorylated and non-phosphorylated peptides, but the highly duplicated F3 clone had an average $A_{405}(+) / A_{405}(-)$ ratio of 2.28. The ratios for the top 7 duplicates of the F3 are all higher than 3.0 (F3: 4.35, B2: 4.25, F2: 3.79, D3: 3.69, F4: 3.37, E2: 3.22, H8: 3.07). The more stringent washing conditions seem to produce fewer clones with better affinity and specificity because of the stronger selection pressure, but it also impose higher risk of losing positive clones if there are only scFvs with intermediate affinities available in the library. For difficult selections against small, specific epitopes, testing different washing conditions may be required to achieve the best performance.

While the 17aa-SSA-scFv library has proved its diversity in multiple successful selections, the 18aa-SX-scFv has been used for only one selection against human CD4, leading to 6 distinct clones after 4 rounds of selection. One of these clones has the 17aa-SSA linker instead of the 18aa-SX linker, which is probably caused by

incomplete digestion of the 17aa-SSA-V_H plasmids during the library construction. The characterization of these clones is currently underway, and the further validation of the 18aa-SX-scFv library depends on selections against more targets in the future.

Successful phage selections depend on optimized washing stringency for each round. Different researchers may have different washing techniques, so the exact washing protocol should be optimized accordingly. The more practical standard is the input and output phage titer for each round of selection. The number of positive clones is very small in the naïve phage pool, so the washing should be mild for the first round in order to retain more of the positive clones to allow amplification and enrichment in the subsequent rounds. Usually, about 10^{13} input phage are used for the first round, and the output phage titer should be around 10^8 to 10^9. The washing stringency can be greatly increased in the second round to get rid of most of the negative clones. Optimized washing stringency should lead to an output / input ratio of 10^{-8}. For the third round, the washing stringency should be the same as or stronger than that of the second round. Random clones should be sequenced after three rounds of selection to identify enriched clones. If no functional clones are enriched, a fourth round may be necessary.

The purpose of building these two libraries was to provide built-in restriction sites in the linker region to promote rapid linker length reduction to make diabody constructs. The linker designs worked well for this purpose. The 17aa-SSA linker or the 18aa-SX

linker can be shortened to 7 residues or 5 residues by simple digestion, spin column purification and re-ligation. There is no need for PCR, gel purification, and primer design. To investigate whether the linkers of different lengths can fit the needs of different scFvs and diabodies, multiple clones from these libraries were reformatted and produced for size exclusion chromatography analysis. Among the four anti-Ncad clones from the 17aa-SSA-scFv library, the 17aa-SSA linker and 7aa-SSA linker work well for half the clones. We designed a relatively long 7-residue linker for the diabodies considering the rigid nature of the proline residue. However, the 7aa-linker A6 diabody formed a mixture of both monomer and dimer, indicating the 7-residue linker is too long to induce complete dimerization for this particular clone. On the other hand, the 17aa-linker D6 scFv also formed a monomer-dimer mixture. This demonstrated the complicated nature of linker length dependent multimerizaiton. As discussed in last chapter, although 3- to 10-residue linkers can induce dimerization for many scFv clones, the specific requirement on the linker length is also highly dependent on the nature of the antibody clones. There are cases that scFv clones with 12-residue or even 18-residue linkers still formed dimers (4, 5). Our lab has also made a diabody clone with flexible 8-residue linker (GGGGSGGG) that formed monomer instead of dimer (unpublished data). Considering the high diversity of the phage display libraries, it is not surprising to see clones showing different multimerization behaviors. Even if the linker design only works well for half of the clones in the library, it can still save considerable time and effort. For the 18aa-5aa linker design, we tested two random clones, and both clones behaved as expected.

Since the number of tested clones is limited, it is difficult to tell whether the better behaviors are caused by better linker design or simply cause by the properties of individual clones. According to the data presented here, these new libraries can definitely help accelerate the antibody fragments reformatting for some of the clones. Exactly how well these linker designs will work for other clones remain to be verified in the future applications of these libraries.

5.5 Bibliography

1. Schier R, Marks JD, Wolf EJ, Apell G, Wong C, McCartney JE, et al. *In vitro* and *in vivo* characterization of a human anti-c-erbB-2 single-chain Fv isolated from a filamentous phage antibody library. Immunotechnology : an international journal of immunological engineering. 1995;1:73-81.

2. Bai J, Sui J, Zhu RY, Tallarico AS, Gennari F, Zhang D, et al. Inhibition of Tat-mediated transactivation and HIV-1 replication by human anti-hCyclinT1 intrabodies. J Biol Chem. 2003;278:1433-42.

3. Sheets MD, Amersdorfer P, Finnern R, Sargent P, Lindquist E, Schier R, et al. Efficient construction of a large nonimmune phage antibody library: the production of high-affinity human single-chain antibodies to protein antigens. Proceedings of the National Academy of Sciences of the United States of America. 1998;95:6157-62.

4. Whitlow M, Filpula D, Rollence ML, Feng SL, Wood JF. Multivalent Fvs: characterization of single-chain Fv oligomers and preparation of a bispecific Fv. Protein engineering. 1994;7:1017-26.

5. Le Gall F, Kipriyanov SM, Moldenhauer G, Little M. Di-, tri- and tetrameric single chain Fv antibody fragments against human CD19: effect of valency on cell binding. FEBS letters. 1999;453:164-8.

Chapter 6: Summary and future directions

6.1 Summary

The studies presented in this dissertation focused on the fast development of fully human antibody fragments for immunoPET imaging applications. Traditionally, monoclonal antibodies were generated using the murine hybridoma technology (1), and the murine antibodies were then humanized to reduce immunogenicity for clinical applications (2). The antibody reformatting and humanization process can sometimes lead to a reduction of affinity, requiring additional affinity maturation (3). It usually takes several months to just get an antibody fragment candidate, let alone the subsequent characterizations and imaging studies. Phage display technology provides a convenient alternative approach this task. Using fully human antibody phage display libraries, researchers can identify and reformat fully human antibody candidate clones into desired formats in just a few weeks (1 week for 3 rounds of selection, 1 week for sequencing and phage ELISA, and 1 to 2 weeks for antibody fragment production). It will greatly accelerate the development process of fully human antibody fragments for *in vivo* imaging and other applications.

Chapter 2 and chapter 3 demonstrate the fast development of fully human anti-MET antibody fragments for *in vivo* PET imaging of MET positive non-small cell lung cancer

xenografts in preclinical murine models. Multiple anti-human MET phage clones were isolated from a large naïve scFv phage display library generated by Sheets *et al.* (4). Three clones were successfully reformatted into cys-diabodies for *in vitro* characterizations. Among these cys-diabodies, the H2 clone demonstrated highest affinity and best anti-MET inhibitory effect on the MET dependent non-small cell lung cancer cell lines, and it also showed cross reactivity to mouse MET protein. Therefore, it was chosen for the anti-MET immunoPET studies. Compared to previous anti-MET immunoPET studies using intact or one-armed antibodies (5, 6), imaging with the H2 cys-diabody and minibody can provide high contrast images at earlier time points (4 to 20 hours post injection). They were able to distinguish the MET over-expressing gefitinib resistant Hcc827-GR6 tumor from the parental Hcc827 tumor, showing clear potential for same day imaging to evaluate *in vivo* MET expression levels to direct MET-targeted therapies. The anti-MET inhibitory effect of the bivalent H2 antibody fragments also indicated their potential for therapeutic applications.

Although phage display technology has already been accelerating the development of fully human antibody fragments compared to the traditional humanization approach, we have met another bottleneck in our practice. Due to the small size and avidity effect of the bivalent diabody format, it is widely used for various applications including *in vivo* imaging and nanoparticle labeling (7-12). However, it is relatively difficult to reformat the scFvs isolated from the phage display library into diabodies. The dimerization of diabodies is only induced when a short linker is used to connect

the V_H and V_L domains. The steric hindrance forbids self-paring, and the V_H domains are forced to pair with the V_L domains of other molecules (13, 14). The traditional overlap extension PCR method to reduce the linker length is time consuming and sometimes technically challenging, especially when multiple lead candidates need to be reformatted. Therefore, we sought out to further optimize this already great tool to better fit our specific needs.

Most scFv phage display libraries have already included upstream and downstream restriction sites that can be utilized to conveniently subclone the isolated scFvs to other expression vectors or to generate antibody fragments like minibodies or scFv-Fcs. Inspired by this, we designed scFv linkers that can be easily shortened using the built-in restriction sites. Two novel fully human scFv phage display libraries with two different linker designs were constructed using pre-existing V_H and V_L libraries that were used for the construction of the Sheets library. The 17aa-SSA-scFv library has about 9×10^9 functional members, and it has two SalI sites and 1 AscI site in the 17-residue linker region. The two SalI sites can be used to reduce the linker length to 7 residues. The AscI site was used for scFv library construction and it can also be used for V gene shuffling in the future to either increase the library size or to perform affinity maturations on selected scFvs. The 18aa-SX-scFv library has about 2×10^9 functional members. It has an 18-residue linker with one SalI site and one XhoI site. Both sites can be used for V gene shuffling, and they can also be used for the linker length reduction (18-residue to 5-residue) because of the same cohesive ends

after digestion. Both libraries have generated positive clones in phage selections, and the preliminary results showed the anti-Ncad scFvs from the 17aa-SSA-scFv library has low nanomolar affinities ranging from 1.5 nM to 28 nM. The scFvs from these libraries were reformatted into diabody constructs using the restriction sites, and the purified antibody fragments were analyzed by size exclusion chromatography. Among the six pairs of antibody fragments, two fragments did not behave as expected. One scFv with the 17aa-SSA linker and one diabody with the 7aa-SSA linker formed mixtures of monomers and dimers. This demonstrated the complexity of the scFv multimerization, which is determined by not only the linker length but also the linker flexibility, V domain structure and the orientation of the V_H and V_L domains (14-19). Although all four antibody fragments adopting the 18aa-5aa linker design behaved just as expected in the SEC analysis, it is difficult to conclude the 18aa-5aa linker design is better than the 17aa-7aa design due to the limited sample size. Considering the enormous amount of scFv clones in these libraries, It is really difficult for either of these linker designs to fit the need of every individual clone. However, considerable time and effort can still be saved even if these linkers only work well for half of the clones in the library. By using these libraries for more phage selections in the future, we can have a better evaluation of the advantages of these specially designed linkers.

6.2 Future Directions

Given the promising results of the anti-MET antibody fragments in the *in vitro* characterizations and *in vivo* imaging studies, the obvious next step is to continue developing these fragments for both therapeutic and diagnostic applications. Other types of MET positive tumors such as MKN-45 and GTL-16 (5, 6) should also be used for the immunoPET imaging to further validate the cys-diabody and minibody imaging probes. The detailed mechanism for the anti-MET inhibitory effect should be investigated. Considering the fact that many therapeutic anti-MET antibodies are intentionally engineered into monovalent formats, the failure of the H2 scFv to inhibit cell growth and signaling implies it may have a very different mechanism of inhibition. The surprising effects of H2 antibody fragments on the downstream signaling only add more mystery to the problem. We are now collaborating with James Marks' laboratory to perform epitope mapping for the H2 clone, and it will likely produce more implications for the future plan.

Besides the work on the human MET protein, we have also performed several other selections using phage libraries from James Marks' laboratory, against antigens such as EpCAM and PRDX6. The antibody clones generated in these selections, together with the anti-MET clones, were all shared with other laboratories in the Center for Cancer Nanotechnology Excellence and Translation (CCNE-T) program, which focuses on the application of various nanotechnologies to detect all kinds of cancer biomarkers. The anti-MET H2 antibody is currently used for the development of an

endoscopic Raman imaging probe (20) in collaboration with Sanjiv S. Gambhir's laboratory.

The two large human scFv libraries have potential for numerous selections on different targets in the future. The restriction sites in the linker region not only provide a convenient approach to make diabody constructs, they can also be used for V gene shuffling to generate even larger naïve libraries or to improve the affinities of selected scFvs. For example, the 18aa-SX-scFv phage clones from the anti-human CD4 selection showed relatively low signals in the preliminary phage ELISA, probably caused by limited affinities. The V_H genes in the enriched phage pool can be cut out with NcoI and SalI enzymes and cloned back into the 18aa-SX-V_L library. A large enough new library (10^7 -10^8 members) containing only the enriched V_H genes randomly paired with different V_L genes can be generated with just one transformation thanks to the high transformation efficiency of plasmid fragment shuffling (~10^8 /μg). This new library can then be used for the anti-human CD4 selection again to generate scFvs with higher affinities. With these customized phage display libraries, the development of diabodies and other antibody fragments for immunoPET imaging or other applications will be much more convenient and efficient.

6.3 Bibliography

1. Kohler G, Milstein C. Continuous cultures of fused cells secreting antibody of predefined specificity. Nature. 1975;256:495-7.

2. Jones PT, Dear PH, Foote J, Neuberger MS, Winter G. Replacing the complementarity-determining regions in a human antibody with those from a mouse. Nature. 1986;321:522-5.

3. Lepin EJ, Leyton JV, Zhou Y, Olafsen T, Salazar FB, McCabe KE, et al. An affinity matured minibody for PET imaging of prostate stem cell antigen (PSCA)-expressing tumors. Eur J Nucl Med Mol Imaging. 2010;37:1529-38.

4. Sheets MD, Amersdorfer P, Finnern R, Sargent P, Lindquist E, Schier R, et al. Efficient construction of a large nonimmune phage antibody library: the production of high-affinity human single-chain antibodies to protein antigens. Proc Natl Acad Sci U S A. 1998;95:6157-62.

5. Perk LR, Stigter-van Walsum M, Visser GW, Kloet RW, Vosjan MJ, Leemans CR, et al. Quantitative PET imaging of Met-expressing human cancer xenografts with 89Zr-labelled monoclonal antibody DN30. Eur J Nucl Med Mol Imaging. 2008;35:1857-67.

6. Jagoda EM, Lang L, Bhadrasetty V, Histed S, Williams M, Kramer-Marek G, et al. Immuno-PET of the hepatocyte growth factor receptor Met using the 1-armed antibody onartuzumab. Journal of nuclear medicine : official publication, Society of Nuclear Medicine. 2012;53:1592-600.

7. Shimazaki K, Lepin EJ, Wei B, Nagy AK, Coulam CP, Mareninov S, et al. Diabodies targeting epithelial membrane protein 2 reduce tumorigenicity of human endometrial cancer cell lines. Clin Cancer Res. 2008;14:7367-77.

8. Sirk SJ, Olafsen T, Barat B, Bauer KB, Wu AM. Site-specific, thiol-mediated conjugation of fluorescent probes to cysteine-modified diabodies targeting CD20 or HER2. Bioconjugate chemistry. 2008;19:2527-34.

9. McCabe KE, Liu B, Marks JD, Tomlinson JS, Wu H, Wu AM. An engineered cysteine-modified diabody for imaging activated leukocyte cell adhesion molecule (ALCAM)-positive tumors. Molecular imaging and biology : MIB : the official publication of the Academy of Molecular Imaging. 2012;14:336-47.

10. Olafsen T, Sirk SJ, Olma S, Shen CK, Wu AM. ImmunoPET using engineered antibody fragments: fluorine-18 labeled diabodies for same-day imaging. Tumour biology : the journal of the International Society for Oncodevelopmental Biology and Medicine. 2012;33:669-77.

11. Girgis MD, Federman N, Rochefort MM, McCabe KE, Wu AM, Nagy JO, et al. An engineered anti-CA19-9 cys-diabody for positron emission tomography imaging of pancreatic cancer and targeting of polymerized liposomal nanoparticles. The Journal of surgical research. 2013;185:45-55.

12. Barat B, Sirk SJ, McCabe KE, Li J, Lepin EJ, Remenyi R, et al. Cys-diabody quantum dot conjugates (immunoQdots) for cancer marker detection. Bioconjugate chemistry. 2009;20:1474-81.

13. Kortt AA, Lah M, Oddie GW, Gruen CL, Burns JE, Pearce LA, et al. Single-chain Fv fragments of anti-neuraminidase antibody NC10 containing five- and ten-residue linkers form dimers and with zero-residue linker a trimer. Protein engineering. 1997;10:423-33.

14. Atwell JL, Breheney KA, Lawrence LJ, McCoy AJ, Kortt AA, Hudson PJ. scFv multimers of the anti-neuraminidase antibody NC10: length of the linker between VH and VL domains dictates precisely the transition between diabodies and triabodies. Protein engineering. 1999;12:597-604.

15. Hudson PJ, Kortt AA. High avidity scFv multimers; diabodies and triabodies. Journal of immunological methods. 1999;231:177-89.

16. Whitlow M, Filpula D, Rollence ML, Feng SL, Wood JF. Multivalent Fvs: characterization of single-chain Fv oligomers and preparation of a bispecific Fv. Protein engineering. 1994;7:1017-26.

17. Arndt KM, Muller KM, Pluckthun A. Factors influencing the dimer to monomer transition of an antibody single-chain Fv fragment. Biochemistry. 1998;37:12918-26.

18. Le Gall F, Kipriyanov SM, Moldenhauer G, Little M. Di-, tri- and tetrameric single chain Fv antibody fragments against human CD19: effect of valency on cell binding. FEBS letters. 1999;453:164-8.

19. Dolezal O, Pearce LA, Lawrence LJ, McCoy AJ, Hudson PJ, Kortt AA. ScFv multimers of the anti-neuraminidase antibody NC10: shortening of the linker in single-chain Fv fragment assembled in V(L) to V(H) orientation drives the formation of dimers, trimers, tetramers and higher molecular mass multimers. Protein engineering. 2000;13:565-74.

20. Zavaleta CL, Garai E, Liu JT, Sensarn S, Mandella MJ, Van de Sompel D, et al. A Raman-based endoscopic strategy for multiplexed molecular imaging. Proc Natl Acad Sci U S A. 2013;110:E2288-97.